

**EVALUATING DIFFERENT CONTROL SCHEMES FOR  
IMPROVING THE EFFICIENCY IN LOW POWER CONVERTERS  
USED IN REDUCED-SPACE SYSTEMS**

By

*John Edward Salazar Duque*

A thesis submitted in partial fulfillment of the requirements for the degree of

MASTER OF SCIENCE

in

ELECTRICAL ENGINEERING

UNIVERSITY OF PUERTO RICO  
MAYAGÜEZ CAMPUS

July, 2016

Approved by:

---

Eduardo I. Ortiz Rivera, Ph.D.  
Chairman, Graduate Committee

---

Date

---

Guillermo Serrano Rivera, Ph.D.  
Member, Graduate Committee

---

Date

---

Fabio Andrade Rengifo, Ph.D.  
Member, Graduate Committee

---

Date

---

Jesús D. González Llorente, MSc.  
Member, Graduate Committee

---

Date

---

Wandaliz Torres Garcia, Ph.D.  
Graduate Studies Representative

---

Date

---

Jose Colom , Ph.D.  
Department Chairperson

---

Date

Abstract of Thesis Presented to the Graduate School  
of the University of Puerto Rico in Partial Fulfillment of the  
Requirements for the Degree of Master of Science

**EVALUATING DIFFERENT CONTROL SCHEMES FOR  
IMPROVING THE EFFICIENCY IN LOW POWER CONVERTERS  
USED IN REDUCED-SPACE SYSTEMS**

By

*John Edward Salazar Duque*

July 2016

Chair: Dr. Eduardo I. Ortiz Rivera

Department: Electrical and Computer Engineering Department

The DC/DC converters are one of the main blocks of most electronic systems, allowing communication between energy sources and the rest of the system. The DC / DC converters are widely used systems because they allow power control by controlling the input voltage, control of the output voltage, and optimization of energy systems such as solar cells. This thesis presents the analysis, design, implementation and comparison of some control techniques applied to these DC / DC converters. Specifically, control techniques are evaluated in terms of efficiency and response times on the DC/DC SEPIC converter (Single Ended Primary Inductor Converter ) in order to determine suitability for use in reduced space systems where these parameters determine an important factor in the performance. As a case study, the use of a DC/DC converter is evaluated on a CubeSat (U-class spacecraft). These systems are miniature satellites used for space exploration and thanks to its low cost and level of implementation has become an essential tool for research.

Resumen de tesis presentado a la Escuela Graduada  
de la Universidad de Puerto Rico como requisito parcial de los  
requerimientos para el grado de Maestría en Ciencias

**EVALUACIÓN DE DIFERENTES TÉCNICAS DE CONTROL PARA  
MEJORAR LA EFICIENCIA DE CONVERTIDORES DE BAJA  
POTENCIA UTILIZADOS EN SISTEMAS DE ESPACIO REDUCIDO**

Por

*John Edward Salazar Duque*

Julio 2016

Consejero: Dr. Eduardo I. Ortiz Rivera

Departamento: Ingeniería Eléctrica y Computadoras

Los convertidores DC/DC son uno de los bloques principales de la mayoría de sistemas electrónicos, ya que permite la comunicación entre las fuentes de energía y el sistema como tal. Los convertidores DC/DC son sistemas muy utilizados debido a que permiten el control de la potencia mediante el control de la tensión de entrada, control de la tensión de salida y la optimización de sistemas generadores de energía como las celdas solares. Esta tesis presenta el análisis, diseño, implementación y comparación de algunas técnicas de control aplicadas a estos convertidores DC/DC. Específicamente, las técnicas de control son evaluadas en términos de eficiencia y tiempos de respuesta sobre el convertidor Single Ended Primary Inductor Converter (SEPIC) con el fin de determinar la conveniencia sobre el uso en sistemas de espacio reducido donde estos parámetros determinan un factor importante en el rendimiento del mismo. Como caso de estudio, se evalúa la utilización de un convertidor DC/DC en un CubeSat (U-class spacecraft). Estos sistemas son satélites miniatura utilizados para exploración espacial y que gracias a su bajo costo y nivel de implementación se han convertido en una herramienta esencial para la investigación.

Copyright © 2016

by

*John Edward Salazar Duque*



*To my parents,*  
*Maria and Eduardo,*  
*And my brothers, Alejandro and Hector,*  
*Without whom, none of my success would be possible*

# Acknowledgements

I would like to express my thanks to my advisor Professor Dr. Eduardo Ortiz Rivera, thank you for encouraging my research and for allowing me to grow as a student, researcher, and professional. I would like to thank my committee members, Professor Guillermo Serrano Rivera, Dr. Fabio Andrade Rengifo, M.Sc. Jesus Gonzalez Llorente, and Dr. Wandaliz Torres Garcia, for serving as my committee and for taking part in the review of my work.

Also I would especially like to express deepest appreciation to Sandy, my Puerto Rican mother, who knew how to guide me and be with me at all times.

I would like to thank all my Puerto Rican friends and professors, who always made me feel at home and showed me the amazing things of this beautiful island. I would like to express my gratitude to my Colombian friends, who became a second family and supported me during good and bad moments.

Last but not least, I want to thank Natalia Cerón, who despite the distance never made me feel alone.

This master thesis was developed, under research project “Study and analysis of obtaining solar energy and its efficient use of the orientation of a CubeSat 3U nanosatellite”. The author is grateful for financial support from the COLCIENCIAS under research grant No. 0208-2013 with resources of “El Patrimonio Autónomo Fondo Nacional de Financiamiento para la Ciencia, la Tecnología y la Innovación”, Colombia.

# Table of Contents

Abstract in English . . . . .	ii
Abstract in Spanish . . . . .	iii
Copyright . . . . .	iv
Dedicated to... . . . .	v
Acknowledgements . . . . .	vi
List of Tables . . . . .	xi
List of Figures . . . . .	xii
<b>1 INTRODUCTION . . . . .</b>	<b>1</b>
1.1 Justification . . . . .	2
1.2 Objectives . . . . .	3
1.2.1 General Objective . . . . .	3
1.2.2 Specific Objectives . . . . .	3
<b>2 PREVIOUS WORK &amp; ARCHITECTURE SELECTION . . . . .</b>	<b>4</b>
2.1 Literature review & Topologies Overview . . . . .	4
2.1.1 Background . . . . .	5
2.1.2 Photovoltaic System . . . . .	6
2.1.3 Converter Topologies . . . . .	9
2.2 Topology Selected . . . . .	13
2.2.1 SEPIC Design . . . . .	15
2.2.2 Summary of components . . . . .	21
<b>3 CONTROL DESIGN TOOLS . . . . .</b>	<b>22</b>
3.1 Fuzzy Logic Control . . . . .	22

3.1.1	Fuzzy Sets . . . . .	23
3.1.2	Membership Function . . . . .	23
3.1.3	Fuzzification . . . . .	24
3.1.4	The defuzzification . . . . .	25
3.2	Passivity-Based Control . . . . .	26
<b>4</b>	<b>SYSTEM'S DESIGN &amp;</b>	
	<b>COMPONENTS OVERVIEW . . . . .</b>	<b>29</b>
4.1	SEPIC Analysis . . . . .	30
4.2	Maximum Power Point Tracking - MPPT . . . . .	37
4.2.1	Linear Reoriented Coordinates Method - LRCM . . . . .	40
4.2.2	Linear Approximation of the I-V curve . . . . .	42
4.2.3	Existence . . . . .	48
4.3	Output Voltage Control . . . . .	51
4.3.1	Fuzzy Logic Control . . . . .	51
4.3.2	Passivity-Based Control . . . . .	54
<b>5</b>	<b>ANALYSIS OF SIMULATION &amp;</b>	
	<b>EXPERIMENTAL RESULTS . . . . .</b>	<b>58</b>
5.1	Photovoltaic Module System . . . . .	59
5.1.1	Simulation results . . . . .	60
5.1.2	Experimental results . . . . .	61
5.2	Developed system based on Microcontroller and SEPIC converter . . . . .	63
5.3	DC/DC Converter . . . . .	65
5.3.1	Open-Loop Performance . . . . .	65
5.3.2	Maximum Power Point Tracking . . . . .	85
5.3.3	Output Voltage Control . . . . .	89
5.4	Summary of results . . . . .	97
5.4.1	Open-Loop Performance . . . . .	97

5.4.2	MPPT	. . . . .	98
5.4.3	Close-Loop Performance	. . . . .	99
<b>6</b>	<b>CONCLUSIONS</b>	. . . . .	<b>102</b>
<b>Bibliography</b>		. . . . .	<b>103</b>

# List of Tables

2.1	Mathematical Description of PMCS . . . . .	6
2.2	SX-10 SOLAREX PVM basic electrical characteristics . . . . .	7
2.3	Buck, Boost and Buckboost Converter Topologies . . . . .	10
2.4	Optimal D for different DC-DC converters for load matching . . . . .	11
2.5	Summary of CCM-DCM characteristics for the Buck, Boost, and Buck- boost converter . . . . .	12
2.6	System requirements . . . . .	15
2.7	Summary of components . . . . .	21
4.1	Fuzzy Logic Controller rules . . . . .	52
5.1	Triple Junction Solar Cell 5E14 - Azur Space [1] . . . . .	59
5.2	Case Study . . . . .	59
5.3	Case Study - Matlab Simulation . . . . .	61
5.4	Case Study - Solar Array Emulator . . . . .	62
5.5	Simulation results of P&O method . . . . .	86
5.6	Open-Loop efficiency - fixed power supply . . . . .	97
5.7	Open-Loop efficiency - Solar array simulator . . . . .	98
5.8	Convergence time of the MPPT algorithm . . . . .	98
5.9	Average Output Voltage Control efficiency - Fuzzy Logic Controller . . . . .	99
5.10	Output Voltage Control efficiency - Passivity-Based Controller . . . . .	100
5.11	Output Voltage Control efficiency - Summary . . . . .	100
5.12	Settling Time . . . . .	101

# List of Figures

2.1	General System - PMCS . . . . .	5
2.2	I-V characteristic curves . . . . .	8
2.3	P-V characteristic curves . . . . .	9
2.4	SEPIC Topology . . . . .	14
2.5	SEPIC Stages . . . . .	14
3.1	Graphical representation of a conventional set (left) and a fuzzy set (right)	23
3.2	Example of membership function . . . . .	24
3.3	Example of fuzzification of one variable. . . . .	24
3.4	Example of fuzzy implication with conjunction OR translated into a MAX	24
3.5	Example of fuzzy implication using some rules . . . . .	25
3.6	Defuzzification with the method of the mean of maxima (MeOM) . . .	26
3.7	Defuzzification with the method of center of gravity (COG) . . . .	26
4.1	SEPIC converter and PVM configuration . . . . .	30
4.2	SEPIC Stages . . . . .	31
4.3	Duty cycle regions . . . . .	35
4.4	P&O Algorithm . . . . .	39
4.5	Relation between the I-V curve an the LRCM . . . . .	40
4.6	Upper region of the search of the new P&O technique . . . . .	42
4.7	Getting the Fill Factor From the I-V Sweep . . . . .	42
4.8	Simplified Equivalent Circuit Model for a Photovoltaic Cell . . . .	43
4.9	Linear approximation of the I-V Curve . . . . .	44
4.10	Bounded Region of the I-V Curve . . . . .	46
4.11	Bounded Region of the P-V Curve . . . . .	46



4.12	Derivative of Power for each b . . . . .	47
4.13	Fuzzy Membership Function Inputs and Output . . . . .	53
4.14	Block diagram of the FLC for DC/DC converters [2] . . . . .	53
5.1	EPVM Model implementation - Simulink® . . . . .	60
5.2	Simulation characteristic curves . . . . .	61
5.3	Simulation and Experimental characteristic curves . . . . .	62
5.4	Triple Junction Solar Cell 5E14 - Azur Space [1] . . . . .	63
5.5	Block Diagram of the developed system . . . . .	64
5.6	PCB Boards . . . . .	64
5.7	Experimental Setup . . . . .	65
5.8	Open Loop simulation systems - a) LT-Spice b) Matlab Simulink® .	66
5.9	Input Current response - SEPIC as a Buck converter . . . . .	68
5.10	Output Current response - SEPIC as a Buck converter . . . . .	69
5.11	Input Voltage response - SEPIC as a Buck converter . . . . .	70
5.12	Output Voltage response - SEPIC as a Buck converter . . . . .	71
5.13	Input Current response - SEPIC at 50% duty cycle . . . . .	72
5.14	Output Current response - SEPIC at 50% duty cycle . . . . .	73
5.15	Input Voltage response - SEPIC at 50% duty cycle . . . . .	74
5.16	Output Voltage response - SEPIC at 50% duty cycle . . . . .	75
5.17	Input Current response - SEPIC as a Boost converter . . . . .	76
5.18	Output Current response - SEPIC as a Boost converter . . . . .	77
5.19	Input Voltage response - SEPIC as a Boost converter . . . . .	78
5.20	Output Voltage response - SEPIC as a Boost converter . . . . .	79
5.21	PVM-SEPIC simulation system - Simulink® . . . . .	80
5.22	PVM Model Open-Loop simulation response . . . . .	81
5.23	PVM Model Experimental response . . . . .	83
5.24	Flow chart of P&O algorithm . . . . .	85

5.25	P&O simulation responses . . . . .	87
5.26	Zoom-in of Figure 5.25 . . . . .	88
5.27	Fuzzy-Logic Control implementation - Simulink® . . . . .	89
5.28	Fuzzy-Logic Control rules validation - Simulink® . . . . .	90
5.29	3-D surface of Memberships in Figure 4.13 . . . . .	91
5.30	Fuzzy Logic Control simulation response . . . . .	92
5.31	Fuzzy Logic Control Experimental response . . . . .	93
5.32	Passivity-Based Control simulation response . . . . .	95
5.33	Passivity-Based Control Experimental response . . . . .	96

# Chapter 1

## INTRODUCTION

The generation of electric energy coming from renewable energy sources like a solar cells, which generate electrical current from the Suns lights, wind turbines, which generate electrical power by converting the winds kinetic energy into electrical energy, Fuel cells, Bio mass among others, must be made efficient and effective due to that the non-renewable energy sources are quickly depleting day by day [3]. Reducing the physical size of electronic equipment in power applications aims to include both new features and integrate power converters in places normally unfit for such equipment [4]. There are several types of power converters. Among the best known DC/DC converters the Buck Converter, the Boost converter and Buck-Boost are the most common [5]. The output voltage for the Boost converter is above the input, while for the Buck converter is below. The output of the Buck-Boost converter can be either higher or lower than the input signal, but the polarity will be inverse with respect to the input signal [6]. On the other hand, a SEPIC (Single-Ended Primary-Inductor Converter) converter is a type of converter that regardless of variations in the input signal or load changes maintains a constant output. Also it preserves the polarity of the input signal, a decisive factor in many fields [7]. Design methodology and selection of components of SEPIC converter is described in [8–10].

## 1.1 Justification

Switching power converters are present in almost every electrical/electronic device in today's world [11]. The ever-increasing demand of higher power densities (reduced size for the same power) and higher efficiencies, has made power electronics essential in any device [12]. This problem will create a need for obtaining the necessary power from a source which will be able to supply this energy on reduced-space systems. Thus, closed-loop controllers such as current-mode control, voltage-mode control, direct control method, among others are usually implemented in power conversion systems in order to obtain a tight regulation of the output variables at the desired values [13, 14].

Higher efficiency, better performance, smaller size and reduced cost can be reached just by improving these controllers. Reducing the physical size of electronic equipment in power applications is desirable in order to add more features into existing products, integrate power converters in places normally unfit for such equipment, and reduce system cost. On the other hand, non-renewable energy sources are quickly depleting as their demand increases day by day [15]. To overcome this problem the generation of electric energy coming from renewable energy sources must be made efficient and effective.

Having mentioned this, it is necessary to develop a system that will increase the efficiency of the converters used in reduced space systems such as cell phones, computers, video games, among others and systems based on renewable energy such as nanosatellites, where the efficiency plays an important role on the system performance.

## **1.2 Objectives**

This Section describes the objectives that have been formulated for the proposed work.

### **1.2.1 General Objective**

To evaluate the performance of different controllers of DC/DC low power converters used in reduced-space systems to improve their efficiency.

### **1.2.2 Specific Objectives**

1. To identify the main control techniques for DC/DC converters used in low power systems.
2. To design and implement control strategies for low power DC/DC converters to evaluate their performance for different load conditions.
3. To design and implement different control strategies to maximize energy in low power photovoltaic systems in different environment conditions.

## Chapter 2

# PREVIOUS WORK & ARCHITECTURE SELECTION

### 2.1 Literature review & Topologies Overview

The research topic will be the study the topology of DC/DC converters to determine a nonlinear control technique which promotes the efficient operation of the converter and prolongs the batteries or utilizes the photovoltaic panels improving their efficiency. Some of the techniques used in the literature can be found in [Chapter 3](#). In order to select the proper technique to avoid losses of energy, the literature in DC/DC converters for low power applications and nonlinear control was reviewed in [Section 2.1.3](#). Several examples of the most common power converters used in the industry are presented in [Section 2.1.3](#). The approaches documented here can be classified as DC/DC converters and nonlinear control techniques. In this Chapter, we make a review of the works considered more relevant in these kinds of studies.

### 2.1.1 Background

Embedded applications have emerged appreciably during the past few years due to the considerable increase of nomadic and traveling ways of life. These kinds of itinerant lifestyles induce the apparition and development of more portable and autonomous systems. As a consequence, the energy sources, and their corresponding storage devices and power management control systems (PMCS), should be improved substantially to obtain an optimal and long-lasting working operation. Usually, a PMCS has the following form:

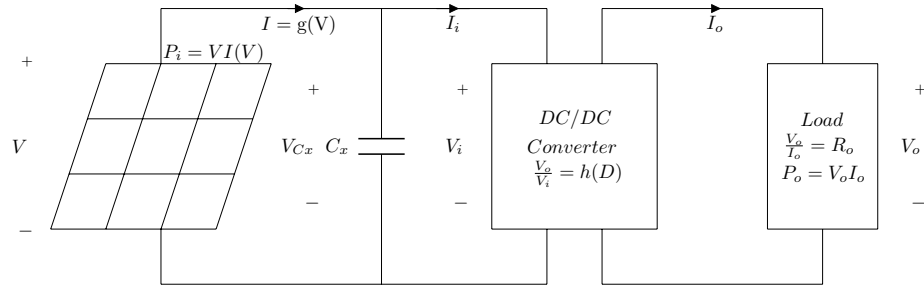


Figure 2.1 : General System - PMCS

This system is composed of three fundamental parts. The first part is a power source, which in this case is a Photovoltaic System (PV), then, a DC/DC Converter and, finally, a charging System. The following mathematical description is assumed under the premise that the output and input power is the same.

$$P_o = P_i$$

A general mathematical form to express the above DC/DC Converters is shown in [Table 2.1](#). This table summarizes each state of the systems composed of photovoltaic system, loads, and DC/DC converters as mathematical form

In [Table 2.1](#) (b),  $D$  is the duty cycle or the fraction of the time that the inductor is being charged, and  $V_x$  and  $I_x$  are the photovoltaic panel parameters.

(a)	(b)	(c)
Source	DC/DC Converter	Load
$I_x \geq g(V) \geq 0$	$V_o = h(D)V_i$	$V_o = I_o R_o$
$V_x \geq V \geq 0$	$I_i = h(D)I_o$	$P_o = \frac{V_o^2}{R_o}$
$P_{max} \geq Vg(V) \geq 0$	$R_o = h(D)^2 R_i$	$R_o = \frac{V_o^2}{P_o} = \frac{V_o^2}{P_i}$

Table 2.1 : Mathematical Description of PMCS

### 2.1.2 Photovoltaic System

Solar photovoltaic energy has gained recognition as a great alternative source of energy. In photovoltaics, the basic building block is the solar cell, which is a pn junction diode where the incidence of light on the pn junction causes the development of a potential difference across the junction. This then initiates the flow of a current in an external circuit. Several of these kinds of cells are connected in a series-parallel connection to form a solar array.

These devices, solar cells, can be modeled by mathematical models. Some theoretical equations to model the I-V characteristic of the PV cells are given in [Equation \(2.1\)](#) from [16]. First, the [Equation \(2.1a\)](#) is a model described through the fractal polynomials (FPVM) [17]. On the other hand, the [Equation \(2.1b\)](#) is an exponential PV Module Model (EPVM) that considers the irradiance level ( $E_i$ ) and temperature ( $T$ ), making it excellent for real-time applications [16]. As can be seen in [Equation \(2.1a\)](#) and [Equation \(2.1b\)](#), the solar array can have linear and nonlinear characteristics. These characteristics can be seen shown in [Figure 2.2](#).

$$I(V) = I_x - I_x \left( \frac{V}{V_x} \right)^{n+q} \quad (2.1a)$$

$$I(V) = \frac{I_x - I_x e^{\left(\frac{V}{bV_x} - \frac{1}{b}\right)}}{1 - e^{\left(\frac{-1}{b}\right)}} \quad (2.1b)$$



In the previous equations,  $I_x$  and  $V_x$  are the short-circuit current and the open-circuit voltage at any given  $E_i$  and  $T$  respectively, and  $b$  is the PVM characteristic constant [16]. These two models presented by Ortiz-Rivera [16] describes the behavior of a PVM considering its basic electrical conditions. Also, they can be related through the dimensionless constants of each model ( $b$ ,  $n$  and  $q$ ). If the maximum power value is the same in these two models it can be demonstrated that this relationship exists.

$$P_{max_{fp}} = V_{op}I_x - V_{op}I_x \left( \frac{V_{op}}{V_x} \right)^{n+q} \quad (2.2a)$$

$$P_{max_{exp}} = \frac{V_{op}I_x - V_{op}I_x e^{\left(\frac{V_{op}}{bV_x} - \frac{1}{b}\right)}}{1 - e^{\left(\frac{-1}{b}\right)}} \quad (2.2b)$$

where

$$P_{max_{fp}} = P_{max_{exp}} \quad (2.3)$$

$$n + q = \frac{\ln \left( 1 - \frac{e^{\left(\frac{V_{op}}{bV_{oc}} - \frac{1}{b}\right)} - 1}{e^{\left(\frac{-1}{b}\right)} - 1} \right)}{\ln \left( \frac{V_{op}}{V_{oc}} \right)} \quad (2.4)$$

also

$$\begin{aligned} & \text{While } |b_{n+1} - b_n| > \varepsilon_{error} \\ b_{n+1} &= \frac{V_{op} - V_{oc}}{V_{oc} \ln \left[ 1 - \frac{I_{op}}{I_{sc}} \left( 1 - e^{\left(\frac{-1}{b_n}\right)} \right) \right]} \end{aligned} \quad (2.5)$$

This relationship allows using both equations or one of them to find parameters missing in the other one. The manufacturer data sheet will provide the open circuit voltage under STC,  $V_{oc}$ , and the short circuit current under STC,  $I_{sc}$  [18], e.g.  $T_N$  is  $25^\circ C$  and  $E_{iN}$  is  $1000 \frac{W}{m^2}$ . [Table 2.2](#) shows the basic electrical conditions for a commercial PVM.

Table 2.2 : SX-10 SOLAREX PVM basic electrical characteristics

$V_{oc}(V)$	$I_{sc}(A)$	$V_{op}(V)$	$I_{op}(A)$	$P_{max}(W)$	$b$	$n + q$
21	0.65	16.8	0.59	10	0.08394	10.677

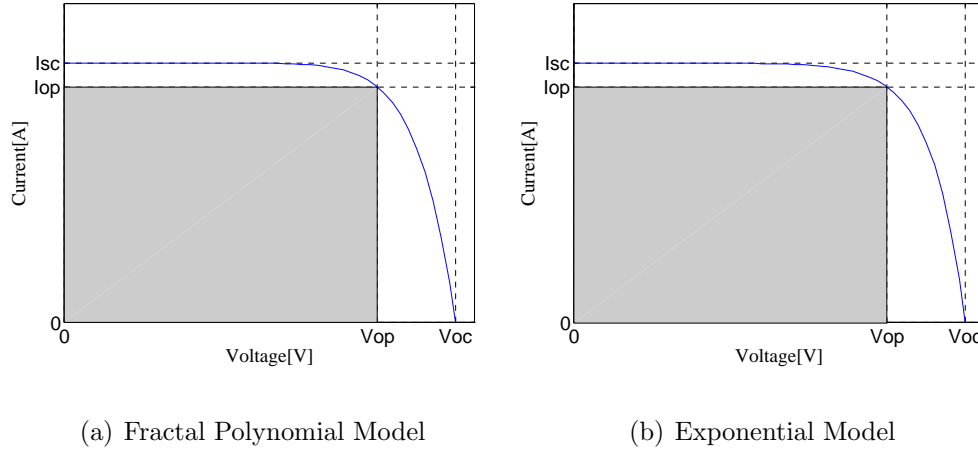


Figure 2.2 : I-V characteristic curves

The PV cell current and voltage depend on cell temperature and the quantity of radiation that incident on the cell since temperature and radiation incident are continuously changing throughout the day when the array is operating. The conversion efficiency of the incident radiation to electrical energy in the PV cell is low and in the order of around 15% [19]. However, the maximum power can be drawn from the array by operating it at the voltage and corresponding current to the knee of the curve, which is the maximum power point of the curve. The maximum power point is continuously changing as the array characteristics changes. The power variation is shown in Figure 2.3 . If a fixed load is connected to the array terminals, the maximum power will not be extracted under changing conditions.

Since the array is a DC power source, the current drawn from the solar array should ideally be ripple free for efficient extraction of energy, but the DC/DC converter is a switching converter which inherently introduces a certain amount of ripple in the array current, thereby reducing the efficiency of which energy can be recovered from the array. Usually, this ripple is minimized by using a filter at the array terminals. However, the use of a large capacitor, which is usually electrolytic, is not preferred, as it is prone to failures [20].

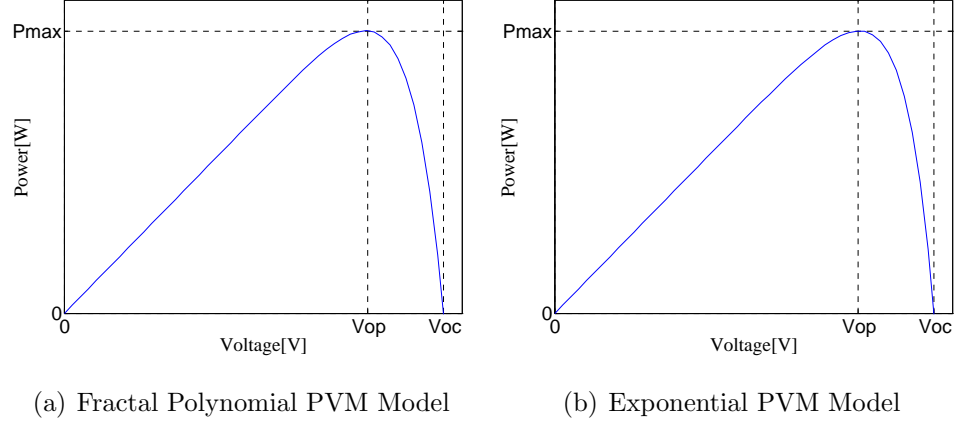


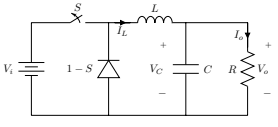
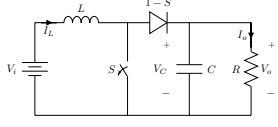
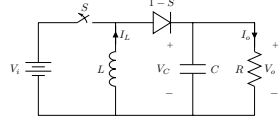
Figure 2.3 : P-V characteristic curves

### 2.1.3 Converter Topologies

DC-DC converters are power electronic circuits that convert a DC voltage to a different DC voltage level, often providing a regulated output [21]. Voltage regulators can be classified in two fundamental topologies: linear regulators and switching regulators (inductive). A linear regulator employs an active (Bipolar Junction Transistor “BJT” or Metal-Oxide-Semiconductor Field-Effect Transistor “MOSFET”) pass device (series or shunt) controlled by a high gain differential amplifier. It compares the output voltage with a precise reference voltage and adjusts the pass device to maintain a constant output voltage. These devices are limited to step-down conversion and exhibit poor efficiencies. The linear regulators' power dissipation is directly proportional to its output current for a given input and output voltage, so typical efficiencies can be 50% or even lower.

A switching regulator converts the DC input voltage to a switched voltage applied to a power MOSFET or BJT switch. This conversion method is more power efficient (often 90%) than linear voltage regulation, which dissipates unwanted power as heat [22]. This efficiency is beneficial for increasing the running time of battery operated devices. However, the noise output of a linear regulator is much lower than a switching

Table 2.3 : Buck, Boost and Buckboost Converter Topologies

Converter	Buck	Boost	Buckboost
			
$V_o/V_i$	$D$	$\frac{1}{1-D}$	$\frac{-D}{1-D}$
$\Delta V_o/V_i$	$\frac{1-D}{8LCf^2}$	$\frac{D}{RCf}$	$\frac{D}{RCf}$
$L_{min}$	$\frac{(1-D)R}{2f}$	$\frac{D(1-D)^2 R}{2f}$	$\frac{(1-D)^2 R}{2f}$

regulator with the same output voltage and current requirements. Typically, the switching regulator can drive higher current loads than a linear regulator.

There are several types of inductive converters. These type of converters can be used as step/up or step/down depending on the topology. Among the best known DC/DC converters are the Buck converter and the Boost converter. There are other topologies, but usually, they are based on these two. The most common combination of these two topologies is called Buck-Boost, which can be used as step/up or step/down. There are other topologies such as SEPIC, Zeta, Ćuk, KY and others, but they basically vary in their specifications. The output voltage of the Boost converter is above the input while for the Buck converter it is below. A particular case of converters is the KY converter, which is a voltage boosting converter and it always operates in continuous conduction mode [23].

The topologies just mentioned can be appreciated in Table 2.3. The most commonly used DC/DC power converters correspond to the SISO (Single-Input Single-Output) second order converters. These are step-down (Buck) converter, step-up (Boost) converter, and step-down/step-up (Buck-boost) converter.

Buck and Boost converter circuits are only capable of stepping-down and stepping-up the input voltage respectively. The circuit implementation is simple but the PV

array current is discontinuous and would require a large capacitor at the array terminals to smooth the input current. In order to determine the maximum power point, there are methods that extract this value through different algorithms. Those algorithms do not take into account that weather conditions are changing very fast. Ortiz-Rivera et al, [18], presents an analytical method for load matching using the optimal duty ratio for a DC/DC converter to transfer the maximum power to the load. This method uses the relationship between the voltage input and output for a DC/DC converter relationship. The load resistance,  $R_o$ , can be seen as voltage output,  $V_o$ , divided by current output,  $I_o$ .

Table 2.4 shows the conditions and optimal duty ratio for a Buck converter, Boost converter, and Buck-Boost converter. From Table 2.4, the only disadvantage of using a Buck or Boost converter is the restriction in the values between  $R_{op}$  and  $R_o$  for both cases. As can be seen for Buck and Boost converter  $R_{op} > R_o$  and  $R_o > R_{op}$  respectively.

Table 2.4 : Optimal D for different DC-DC converters for load matching

DC/DC Converter	D for any $P_o$	D when $P_i = P_o = P_{max}$	Required
Buck-boost	$D = \frac{\sqrt{R_o}}{\sqrt{R_o} + \sqrt{R_i}}$	$D = \frac{V_o}{V_o + V_{op}}$	None
Boost	$D = 1 - \sqrt{\frac{R_i}{R_o}}$	$D = 1 - \frac{V_{op}}{V_o}$	$R_o > R_{op}$
Buck	$D = \sqrt{\frac{R_o}{R_i}}$	$D = \frac{V_o}{V_{op}}$	$R_{op} > R_o$

A very important factor for designing a DC/DC converter is the current that passes through the inductor present in the converter. This current has two operation modes: continuous and discontinuous conduction mode (CCM and DCM respectively). In CCM, the inductor current is always positive and greater than zero; while in DCM, the inductor current reaches zero. The DCM mode occurs because switching ripple in inductor current or capacitor voltage causes polarity of applied

switch current or voltage to reverse. This causes the current or voltage unidirectional assumptions made in realizing the switch to be violated [24]. A typical example is DC/DC converters operating at light load (small load current). This is important to know when designing the system controller. Table 2.5 shows the CCM-Gain, DCM-Gain expressions for each basic topology.

Table 2.5 : Summary of CCM-DCM characteristics for the Buck, Boost, and Buck-boost converter

Converter	$K_{crit}$	DCM M(D,K)	CCM M(D,K)
Buck-boost	$(1 - D)^2$	$-\frac{D}{\sqrt{K}}$	$-\frac{D}{1-D}$
Boost	$D(1 - D)^2$	$\frac{1+\sqrt{1+4D^2/K}}{2}$	$\frac{1}{1-D}$
Buck	$(1 - D)$	$\frac{2}{1+\sqrt{1+4K/D^2}}$	$D$

---

with  $K = 2L/RT_s$  DCM occurs for  $K < K_{crit}$ .

If the value of  $K$  is less than the value of  $K_{crit}$ , the converter will be forced to operate in DCM; otherwise, it would be operating in CCM. It can be observed that when the output current increases, the converter is nearer to CCM operation. Although this  $K_{crit}$  changes for some topologies, the criterion for DCM is always the same. The only difference between topologies will be the definition of  $K_{crit}$ .

Each system above, Buck, Boost or the Buck-boost can work in each of these operation modes. Performing an analysis for each of the topologies, equations describing each system are obtained. Usually, the mode of operation is CCM, but the analysis is performed for both modes. The complete methodology for the derivation

of the models of the basic converters has been discussed by Daniel W Hart, Ned Mohan, and Sira-Ramirez [21, 25, 26].

## 2.2 Topology Selected

As discussed in the previous Section, inductive converters offer high efficiency, hence are best suited for the target application. Some applications of converters only need to buck or boost the voltage and can simply use the corresponding converters. However, sometimes the desired output voltage will be in the range of input voltage. When this is the case, it is still convenient to use a converter that can decrease or increase the voltage. Buck-boost converters can be cheaper because they only require a single inductor and a capacitor. However, these converters suffer from a high amount of input current ripple. This ripple can create harmonics; in many applications, these harmonics need a large capacitor or an LC filter. This often makes the Buck-boost expensive or inefficient. Another issue that can complicate the usage of buck-boost converters is the fact that they invert the voltage. Ćuk converters solve both of these problems by using an extra capacitor and inductor. However, both Ćuk and buck-boost converter operation cause large amounts of electrical stress on the components, this can result in device failure or overheat. SEPIC converter solves both of these problems. For this reason, a SEPIC converter will be used to evaluate different non-linear control techniques to estimate the maximum power point and to control the output signal of the DC/DC converter.

The SEPIC converter shown in [Figure 2.4](#) uses two inductors,  $L_1$  and  $L_2$ . These two inductors can be on the same core if it is applied the same voltage through switching cycles. Using this type of inductors can reduce the space used on a PCB (Print Circuit Board) and tends to have a lower cost than two separate inductors. The  $C_1$  capacitor isolates the input from the output and provides protection against short in the load. [Figure 2.5](#) shows the current flow for switching cycles.

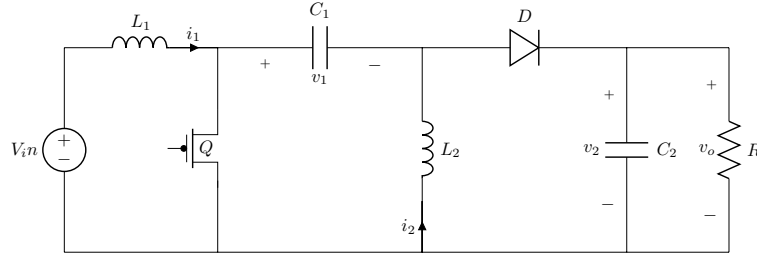
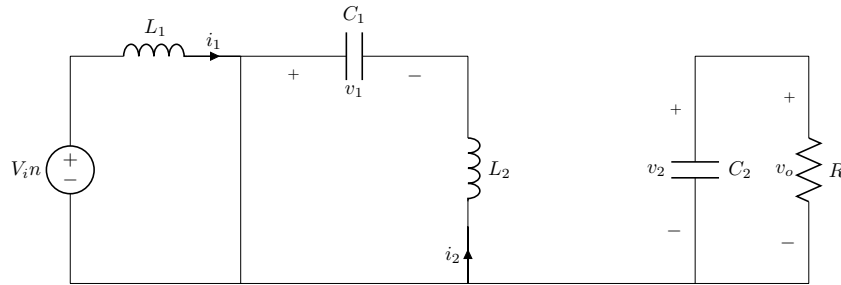
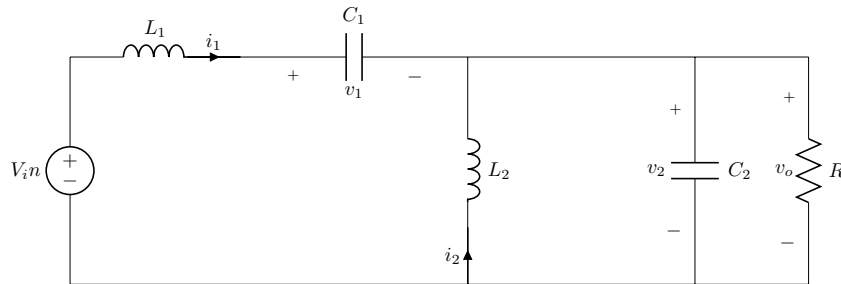


Figure 2.4 : SEPIC Topology

When  $Q$  turns ON, the energy is stored in the inductor  $L_1$ . At this time, the inductor voltage equals to input voltage, and the energy stored in capacitor  $C_1$  will be transferred to inductor  $L_2$ . The load is supplied by capacitor  $C_2$ . When  $Q$  turns OFF, the energy stored in inductor  $L_1$  is transferred to  $C_1$ . The energy stored in  $L_2$  is transferred to  $C_2$  through  $D$  and supplying the energy to load. The equivalent circuits during ON and OFF states are shown in [Figure 2.5](#).



(a) SEPIC - On State



(b) SEPIC - Off State

Figure 2.5 : SEPIC Stages



### 2.2.1 SEPIC Design

As discussed in the [Section 2.1.3](#), the operation mode in which a DC/DC converter works is very important. CCM is selected because the current of the inductors will flow through the DC/DC converter is always positive and greater than zero.

Based on the objectives of this work, the system must have the following characteristics:

Table 2.6 : System requirements

Parameter		Value	Units
Output Power	$P_o$	4 - 6.8	W
Input Voltage	$V_{in}$	0 - 7.962	V
Output Voltage	$V_o$	0-12	V
Output Current	$I_o$	0-570	mA
Output Ripple Voltage	$V_{rip}$	3	%

### Duty Cycle Consideration

For a SEPIC converter operating in a CCM, the duty cycle is given by:

$$D = \frac{V_{OUT} + V_D}{V_{IN} + V_{OUT} + V_D} \quad (2.6)$$

Taking into account the losses caused by the diode in the circuit( $V_D$ , the forward voltage drop), the maximum duty cycle is determined by:

$$D_{max} = \frac{V_{OUT} + V_D}{V_{IN_{min}} + V_{OUT} + V_D} \quad (2.7)$$

Assume that  $V_D = 0.5V$ ,  $V_{IN_{min}} = 4V$ , and  $V_{OUT} = 12V$  as shown in [Table 2.6](#).

$$D_{max} = \frac{V_{OUT} + V_D}{V_{IN_{min}} + V_{OUT} + V_D}$$

$$D_{max} = \frac{12 + 0.5}{4 + 12 + 0.5} = 0.757$$

$$D_{min} = \frac{V_{OUT}V_D}{V_{IN_{max}} + V_{OUT} + V_D}$$

$$D_{min} = \frac{12 + 0.5}{7.2 + 12 + 0.5} = 0.634$$

### Inductor Selection

Usually based on the operation of power converters, the industry it has used in electronic systems near 40% ripple current [27]. Considering this statement as a starting point and taking into account that current flows through inductors with the same value for both, the change of the current in them is determined by:

$$\Delta I_L = I_{IN} \times 40\% = I_{OUT} \times \frac{V_{OUT}}{V_{IN_{min}}} \times 40\% \quad (2.8)$$

The inductor value can be calculated by [27]:

$$L_1 = L_2 = L = \frac{V_{IN_{min}}}{\Delta I_L \times F_{sw}} \times D_{max} \quad (2.9)$$

$F_{sw}$  is the switching frequency and  $D_{max}$  is the duty cycle at the minimum  $V_{in}$ . The peak current in the inductor, to ensure the inductor does not saturate, is given by:

$$I_{L1_{peak}} = I_{OUT} \times \frac{V_{OUT} + V_D}{V_{IN_{min}}} \times \left(1 + \frac{40\%}{2}\right) \quad (2.10)$$

$$I_{L2_{peak}} = I_{OUT} \times \left(1 + \frac{40\%}{2}\right)$$

The input inductor  $L_1$  ripple current is:

$$\Delta I_L = I_{OUT} \times \frac{V_{OUT}}{V_{IN_{min}}} \times 40\% \quad (2.11)$$

$$\Delta I_L = 0.570 \times \frac{12}{4} \times 40\%$$

$$\Delta I_L = 687.82mA$$

And the inductance for  $L_1$  and  $L_2$  is:

$$L_1 = L_2 = L = \frac{V_{IN_{min}}}{\Delta I_L \times F_{sw}} \times D_{max} \quad (2.12)$$

$$L_1 = L_2 = L = \frac{4}{0.68782 \times 100000} \times 0.757 = 44.056\mu H$$

The peak inductor current is:

$$I_{L1_{peak}} = I_{OUT} \times \frac{V_{OUT} + V_D}{V_{IN_{min}}} \times \left(1 + \frac{40\%}{2}\right) \quad (2.13)$$

$$I_{L1_{peak}} = 0.570 \times \frac{12 + 0.5}{4} \times \left(1 + \frac{40\%}{2}\right) = 2149mA$$

$$I_{L2_{peak}} = I_{OUT} \times \left(1 + \frac{40\%}{2}\right) \quad (2.14)$$

$$I_{L2_{peak}} = 0.570 \times \left(1 + \frac{40\%}{2}\right) = 687.82mA$$

### Coupling Capacitor Selection

The selection of coupling capacitor,  $C_1$ , depends on the RMS current, which is given by:

$$I_{C1_{rms}} = I_{OUT} \times \sqrt{\frac{V_{OUT} + V_o}{V_{IN_{min}}}} \quad (2.15)$$

The coupling capacitor must be rated for a large *RMS* current relative to the output power. This property makes the SEPIC much better suited to lower power applications where the *RMS* current through the capacitor is relatively small (relative to capacitor technology). The voltage rating of it must be greater than the maximum input voltage. Electrolytic capacitors work well for through-hole applications, where the size is not limited and they can accommodate the required RMS current rating. The peak-to-peak ripple voltage on  $C_s$  is:

$$\Delta V_{C_1} = \frac{I_{OUT} \times D_{max}}{C_s \times F_{sw}} \quad (2.16)$$

A capacitor that meets the *RMS* current requirement would mostly produce small ripple voltage on  $C_1$ . Hence, the peak voltage is typically close to the input voltage.

The *RMS* current of  $C_1$  is:

$$I_{C_{1rms}} = 0.570 \times \sqrt{\frac{12 + 0.5}{4}} = 1013mA$$

And the ripple voltage is:

$$\Delta V_{C_1} = \frac{0.570 \times 0.757}{10\mu \times 100000}$$

### Output Capacitor Selection

In a SEPIC converter, when the power switch  $Q_1$  is turned on, the inductor is charging and the output current is supplied by the output capacitor. As a result, the output capacitor sees large ripple currents. Thus, the selected output capacitor must be capable of handling the maximum *RMS* current. The *RMS* current in the output capacitor is:

$$I_{C_{outrms}} = I_{OUT} \times \sqrt{\frac{V_{OUT} + V_D}{V_{INmin}}} \quad (2.17)$$

The Equivalent Series Resistance(*ESR*), Equivalent Series Inductance (*ESL*), and the bulk capacitance of the output capacitor directly control the output ripple. Assume half of the ripple is caused by the *ESR* and the other half is caused by the amount of capacitance. Hence,

$$ESR = \frac{V_{ripple} \times 0.5}{I_{L_{1peak}} + I_{L_{2peak}}} \quad (2.18)$$

$$C_{OUT} = \frac{I_{OUT} \times D}{V_{ripple} \times 0.5 \times F_{sw}} \quad (2.19)$$

The *RMS* current of the output capacitor is:

$$I_{C_{outrms}} = I_{C_{srms}} = 1013mA$$

$$ESR = \frac{V_{ripple} \times 0.5}{I_{L_{1peak}} + I_{L_{2peak}}}$$

$$ESR = \frac{0.02 \times 0.5}{2.149 + 0.6878} = 42m\Omega$$

$$C_{OUT} = \frac{I_{OUT} \times D_{max}}{V_{ripple} \times 0.5 \times F_{sw}}$$

$$C_{OUT} = \frac{0.570 \times 0.757}{0.02 \times 0.5 \times 100000} = 36.18\mu F$$

### Input Capacitor Selection

The input current waveform is continuous and triangular due to the SEPIC converter has an inductor at the input. The input capacitor is not much important in a SEPIC application, a  $10\mu f$  or higher value, good quality capacitor would prevent impedance interaction with the input supply [27]. The *RMS* current in the input capacitor is given by:

$$I_{C_{in_{rms}}} = \frac{\Delta I_L}{\sqrt{12}} \quad (2.20)$$

$$I_{C_{in_{rms}}} = \frac{0.6878}{\sqrt{12}} = 198.55mA$$

### SWITCH Selection

There are two switching element in SEPIC. That is diode and MOSFET.

### Power MOSFET Selection

For the selection of a MOSFET transistor must take into account certain parameters that are important such as the minimum threshold voltage  $V_{th_{min}}$ , the on resistance  $R_{DS_{ON}}$ , gate-drain charge  $Q_{GD}$ , and the maximum drain to source voltage,  $V_{DS_{max}}$ .

The peak switch voltage is equal to:

$$V_{Q_{peak}} = V_{in} + V_{OUT} \quad (2.21)$$

The peak switch current is given by:

$$L_{Q_{1_{peak}}} = I_{L1_{peak}} + I_{L2_{peak}} \quad (2.22)$$

The *RMS* current through the switch is given by:

$$L_{Q1_{rms}} = I_{OUT} \times \sqrt{\frac{(V_{OUT} + V_{IN_{min}} + V_D) \times (V_{OUT} + V_D)}{V_{IN_{min}}^2}} \quad (2.23)$$

A good approximation for the MOSFET power dissipation  $P_{Q_1}$  is given by:

$$P_{Q_1} = I_{Q1_{rms}}^2 \times R_{DS_{ON}} \times D_{max} + (V_{IN_{min}} + V_{OUT}) \times I_{Q1_{peak}} \times \frac{Q_{GD} \times F_{sw}}{I_G} \quad (2.24)$$

$P_{Q_1}$  includes conduction loss and switching loss. The  $R_{DS_{ON}}$  value should be selected at maximum operating junction temperature and is typically given in the MOSFET data sheet. Conduction losses plus the switching losses do not exceed the package ratings or exceed the overall thermal budget.

The MOSFET peak current is:

$$L_{Q1_{peak}} = 2.149 + 0.68782 = 2837.27mA$$

And the *RMS* current is:

$$L_{Q1_{rms}} = 0.570 \times \sqrt{\frac{12 + 4 + 0.5}{4^2} \times (12 + 0.5)} = 2057.94mA$$

### Output Diode Selection

The output diode must be selected to handle the peak current and the reverse voltage. In a SEPIC, the diode peak current is the same as the switch peak current  $I_{Q_1}$ . The minimum peak reverse voltage is related with the diode must withstand is:

$$V_{R_D} = V_{IN_{max}} + V_{OUT_{max}} \quad (2.25)$$

The power dissipation of the diode is equal to the output current multiplied by the forward voltage drop of the diode. Schottky diodes are recommended in order to minimize the efficiency loss.

### 2.2.2 Summary of components

Below, [Table 2.7](#) shows the components selected for the system that will be implemented.

Table 2.7 : Summary of components

Component		Value	Units
Input Capacitor	$C_x$	22	$\mu f$
Coupling Capacitor	$C_1$	22	$\mu f$
Output Capacitor	$C_2$	44	$\mu f$
Inductor	$L_1$	47	$\mu H$
Inductor	$L_2$	47	$\mu H$
Diode	$D$	B560C	NA
MOSFET - Transistor	$Q$	csd17556q5b	NA

## Chapter 3

# CONTROL DESIGN TOOLS

### 3.1 Fuzzy Logic Control

The fuzzy logic control (FLC) has been successfully applied to many control problems that the conventional one has difficulties to deal with when the controlled systems are complex, not well defined and/or model-free and can be controlled by a skilled human operator with the knowledge of their underlying dynamics.

Many of the things that humans do every day can be considered as a type of control. Some of these things or daily activities are ride a bike, hit a ball with a bat or kick a ball across a football field. Humans does not has a complex system of control to decide what to do in certain moments and how to control the movements needed to react to unpredictable situations. However humans can become very skilled to perform very complicated tasks [28]. One explanations is that the humans learn through experience, common sense, and coaching to follow an untold number of basic rules of the form "if... then...". Below some examples are presented.

If the bicycle leans to the right, then turn the wheel to the right.

If the light is red, then brake hard.

If the ball is coming fast, then swing the bat soon.

The use of the basic rules in this way is the basic idea behind the fuzzy control. Variables such as fast, slow, long, medium, and small are moved to fuzzy sets. The combination of these fuzzy sets creates mathematical rules that can be describes of the form "If...Then...".



Fuzzy sets trying to model the ambiguity with which a variable is perceived. The fuzzy sets are the basis for fuzzy logic like classical set theory is the basis for Boolean logic.

### 3.1.1 Fuzzy Sets

The classic sets has limitations, and are defined in a system where are completely defined. An element that is contained in a set cannot be part of other one. One thing is true or false, there are not intermediate situations. [Figure 3.1](#) shows the difference between a conventional set and a fuzzy set.

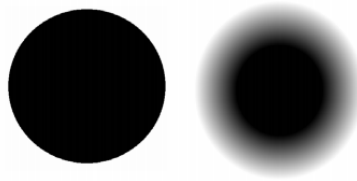


Figure 3.1 : Graphical representation of a conventional set (left) and a fuzzy set (right)

The fuzzy sets are an extension of classic sets, where a membership function is added and defined as a real number between 0 and 1. Each set deduces to add a membership function.

### 3.1.2 Membership Function

The shape of the membership function is chosen arbitrarily by following the advice of the expert or by statistical studies: sigmoid, triangular, Gaussian or any other form can be used. The membership functions represent the membership degree of an element to a subset defined by a label. One membership function indicates the extent to which the variable being evaluated is included in the set according to the taken value, if this membership takes the value of 0 indicates that there is included and if takes the value of 1 indicates that this absolutely included in the set.

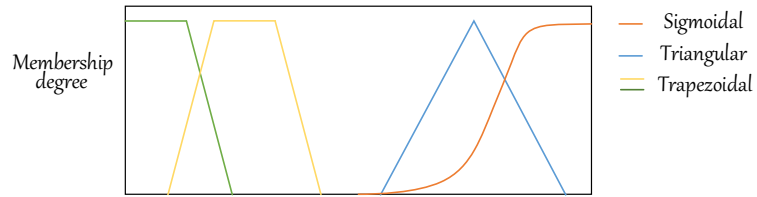


Figure 3.2 : Example of membership function

### 3.1.3 Fuzzification

The fuzzy control process always involves fuzzification, this is done at every instant of time, is the gateway to the fuzzy inference system. It is a mathematical procedure in which an element of the system is converted to a value in each membership function to which it belongs.

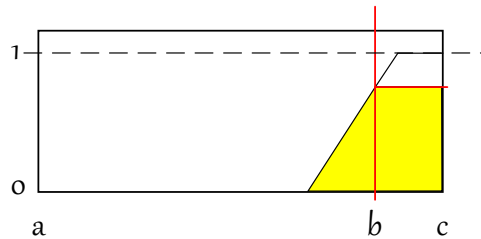


Figure 3.3 : Example of fuzzification of one variable.

There are operators to perform this mathematical process between fuzzy sets. These include complement (NOT), the intersection (AND) and union (OR).

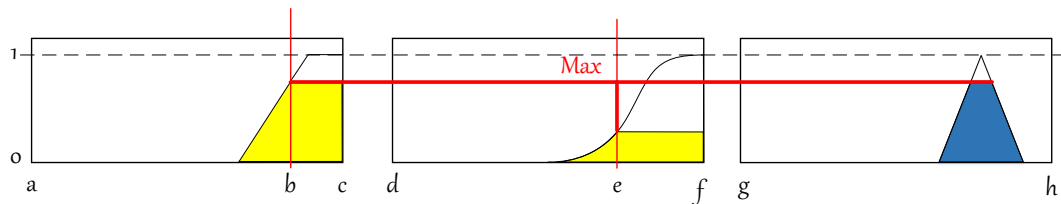


Figure 3.4 : Example of fuzzy implication with conjunction OR translated into a MAX

### 3.1.4 The defuzzification

The defuzzification is a mathematical process used to convert one fuzzy set to real one. The fuzzy inference system gets a conclusion from the input information, but in vague terms, on this fuzzy output or conclusion is obtained by the fuzzy inference stage, a fuzzy set is generated but the generated value should be a real number. Due to this there are different types of defuzzification methods.

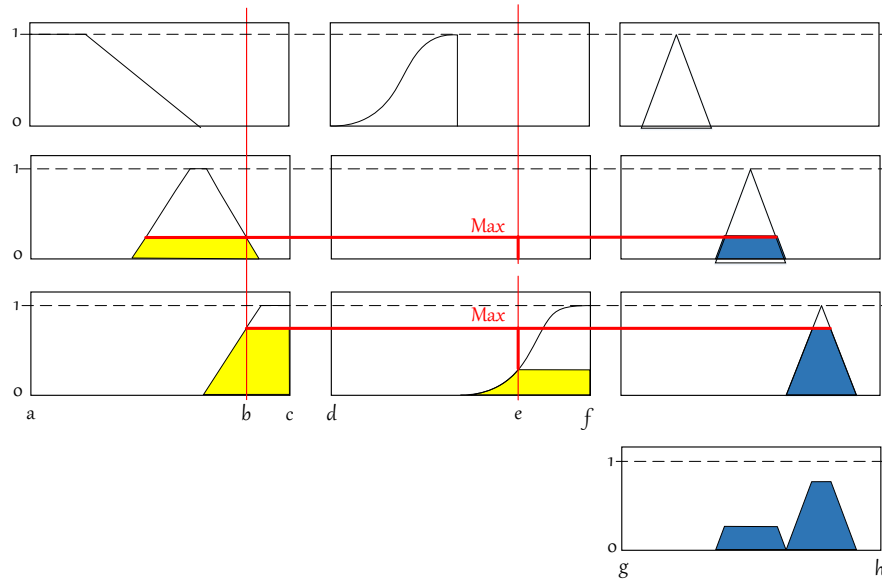


Figure 3.5 : Example of fuzzy implication using some rules

Below a briefly presentation the two main methods of defuzzification. The method of the mean of maxima (MeOM) and the method of center of gravity (COG). The MeOM defuzzification sets the output (decision of the tip amount) as the average of the abscissas of the maxima of the fuzzy set resulting from the aggregation of the implication results. See [Figure 3.6](#).

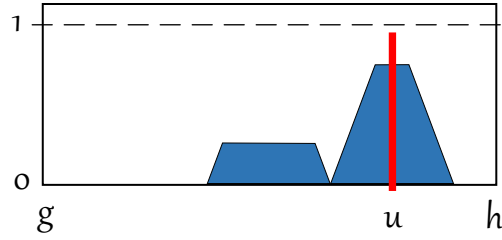


Figure 3.6 : Defuzzification with the method of the mean of maxima (MeOM)

The COG defuzzification is more commonly used. It defines the output as corresponding to the abscissa of the center of gravity of the surface of the membership function characterizing the fuzzy set resulting from the aggregation of the implication results

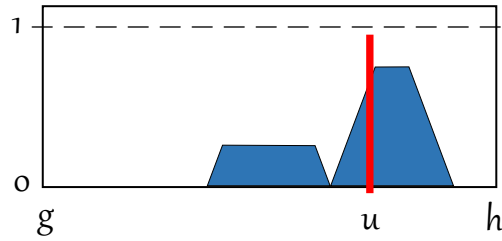


Figure 3.7 : Defuzzification with the method of center of gravity (COG)

The result of the application of a fuzzy rule thus depends on three factors:

1. The definition of fuzzy implication chosen,
2. The definition of the membership function of the fuzzy set of the proposition located at the conclusion of the fuzzy rule.
3. The degree of validity of propositions located premise.

### 3.2 Passivity-Based Control

Suppose a system, in which  $u(t)$  and  $y(t)$  respectively represent its input and output variables, at the same time,  $x(t)$  represents its space variables.

$$\dot{x} = f(x, u) \tag{3.1}$$

$$y = h(x) \quad (3.2)$$

where  $f$  is locally Lipschitz in  $(x, u)$  and  $h$  is continuous in  $x$ , for all  $x \in R^n$  y  $u \in R^m$ . If  $f(0, 0) = 0$  y  $x = 0$  is an open-loop equilibrium point, and  $h(0) = 0$  it said that the system is passive if there exists a continuously differentiable positive semidefinite function  $V(x)$  (called the storage function) such that

$$u^T y \geq \dot{V} = \frac{\partial V}{\partial x} f(x, u), \quad \forall (x, u) \in R^n \times R^m \quad (3.3)$$

Then we can deduce that this system is passive.

$$If \quad u(t) = 0, \quad y(t) = 0 \quad (3.4)$$

And it follows that

$$\lim_{t \rightarrow \infty} x(t) = 0 \quad (3.5)$$

Then this system can be a strictly passive system, and the storage function can also be Lyapunov function. Moreover, the feedback controller can ensure the closed-loop system to be global asymptotic stability at the state zero point, passive with a radially unbounded positive definite storage function and zero-state observable [29]. The feedback controller can be given by:

$$u = -\phi(y) \quad (3.6)$$

where  $\phi$  is any locally Lipschitz function such that  $\phi(0) = 0$  and  $y^T \phi(y) > 0$  for all  $y \neq 0$ .

A passive system has a stable origin. All that is needed to stabilize the origin is the injection of damping so that energy will dissipate whenever  $x(t)$  is not identically zero. The required damping is injected by the function  $\phi$ .

### Example

Consider the system

$$\dot{X}_1 = X_2 \quad (3.7)$$

$$\dot{X}_2 = -X_1^3 + u \quad (3.8)$$

Let  $V(x) = \frac{X_1^4}{4} + \frac{X_2^2}{2}$ , Then

$$\dot{V} = X_1^3 X_2 - X_2 X_1^3 + X_2 u = X_2 u \quad (3.9)$$

Set  $y = x_2$  and note that, with  $u = 0$ ,  $y(t) \equiv 0$  implies that  $x(t) \equiv O$ . Thus, the system is passive with a radially unbounded positive definite storage function and zero-state observable, and a globally stabilizing state feedback control can be taken as  $u = -kx_2$  or  $u = -(2k/\pi)\tan^{-1}(x_2)$  with any  $k > 0$ , [30].

## **Chapter 4**

# **SYSTEM'S DESIGN & COMPONENTS OVERVIEW**

This Chapter discusses in detail different methods in power management through the modification of the power converter duty ratio. The systems design was done using Matlab<sup>®</sup>. This Chapter describes these methods, whose theory has been explained in [Section 2.1.2](#) and in [Chapter 3](#). These methods are: Maximum Power Point Tracking (MPPT), Input-Voltage Control, and Output-Voltage Control. In addition, a mathematical analysis of the SEPIC converter has been shown in order to demonstrate stability of the converter.

The MPPT was performed using a modification of Perturb and Observe algorithm (P&O). Moreover, two control techniques were implemented for Output-Voltage Control. These controls methods are: Fuzzy Logic control(FLC), and Passivity-Based Control(PBC).

#### 4.1 SEPIC Analysis

##### Operation

The SEPIC converter is a converter in which the output voltage is a function of the duty cycle of the switching device [9]. A basic scheme for a SEPIC converter is shown in Figure 2.4, but the inductors and capacitors have a series resistance ( $R_{SL}, R_{SC}$ ). For this reason, a new scheme for a SEPIC converter in Figure 4.1 is presented. The SEPIC converter is composed of a switch ( $S$ ), a diode ( $D$ ), two inductors ( $L_1$  y  $L_2$ ), two capacitors ( $C_1$  y  $C_2$ ) and a resistive load  $R$ .

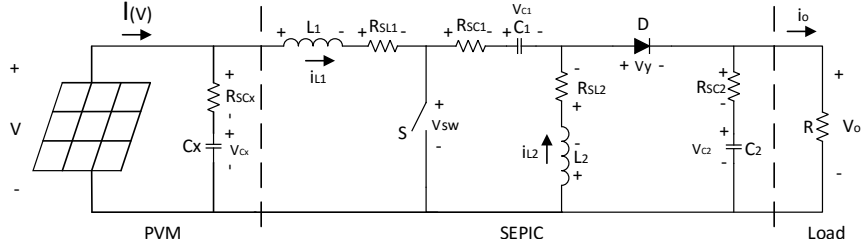


Figure 4.1 : SEPIC converter and PVM configuration

In addition, the SEPIC converter states are as can be seen in Figure 4.2.

The steady state properties and periodicity property say that:

$$V_L = \frac{1}{T} \int_t^{t+T} V_L(\lambda) d\lambda = 0 \quad (4.1)$$

$$I_c = \frac{1}{T} \int_t^{t+T} I_c(\lambda) d\lambda = 0 \quad (4.2)$$

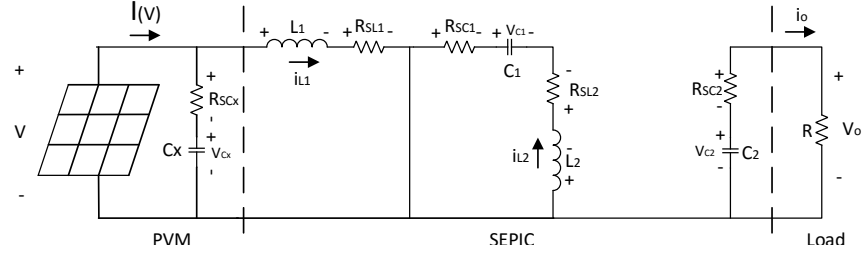
According to this,

$$v_{L1_{on}} = -V_{cx} + i_{L1} * R_{sl1} + V_{sw}$$

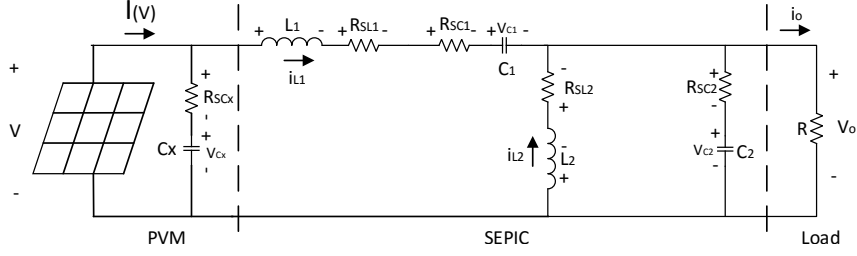
$$v_{L1_{off}} = -V_{cx} + i_{L1} R_{sl1} + i_{L1} R_{sc1} + v_{C1} + V_y + V_o$$

$$V_{L1} = \frac{1}{T} \int_0^{T_{on}} v_{L1_{on}} dt + \frac{1}{T} \int_0^{T_{off}} v_{L1_{off}} dt \quad (4.3)$$





(a) SEPIC - On State



(b) SEPIC -Off State

Figure 4.2 : SEPIC Stages

$$V_{L1} = 0, \frac{T - T_{off}}{T} = S, \text{ and solve for } v_{C1}$$

$$v_{C1} = -\frac{-SV_{sw} + V_{cx} - i_{L1}R_{sl1} - i_{L1}R_{sc1} - V_y - V_o + Si_{L1}R_{sc1} + SV_y + SV_o}{S - 1} \quad (4.4)$$

$$S \neq 1$$

On the other hand,

$$v_{L2on} = -V_{sw} - i_{L2} * R_{sc1} - i_{L2} * R_{sl2} + v_{C1}$$

$$v_{L2off} = -i_{L2} * R_{sl2} - V_y - i_{L2} * R_{sc2} - v_{C2}$$

$$V_{L2} = \frac{1}{T} \int_0^{T_{on}} v_{L2on} dt + \frac{1}{T} \int_0^{T_{off}} v_{L2off} dt \quad (4.5)$$

$$V_{L2} = 0, \text{ and solve for } v_{C1}$$

$$v_{C1} = -\frac{-SV_{sw} - Si_{L2}R_{sc1} - i_{L2}R_{sl2} - V_y - i_{L2}R_{sc2} - v_{C2} + SV_y + Si_{L2}R_{sc2} + Sv_{C2}}{S} \quad (4.6)$$

$$S \neq 0$$

The voltage Equation (4.6) and the voltage Equation (4.4), are set equal to each other to solve for  $V_o$ , this solution will be known as  $V_{out}$ .

$$V_o = \frac{AS^2 + BS + C}{S(S - 1)} \quad (4.7)$$

with

$$\begin{aligned} A &= -i_{l2}R_{SC1} + i_{l2}R_{SC2} + v_{C2} - i_{l1}R_{SC1} \\ B &= V_{sw} + i_{l2}R_{SC1} - i_{l2}R_{SL2} - V_y - 2i_{l2}R_{SC2} - 2v_{C2} - V_{cx} + i_{l1}R_{SL1} + i_{l1}R_{SL1} \\ C &= i_{l2}R_{SL2} + V_y + i_{l2}R_{SC2} + v_{C2} \end{aligned} \quad (4.8)$$

Based on Figure 4.2 SEPIC converter can be modeled by the following equations of state space:

$$\begin{aligned} \dot{i}_1 &= \frac{-(1-S)(v_{C1}+V_o)}{L_1} + \frac{V-i_{L1}R_{SL1}}{L_1} + \frac{(SV_{sw})}{L_1} \\ \dot{i}_2 &= \frac{-i_{L2}R_{SL2}}{L_2} + \frac{S(v_{C1}-V_{sw}-i_{L2}R_{SC1})}{L_2} + \frac{(1-S)(-v_{C2}-V_y-i_{L2}R_{SC2})}{L_2} \\ \dot{v}_{C1} &= \frac{(1-S)i_{L1}}{C_1} - \frac{Si_{L2}}{C_1} \\ \dot{v}_{C2} &= \frac{(1-S)(i_{L1}+i_{L2})}{C_2} - \frac{V_o}{C_2R} \\ \dot{V} &= \frac{I_x}{C_x} - \frac{I_x}{C_x} \left( \frac{V}{V_x} \right)^{n+q} - \frac{i_{L1}}{C_x} \\ S &\in [0, 1] \\ \lim_{t \rightarrow \infty} (S) &= D \\ D &\in (0, 1) \\ I_{in} &= i_{L1} \\ I_o &= \frac{V_o}{R} \end{aligned} \quad (4.9)$$

$V$  is the PVM voltage. In order to facilitate the calculation and assuming the losses are minimal:

$$R_{SL1} = R_{SL2} = R_{SC1} = R_{SC2} = V_{sw} = V_y = 0$$

thus

$$\begin{aligned}
\dot{i}_{L1} &= \frac{-(v_{C1}+v_{C2})}{L_1} + \frac{V_{cx}}{L_1} + \frac{(v_{C1}+v_{C2})D}{L_1} \\
\dot{i}_{L2} &= \frac{-v_{C2}}{L_2} + \frac{(v_{C1}+v_{C2})D}{L_2} \\
\dot{v}_{C1} &= \frac{i_{L1}}{C_1} - \frac{(i_{L1}+i_{L2})D}{C_1} \\
\dot{v}_{C2} &= \frac{(i_{L1}+i_{L2})}{C_2} - \frac{v_{C2}}{C_2 R} + \frac{(v_{C1}+v_{C2})D}{C_2} \\
\dot{V}_{cx} &= \frac{I_x}{C_x} - \frac{I_x}{C_x} \left( \frac{V_{cx}}{V_x} \right)^{n+q} - \frac{i_{L1}}{C_x} \\
V_o &= \frac{D}{1-D} V_{cx}
\end{aligned} \tag{4.10}$$

$$V = V_{cx}$$

$$V_o = v_{C2}$$

$$I_{in} = i_{L1}$$

$$I_o = \frac{V_{C2}}{R}$$

Where  $v_{C1}$ ,  $v_{C2}$  are the capacitors voltages, and  $i_{L1}$ ,  $i_{L2}$  are the inductors currents [8].  $V_{cx}$  is the PVM voltage.

Each equation has the following form:

$$\dot{x} = h(x, D) = f(x) + g(x)D + e \tag{4.11}$$

### Equilibrium Points

Most physical systems are not linear in nature. However, it is possible for these systems to be considered as linear by the use of approximations [30]. The application of non-linear control techniques allows a better understanding of the physical system and thus better results in the control. For this reason, when modeling the physical system it is necessary to consider its stability and equilibrium points. When the SEPIC converter operates at the equilibrium point, the system described above is analyzed at that point.

$$\dot{i}_{L1} = \dot{i}_{L2} = \dot{v}_{C1} = \dot{v}_{C2} = 0 \tag{4.12}$$

Developing the system of [Equations \(4.10\)](#) and [\(4.12\)](#) the following equilibrium point is obtained:

$$\begin{aligned} i_{L1eq} &= \frac{D^2}{(1-D)^2 R} V_{cx} \\ i_{L2eq} &= \frac{D}{(1-D)R} V_{cx} \end{aligned} \quad (4.13)$$

$$v_{C1eq} = V_{cx}$$

$$v_{C2eq} = \frac{D}{1-D} V_{cx}$$

According to this,

$$\dot{V}_{cx} = \frac{I_x}{C_x} - \frac{I_x}{C_x} \left( \frac{V_{cx}}{V_x} \right)^{n+q} - \frac{V_{cx} D^2}{(D-1)^2 R C_x} \quad (4.14)$$

In steady state  $\dot{V}_{cx} = 0$ , and to solve for  $D$  where  $D$  is a duty cycle of the system during steady state.

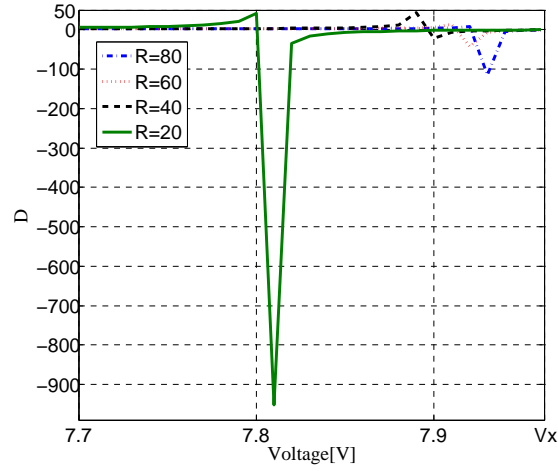
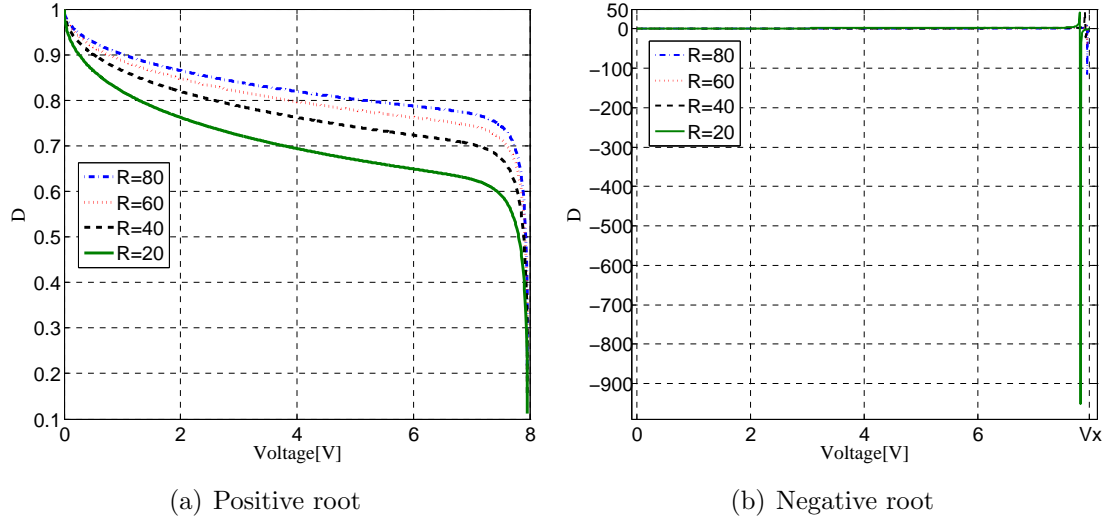
$$D = \frac{-I_x R + I_x R \left( \frac{V_{cx}}{V_x} \right)^{n+q} \pm \sqrt{V_{cx} I_x R - V_{cx} I_x R \left( \frac{V_{cx}}{V_x} \right)^{n+q}}}{-I_x R + I_x R \left( \frac{V_{cx}}{V_x} \right)^{n+q} + V_{cx}} \quad (4.15)$$

In order to determine which of the roots meets the needs of the system, a sweep is performed through the parameters which vary in the system ( $R$  and  $V_{cx}$ ).

As can be seen, [Figures 4.3 \(b\)](#) and [4.3 \(c\)](#) shown that the answer composed of the negative root has values for  $D$  that not are adequate for the system. On the other hand, the answer composed of the positive root, [Figure 4.3 \(a\)](#), has adequate values for the PWM signal.

Thus,

$$D_{eq} = \frac{-I_x R + I_x R \left( \frac{V_{cx}}{V_x} \right)^{n+q} + \sqrt{V_{cx} I_x R - V_{cx} I_x R \left( \frac{V_{cx}}{V_x} \right)^{n+q}}}{-I_x R + I_x R \left( \frac{V_{cx}}{V_x} \right)^{n+q} + V_{cx}} \quad (4.16)$$



(c) Zoom in Figure 4.3 (b) range [7.8-8]

Figure 4.3 : Duty cycle regions

### Stability

The system must be analyzed like a linear system linearized around an operating point to determine the stability. According to this, using Equation (4.11) the linear system can be described the following form:

$$\dot{X}_L = AX + BD \quad (4.17)$$

$$B = \left. \frac{\partial h}{\partial D} \right|_{x_{eq}, D_{eq}} \quad (4.18)$$

Where  $x_{eq}$  is the vector of the state variables on equilibrium. Calculating the Jacobian matrix evaluated at this operation point the system can be written as:

$$A = \begin{bmatrix} 0 & 0 & \frac{-(1-D_{eq})}{L_1} & \frac{-(1-D_{eq})}{L_1} & \frac{1}{L_1} \\ 0 & 0 & \frac{D_{eq}}{L_2} & \frac{-(1-D_{eq})}{L_2} & 0 \\ \frac{1-D_{eq}}{C_1} & -\frac{D_{eq}}{C_1} & 0 & 0 & 0 \\ \frac{1-D_{eq}}{C_2} & \frac{1-D_{eq}}{C_2} & 0 & -\frac{1}{C_2 R} & 0 \\ -\frac{1}{C_x} & 0 & 0 & 0 & -\frac{I_x(n+q)}{C_x V_{cx}} \left( \frac{V_{cx}}{V_x} \right)^{n+q} \end{bmatrix}$$

$$B = \begin{bmatrix} \frac{-V_{cx}}{(D_{eq}-1)L_1} \\ \frac{-V_{cx}}{(D_{eq}-1)L_2} \\ \frac{-V_{cx}D_{eq}}{(D_{eq}-1)^2 RC_1} \\ \frac{-V_{cx}D_{eq}}{(D_{eq}-1)^2 RC_2} \\ 0 \end{bmatrix}$$

This system is a linear representation of [Equation \(4.11\)](#). The characteristic polynomial of the system is given by:

$$\det[\lambda I - A] = a_0 \lambda^5 + a_1 \lambda^4 + a_2 \lambda^3 + a_3 \lambda^2 + a_4 \lambda + a_5 \quad (4.19)$$

with

$$\begin{aligned}
a_0 &= 1 \\
a_1 &= k_1 + k_2 V_{cx}^{23.7225} \\
a_2 &= k_3 V_{cx}^{23.7225} + k_4 R + k_5 D_{eq}^2 R - k_6 R D_{eq} \\
a_3 &= k_7 + k_8 D_{eq}^2 - k_9 D_{eq} + k_{10} V_{cx}^{23.7225} D_{eq}^2 R - k_{11} V_{cx}^{23.7225} R D_{eq} + k_{12} V_{cx}^{23.7225} R \\
a_4 &= k_{13} V_{cx}^{23.7225} + k_{14} R + k_{15} D_{eq}^2 R - k_{16} R D_{eq} + k_{17} D_{eq}^2 V_{cx}^{23.7225} - k_{18} D_{eq} V_{cx}^{23.7225} \\
a_5 &= k_{19} D_{eq}^2 + k_{20} R V_{cx}^{23.7225} - k_{21} R D_{eq} V_{cx}^{23.7225} + k_{22} R D_{eq}^2 V_{cx}^{23.7225} + k_{23} D_{eq}^3 R V_{cx}^{23.7225}
\end{aligned} \tag{4.20}$$

Where  $[K_1, \dots, K_{23}]$  are constants that depend of  $C_1, C_2, C_x, L_1, L_2, I_{sc}, V_{oc}, n + q$ , and are positive constants. These values are can be observed in [Table 2.7](#). Furthermore, each of the coefficients depends on the circuit elements and the photovoltaic panel characteristics. Due to that, the value of circuit elements, and the photovoltaic panel characteristics must be positives; the system is analyzed with the purpose to determine the stability. Each coefficient will depend on directly the factor  $D$ . This factor can be a complex value depending on the relation of the input voltage with respect to the open circuit voltage of the photovoltaic panel. This value can destabilize the system. The coefficients that do not depend on  $D$  are  $a_0$  and  $a_1$ . These terms maintain stable with the same sign of the first coefficient of the polynomial characteristic.

## 4.2 Maximum Power Point Tracking - MPPT

When a solar PV module is used in a system, its operating point is decided by the load to which it is connected. Also since solar radiation falling on a PV module varies throughout the day, the operating point of module also changes throughout the day. When a PV system is deployed for practical applications, the  $I - V$  characteristics keeps on changing with insolation and temperature. For example, the operating point of a PV module and a resistive load for 12 noon, 10 am and 8 am will vary from each other, and under all the operating conditions it is desirable to transfer maximum

power from a PV module to the load. In order to receive maximum power, the load must adjust itself accordingly to track the maximum power point. In order to ensure the operation of PV modules for maximum power transfer, a special method called Maximum Power Point Tracking (MPPT) is employed in PV systems. MPPT is not the same as the mechanical tracking (sun tracking) of solar PV modules. In sun tracking method, PV modules are mechanically rotated so the radiation is maximum while in the case of MPPT, electronic circuitry is used to ensure that maximum amount of generated power is transferred to the load.

The maximum power tracking mechanism makes use of an algorithm and an electronic circuitry. The mechanism is based on the principle of impedance matching between load and PV module, which is necessary for maximum power transfer. Generally, MPPT is an adaptation of DC to DC switching voltage regulator. The impedance matching is done by using a DC to DC converter. Using a DC to DC converter the impedance is matched by changing the duty cycle of the switch. Coupling to the load for maximum power transfer may require either provide a higher voltage for higher current.

As mentioned above, there are various methods to calculate the maximum power point. Most of these methods operate on repetitive iterations what takes a time to find this point. The most commonly used is P&O algorithm. See [Figure 4.4](#) . In this method, the voltage is perturbed (changed) and output power is measured for various perturbation stages. Subsequently, the output is compared with the previous values and the voltage is perturbed accordingly to ensure the point of maximum power. Thus, the algorithm must search through the entire voltage range of the panel. According to this, it is possible to improve the search of this point reducing the search region.





### 4.2.1 Linear Reoriented Coordinates Method - LRCM

The LRCM is a method to find the approximate maximum value for a function  $f(x)$ , where  $f'(x) = r(x) = 0$ , which cannot be solved using traditional methods of differential calculus [31, 32]. The Equation (2.2b), is defined as  $P(V) = VI(V)$  and their maximum value is determined by  $P_{max} = V_{op}I_{op}$ , where  $[V_{op}, I_{op}]$  is the knee point. The main idea of the LRCM is to obtain this point. The maximum power is calculated when the derivative of the power, Equation (4.21), is zero. Unfortunately, this is not possible because there is not a symbolic solution of this equation for  $V$ .

$$\frac{\partial P(V)}{\partial V} = \frac{I_x - I_x e^{\left(\frac{V}{bV_x} - \frac{1}{b}\right)}}{1 - e^{\left(\frac{-1}{b}\right)}} - V \frac{I_x e^{\left(\frac{V}{bV_x} - \frac{1}{b}\right)}}{bV_x - bV_x e^{\left(\frac{-1}{b}\right)}} \quad (4.21)$$

Figure 4.6 shows the I-V curve knee point. The I-V curve knee point is the optimal current ( $I_{op}$ ) and the optimal voltage ( $V_{op}$ ) that produces  $P_{max}$ . As explained above the point that this method will be found is only an approximation of the optimal point and that will be used as the lower limit. Using the boundaries of the I-V Curve i.e. initial and final values, a linear current equation,  $I_L(V)$ , of the form Equation (4.22) it can be determined as given in the Equation (4.23). The current Equation (2.1b), and the linear current Equation (4.23), are differentiated and set equal to each other to solve for  $V$ , this solution will be known as  $V_{ap}$  [16].

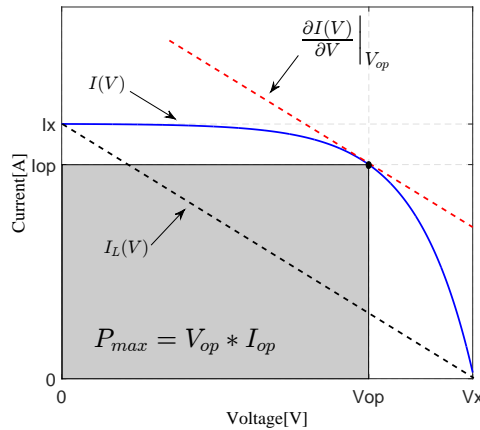


Figure 4.5 : Relation between the I-V curve and the LRCM

$$y = mx + b \quad (4.22)$$

thus

$$I_L(V) = I_x - I_x \frac{V}{V_x} \quad (4.23)$$

The derivatives of  $I(V)$  and  $I_L(V)$  with respect to  $V$  are given by the Equations (4.24) and (4.25).

$$\frac{\partial I(V)}{\partial V} = \frac{-I_x e^{\left(\frac{V}{bV_x} - \frac{1}{b}\right)}}{bV_x - bV_x e^{\left(\frac{-1}{b}\right)}} \quad (4.24)$$

$$\frac{\partial I_L(V)}{\partial V} = -\frac{I_x}{V_x} \quad (4.25)$$

It is important to remember that the slope of the I-V Curve at the knee point is approximated by the slope of the linear current Equation (4.28) hence the solution  $V_{ap}$  is a close approximation of  $V_{op}$  [31, 32].

$$\frac{\partial I(V)}{\partial V} = \frac{\partial I_L(V)}{\partial V} \quad (4.26)$$

$$-\frac{I_x}{V_x} = \frac{-I_x e^{\left(\frac{V}{bV_x} - \frac{1}{b}\right)}}{bV_x - bV_x e^{\left(\frac{-1}{b}\right)}} \quad (4.27)$$

$$V_{ap} = bV_x \ln \left[ be^{\left(\frac{1}{b}\right)} - b \right] \quad (4.28)$$

Now, the equation of the approximate optimal voltage,  $V_{ap}$  is given in the Equation (4.28) [16]. To prove that  $V_{op}$  will be always equal to or greater than  $V_{ap}$  for any given  $b$  more than zero,  $V_{ap}$  is substituted into the Equation (4.21) resulting in the Equation (4.29), where the Equation (4.29) is more than zero for any given  $b$  more than zero.

$$\left. \frac{\partial P(V)}{\partial V} \right|_{V_{ap}} = \frac{I_{sc} \left[ \ln \left( b - be^{\frac{-1}{b}} \right) \left( be^{\frac{-1}{b}} - b \right) + (b+1)e^{\frac{-1}{b}} - b \right]}{1 - e^{\frac{-1}{b}}} \geq 0 \quad (4.29)$$

$$0 < V_{ap} < V_{op} \quad (4.30)$$

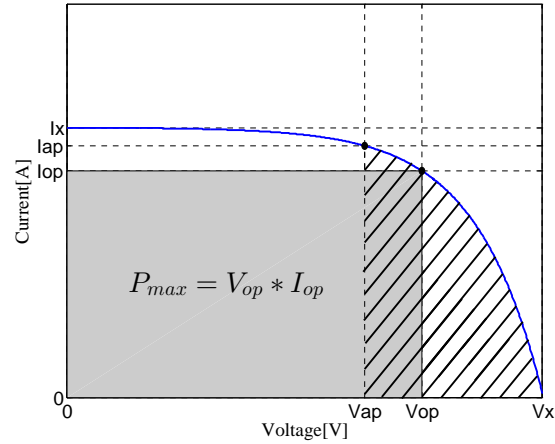


Figure 4.6 : Upper region of the search of the new P&O technique

Thus, the P&O algorithm now has a much smaller range to search for the maximum power that can provide the panel.

#### 4.2.2 Linear Approximation of the I-V curve

The Fill Factor ( $FF$ ) is essentially a measure of the quality of the solar cell. It is calculated by comparing the maximum power to the theoretical power ( $P_T$ ) that would be output at both the open circuit voltage and short circuit current together.  $FF$  can also be interpreted graphically as the ratio of the rectangular areas depicted in Figure 4.7 .

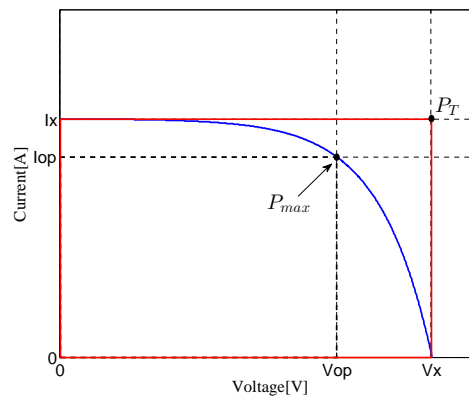


Figure 4.7 : Getting the Fill Factor From the I-V Sweep

$$FF = \frac{P_{max}}{P_T} = \frac{I_{op}V_{op}}{I_xV_x}$$

A larger fill factor is desirable, and corresponds to an I-V sweep that is more square-like. Typical fill factors range from 0.5 to 0.82 [33]. Fill factor is also often represented as a percentage.

During operation, the efficiency of solar cells is reduced by the dissipation of power across internal resistances. These parasitic resistances can be modeled as a parallel shunt resistance ( $R_{SH}$ ) and series resistance ( $R_S$ ), as depicted in Figure 4.8 .

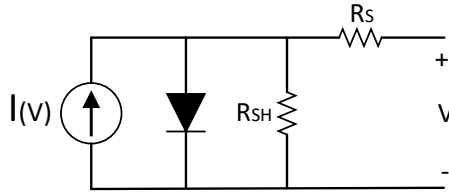


Figure 4.8 : Simplified Equivalent Circuit Model for a Photovoltaic Cell

For an ideal cell,  $R_{SH}$  would be infinite and would not provide an alternate path for current to flow, while  $R_S$  would be zero, resulting in no further voltage drop before the load. It is possible to approximate the series and shunt resistances,  $R_S$  and  $R_{SH}$ , from the slopes of the I-V curve at  $V_{oc}$  and  $I_{sc}$ , respectively. The resistance at  $V_{oc}$ , however, is at best proportional to the series resistance but it is larger than the series resistance.  $R_{SH}$  is represented by the slope at  $I_{sc}$ .

Thus, if the efficiency of the solar array is not 100%, the power delivered is not the total power. Moreover, if the current of the solar panel is described by two linear currents, as can be seen in Figure 4.9 , the power delivered by this current is also less than the  $P_T$ . If these two currents are equal a common point of voltage is found. This voltage always it will be less than the  $V_x$  due to the slope of the linear currents. Furthermore, due to the efficiency of the solar panel this voltage will be between the

$V_{op}$  and the  $V_x$ . According to this, the range of search for the P&O algorithm would be reduced.

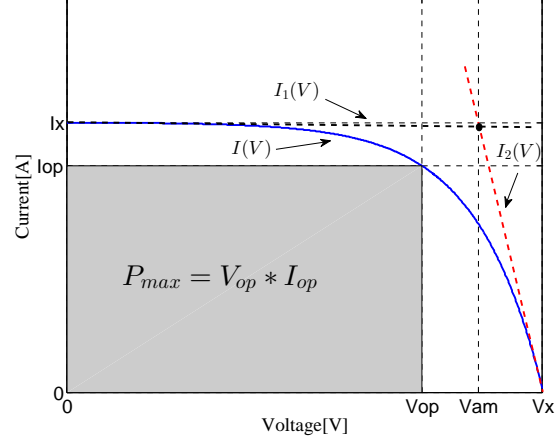


Figure 4.9 : Linear approximation of the I-V Curve

$$I(V) = \begin{cases} I_1(V), & 0 \leq V \leq V_{op} \\ I_2(V), & V_{op} \leq V \leq V_x \end{cases} \quad (4.31)$$

As mentioned above, the linear approximation of the current of the solar panel is done with two currents. Each linear current is described by:

$$y = mx + b$$

$$y_1 = m_1 V + b_1 \quad y_2 = m_2 V + b_2$$

$$I_1(V) = m_1 V + b_1 \quad I_2(V) = m_2 V + b_2$$

$$b_1 = I_1(V) - m_1 V|_{V=0} \quad b_2 = I_2(V) - m_2 V|_{V=V_x}$$

$$b_1 = I_x \quad b_2 = -m_2 V_x$$

$$m_1 = \left. \frac{\partial I(V)}{\partial V} \right|_{V=0} \quad m_2 = \left. \frac{\partial I(V)}{\partial V} \right|_{V=V_x}$$

$$I_1(V) = V \left. \frac{\partial I(V)}{\partial V} \right|_{V=0} + I_x \quad (4.32)$$

$$I_2(V) = (V - V_x) \left. \frac{\partial I(V)}{\partial V} \right|_{V=V_x} \quad (4.33)$$

$$I(V) = \begin{cases} V \left. \frac{\partial I(V)}{\partial V} \right|_{V=0} + I_x, & 0 \leq V \leq V_{am} \\ (V - V_x) \left. \frac{\partial I(V)}{\partial V} \right|_{V=V_x}, & V_{am} \leq V \leq V_x \end{cases} \quad (4.34)$$

The current Equation (4.32) and the current Equation (4.33) are set equal to each other to solve for V, this solution will be known as  $V_{am}$ .

$$\begin{aligned} V \left. \frac{\partial I(V)}{\partial V} \right|_{V=0} + I_x &= (V - V_x) \left. \frac{\partial I(V)}{\partial V} \right|_{V=V_x} \\ V_{am} &= \frac{V_x \left( 1 - b + be^{\left(\frac{-1}{b}\right)} \right)}{1 - e^{\left(\frac{-1}{b}\right)}} \end{aligned} \quad (4.35)$$

Now, the equation of the approximate optimal voltage,  $V_{am}$  is given in the Equation (4.35). To prove that  $V_{op}$  will be always equal to or less than  $V_{am}$  for any given  $b$  more than zero,  $V_{am}$  is substituted into the Equation (4.21) resulting in the Equation (4.36), where the Equation (4.36) is less than zero for any given  $b$  more than zero.

$$\left. \frac{\partial P(V)}{\partial V} \right|_{V_{am}} = - \frac{I_{sc} \left( -b + be^{\frac{-1}{b}} + e^{1 + \frac{e^{\frac{-1}{b}}}{(-1 + e^{\frac{-1}{b}})^b}} \right)}{\left( -1 + e^{\frac{-1}{b}} \right)^2 b} \leq 0 \quad (4.36)$$

thus

$$V_{op} < V_{am} < V_x \quad (4.37)$$

According to this the search region for the P&O technique is now reduced to a smaller region to find the optimal voltage and the knee point of the I-V curve. As can be seen in Figure 4.10 the knee point of the I-V sweep is between  $V_{op} < V_{am} < V_x$ . Furthermore, the Figure 4.11 shows the search region in the P-V curve.

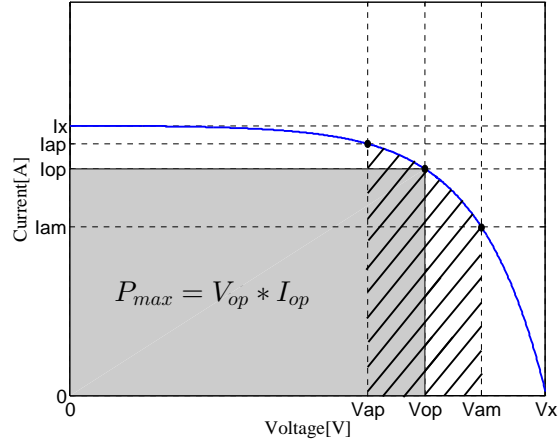


Figure 4.10 : Bounded Region of the I-V Curve

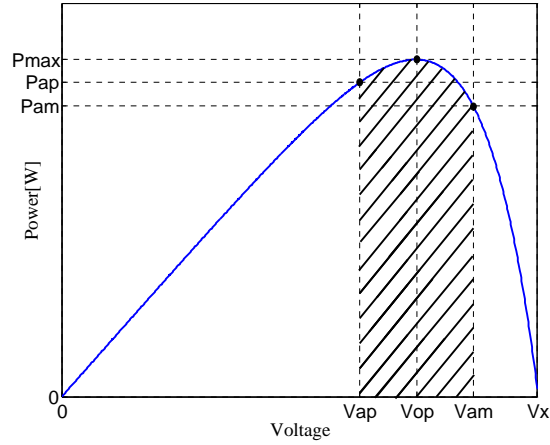
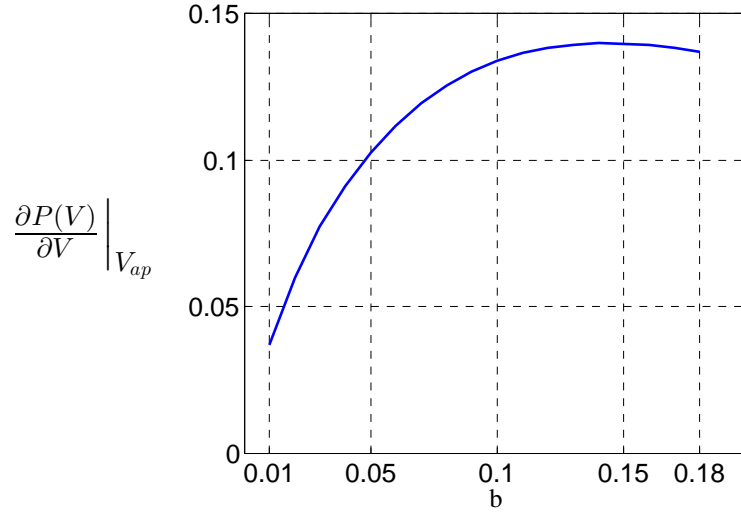


Figure 4.11 : Bounded Region of the P-V Curve

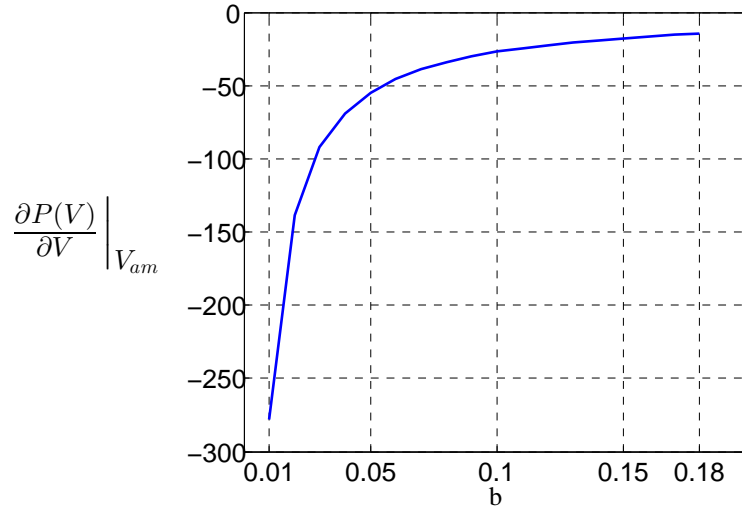
$V_{ap}$  and  $V_{am}$  are two values that are close to the optimum value. In addition, each of these values is on one side of the power curve.  $V_{ap}$  is a point that is on the left of the optimal value, Equation (4.28).  $V_{am}$  is a point that is to the right of the optimal value, Equation (4.35). In order to demonstrate that these two values are always on the left side and the right side of the  $P - V$  curve, the derivative of the power at each point is calculated. Equations (4.29) and (4.36), depend on the characteristic constant for the PVM based on the I-V Curve,  $b$ . Thus, a sweep through the  $b$  is



developed. The characteristic constant for any PVM is positive definite with a typical range for  $b$  from 0.01 to 0.18 [16].



(a) Derivative of  $P$  evaluated in  $V_{ap}$  Equation (4.29)



(b) Derivative of  $P$  evaluated in  $V_{am}$  Equation (4.36)

Figure 4.12 : Derivative of Power for each  $b$

As can be seen, each region of the derivative of power corresponds with the theory. Figure 4.12 (a) shows that the derivative of the power at  $V_{ap}$  always is positive. Additionally, Figure 4.12 (b) shows that the derivative of the power at  $V_{am}$  always is negative. Thus, the search regions for the conventional and modified

P&O algorithm can be described of the following form:

$$P\&O, \quad 0 < V < V_x \quad (4.38)$$

$$P\&O_{Bounded}, \quad 0 < V_{ap} < V < V_{am} < V_x \quad (4.39)$$

### 4.2.3 Existence

Once it has a range in which it is possible to find a solution to achieve the maximum power point it is necessary to demonstrate that the solution exists.

#### Fixed point theorem

A "Fixed Point" of a function is a value that is unchanged by repeating applications of the function [34].

Let  $r$  a fix point,

$$r = g(r)$$

it means a fixed point where  $r$  is a root of  $F(x)$  when  $F(x) = 0$ . The repeating of the function is controlling by:

$$x_{k+1} = g(x_k)$$

After each iteration the error change has the following form:

$$e_k = |x_k - r|$$

and the next step error by definition

$$e_{k+1} = |x_{k+1} - r|$$

$$e_{k+1} = |g(x_k) - g(r)|$$

$$e_{k+1} = |g'(\varrho)(x_k - r)|$$

where  $\varrho$  exist between  $(x_k, r)$

$$|g'(\varrho)(x_k - r)| = |g'(\varrho)|e_k$$

Thus

- if  $|g'(\varrho)| < 1 \Rightarrow e_{k+1} < e_k, \Rightarrow$  *Convergent*
- if  $|g'(\varrho)| > 1 \Rightarrow e_{k+1} > e_k, \Rightarrow$  *Divergent*

and there exists an interval  $I$  around the root  $r$

$$I = [r - a, r + b], \quad \text{for some } a, b > 0$$

Thus, it is found that this solution exists.

### Proof of Existence

let

$$F(x) = \frac{\partial P}{\partial V}$$

such that

$$g(x) = \frac{\partial P}{\partial V} + V$$

Based on the [Equation \(4.21\)](#)

$$\frac{\partial P(V)}{\partial V} = \frac{I_x - I_x e^{\left(\frac{V}{bV_x} - \frac{1}{b}\right)}}{1 - e^{\left(\frac{-1}{b}\right)}} - V \frac{I_x e^{\left(\frac{V}{bV_x} - \frac{1}{b}\right)}}{bV_x - bV_x e^{\left(\frac{-1}{b}\right)}} \quad (4.40)$$

$$g(V) = \frac{I_x - I_x e^{\left(\frac{V}{bV_x} - \frac{1}{b}\right)}}{1 - e^{\left(\frac{-1}{b}\right)}} - V \frac{I_x e^{\left(\frac{V}{bV_x} - \frac{1}{b}\right)}}{bV_x - bV_x e^{\left(\frac{-1}{b}\right)}} + V \quad (4.41)$$

Thus

$$g'(V) = \frac{2bI_x V_x e^{\left(\frac{V-V_x}{bV_x} - \frac{1}{b}\right)} + I_x V e^{\left(\frac{V-V_x}{bV_x} - \frac{1}{b}\right)} - b^2 V_x^2 e^{\left(-\frac{1}{b}\right)}}{b^2 V_x^2 (e^{\frac{-1}{b}} - 1)}$$

thus the  $\max|g(V)|$  must be less than 1. Evaluating term by term,

$$\max \left( 2bI_x V_x e^{\left(\frac{V-V_x}{bV_x} - \frac{1}{b}\right)} \right) = 2bI_x V_x$$

$$\max \left( I_x V e^{\left( \frac{V-V_x}{bV_x} - \frac{-1}{b} \right)} \right) = V_x I_x$$

thus

$$g'(V) = \frac{2bI_x V_x + I_x V_x - b^2 V_x^2 e^{\left( -\frac{1}{b} \right)}}{b^2 V_x^2 \left( e^{\frac{-1}{b}} - 1 \right)}$$

and the maximum value of  $g(V)$  is determined by

$$\max |g(V)| = \lim_{b \rightarrow \infty} |g'(V)|$$

according to this

$$\max |g(V)| = \frac{V_x - 2I_x}{V_x}$$

As can be seen, for all values of  $V_x$  and  $I_x$   $|g'(V)|$  always is less than 1. This demonstrate that the solution of the differential [Equation \(4.21\)](#) exists. Moreover, this solution exists and is on an interval described by

$$I = [V_{ap}, V_{am}]$$

### 4.3 Output Voltage Control

As mentioned above, the batteries are some of the systems that can be used as a final load for DC/DC converters. Moreover, many of these systems used require fixed input signal to work that is not imposed by the system, for this reason, controlling the output signal is one of the most important factors in the development and control of the DC/DC converters.

#### 4.3.1 Fuzzy Logic Control

As mentioned above Fuzzy logic is a way of interfacing analog processes that move through a continuous range of values, to a digital computer, that seems to be well defined discrete numeric values. The fuzzy logic controller can be divided into four part: fuzzification, knowledge base (it includes fuzzy rule base and database), decision making, and defuzzification, where is carry out the conversion from the inferred fuzzy value to real control crisp value [2, 35].

In the design of a fuzzy controller, it must first identify the main control variables and determine a term set, which is at a suitable level for describing the values of each linguistic variable. In FL based feedback controller, the error between the output voltage and reference voltage, and change of error are inputs of FLC [36].

$$V_{error} = V_{ref} - V_{out} \quad (4.42)$$

$$V_{error\_change} = V_{error}(k) - V_{error}(k - 1) \quad (4.43)$$

In the proposed fuzzy controller, the membership functions of the input variables are with classical triangular shapes which are shown in Figures 4.13 (a) and 4.13 (b), and a five-term fuzzy set, Negative Big (N-II), Negative Small (N-I), Zero (Z), Positive Small (PI), Positive Big (P-II), is defined to describe each linguistic variable. The fuzzy rules for the output system, therefore, can be represented in symmetric form, and are collected in Table 4.1 . Also, as in input signals, the membership

functions of the output variables are with classical triangular shapes and a nine-term fuzzy sets, Negative Very-Big (N4), Negative Big (N3), Negative Small (N2), Negative Very-Small (N1), Zero (Z), Positive Very-Small (P1), Positive Small (P2), Positive Big (P3), Positive Very-Big (P4). The memberships of the output variables in [Figure 4.13 \(c\)](#) can be observed.

The fuzzy method was Mamdani where the maximum of minimum composition technique for the inference was used. Center-of-gravity method was used in the defuzzification process.

Table 4.1 : Fuzzy Logic Controller rules

	NII	NI	Z	PI	PII
NII	$P_4$	$P_4$	$P_3$	$P_2$	$Z$
NI	$P_4$	$P_3$	$P_4$	$Z$	$N_2$
Z	$P_3$	$P_4$	$Z$	$N_4$	$N_3$
PI	$P_2$	$Z$	$N_4$	$N_3$	$N_4$
PII	$Z$	$N_2$	$N_3$	$N_4$	$N_4$

The control signal is a little change of the duty cycle  $u(k)$ , because a big change of the duty cycle could cause spikes in the output voltage. Besides PWM control is used to regulate the output voltage. The actual control command  $u(k)$  which is used to control the duty ratio of the switching pulse is calculated by:

$$u(k) = u(k-1) + \Delta u(k) \quad (4.44)$$

The error  $e$  and difference of error  $\Delta e$  are defined as:

$$e(k) = V_{ref}(k) - V_o(k) \quad (4.45)$$

$$\Delta e(k) = e(k) - e(k-1) \quad (4.46)$$

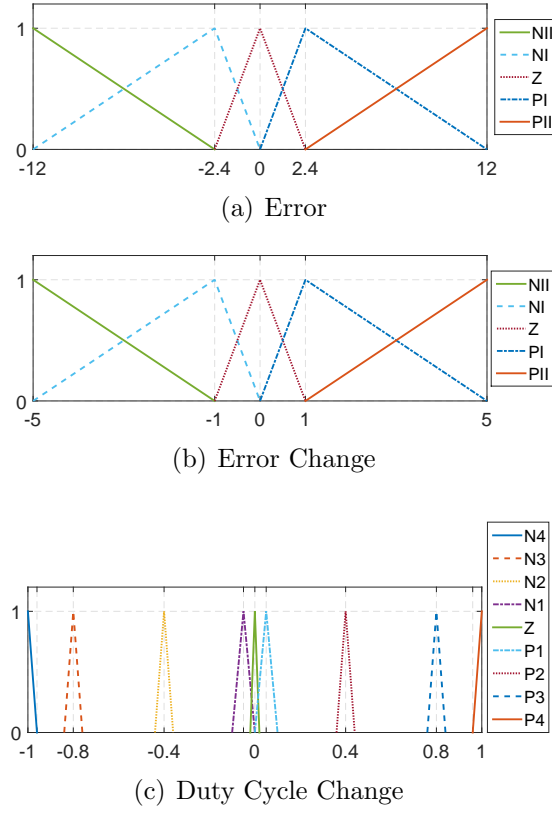


Figure 4.13 : Fuzzy Membership Function Inputs and Output

The block diagram of the FLC for DC/DC converters is shown in Figure 4.14

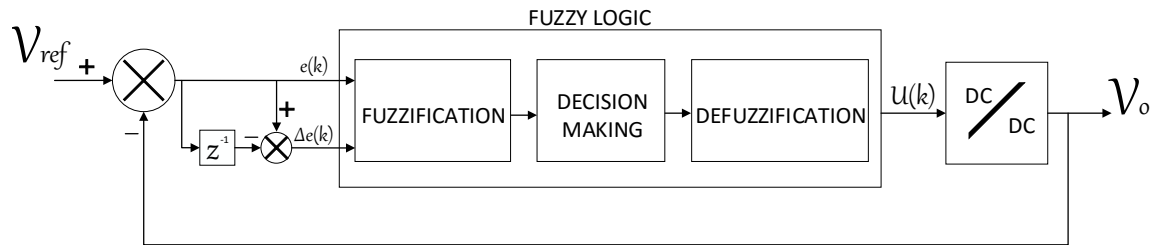


Figure 4.14 : Block diagram of the FLC for DC/DC converters [2]

The range of input variables was defined based on a limit, establishing the maximum difference between the output signal and the reference value would be the maximum output voltage for the system will be implemented.

### 4.3.2 Passivity-Based Control

Suppose a system, in which  $u(t)$  and  $y(t)$  respectively represents its input and output variables, at the same time,  $x(t)$  represents its space variables. Consider positive semidefinite storage function  $V(t)$  and positive definite function  $Q(x)$ , and they are all continuous differentiable [29,37]. If they can satisfy as follows:

$$\dot{V}(x) \leq y^T u - Q(x), \quad \forall (x, u) \in R^m \times R^n \quad (4.47)$$

### Lyapunov Analysis

Then, If the system is a strictly passive system, the storage function can be Lyapunov function. Moreover, the feedback controller can ensure the closed-loop system to be global asymptotic stability at the state zero point, passive with a radially unbounded positive definite storage function and zero-state observable [29]. The feedback controller can be given by:

$$u_p = -\phi(y) \quad (4.48)$$

Thus, a Lyapunov stability analysis with a non-linear input will be analyzed. This input is provided by a photovoltaic panel. The system described above is continuously differentiable at each point. Therefore, we can state that the system is at least locally Lipschitz [38]. With the system described in the Equation (4.10) and the energy function for this circuit like a candidate to Lyapunov stability analysis,



this Lyapunov function is radially unbounded and this allows to realize the analysis.

$$V(e) = \frac{1}{2} (L_1 e_1^2 + L_2 e_2^2 + C_1 e_3^2 + C_2 e_4^2 + C_x e_5^2) \quad (4.49)$$

$$\dot{V}(e) = L_1 e_1 \dot{e}_1 + L_2 e_2 \dot{e}_2 + C_1 e_3 \dot{e}_3 + C_2 e_4 \dot{e}_4 + C_x e_5 \dot{e}_5$$

where,

$$\begin{aligned} e_1 &= i_{L1} - i_{L1eq} & \dot{e}_1 &= \dot{i}_{L1} \\ e_2 &= i_{L2} - i_{L2eq} & \dot{e}_2 &= \dot{i}_{L2} \\ e_3 &= v_{C1} - v_{C1eq} & \dot{e}_3 &= \dot{v}_{C1} \\ e_4 &= v_{C2} - v_{C2eq} & \dot{e}_4 &= \dot{v}_{C2} \\ e_5 &= V_{cx} - V_{cxeq} & \dot{e}_5 &= \dot{V}_{cx} \\ u_e &= D - D_{eq} \end{aligned} \quad (4.50)$$

With  $u_e = 0$  and solving to stay on equilibrium:

$$\frac{-e_4^2 + e_5 I_x R \left( \left( \frac{V_{cx}}{V_x} \right)^{n+q} - \left( \frac{e_5 + V_{cx}}{V_x} \right)^{n+q} \right)}{R} \leq 0 \quad (4.51)$$

The terms present in the [Equation \(4.51\)](#) must be negative to preserve stability on the system. The first term is less than zero, therefore:

$$-\frac{e_4^2}{R} \leq 0 \quad (4.52)$$

to the other term:

$$e_5 I_x \left( \left( \frac{V_{cx}}{V_x} \right)^{n+q} - \left( \frac{e_5 + V_{cx}}{V_x} \right)^{n+q} \right) \leq 0 \quad (4.53)$$

That means that  $e_5$  must be greater or equal to zero for this inequality to be fulfilled and ensure stability [15].

To analyze the system, and to ensure the asymptotically stability, the [Equation \(4.54\)](#) can be used.

$$V(e) = \frac{1}{2} (L_1 e_1^2 + L_2 e_2^2 + C_1 e_3^2 + C_2 e_4^2 + C_x e_5^2) \quad (4.54)$$

$$\dot{V}(e) = L_1 e_1 \dot{e}_1 + L_2 e_2 \dot{e}_2 + C_1 e_3 \dot{e}_3 + C_2 e_4 \dot{e}_4 + C_x e_5 \dot{e}_5$$

with  $u_e \neq 0$ , then

$$\dot{V}(e) = \frac{1}{R} (-e_4^2 + J_1 u_e (e_1 + e_2) + J_2 u_e (e_3 + e_4)) \leq 0 \quad (4.55)$$

with

$$\begin{aligned} J_1 &= R \left( V_{cx} + \sqrt{-I_x R V_{cx} \left( -1 + \left( \frac{V_{cx}}{V_x} \right)^{n+q} \right)} \right) \\ J_2 &= - \left( I_x R + \sqrt{-I_x R V_{cx} \left( -1 + \left( \frac{V_{cx}}{V_x} \right)^{n+q} \right)} - I_x R \left( \frac{V_{cx}}{V_x} \right)^{n+q} \right) \end{aligned} \quad (4.56)$$

The passivity based control requires being in a passive state, thus to employ this technique it is necessary to fulfill this requirement. Based on the above Lyapunov analysis the terms that are not always negative must be analyzed such that the system can be controlled. With  $u_e$  This terms must be taken as control law to take them to a state of passivity that allows the system to be controlled [30]. According to the Lyapunov analysis it chooses an output function:

$$y = \frac{1}{R} (J_1 (e_1 + e_2) + J_2 (e_3 + e_4)) \quad (4.57)$$

With this, the system is passive because  $\dot{V}(e) \leq y^T u$  and asymptotically stable around the equilibrium point defined by the error system and is asymptotically stable with the control input

$$u_p = -k \left( \frac{1}{R} (J_1 (e_1 + e_2) + J_2 (e_3 + e_4)) \right) \quad (4.58)$$

where  $G$  is a positive constant. It is interesting to see that the control signal  $u$  is established from the power variations between inductors and capacitors. The duty cycle control signal is now can be calculated from the real states as following:

$$u = u_p + D_{eq} \quad (4.59)$$

Thus, the system is stable around the equilibrium point defined by  $V_{cx}$  and will be globally asymptotically stable.

## **Chapter 5**

# **ANALYSIS OF SIMULATION & EXPERIMENTAL RESULTS**

This Chapter describes the procedure and partial results after validate the implementation of four proposed control schemes. The target hardware designed for this objective was a PCB Evaluation Platform. Initially, the open loop performance was evaluated in order to validate the PCB Evaluation Platform.

The control schemes first went through a high level of verification. At this point, a Matlab-Simulink program served to validate the strategy by implementing the same block diagram that would then be applied to the hardware version. Schematic diagrams, circuits, and algorithms developed are detailed for each of the methods. To do this the architectures are presented in each Section.

## 5.1 Photovoltaic Module System

Based on a real case study that could use each of the systems to be implemented, a case of a 3U Cubesat nano-satellite is analyzed. This scenario is composed of two strings with three solar cells in series connection, in order to obtain the maximum efficiency for possible cases [39]. The electrical characteristics of the solar cell can be seen in Table 5.1 and the characteristics for the desired scenario are described in Table 5.2 .

Table 5.1 : Triple Junction Solar Cell 5E14 - Azur Space [1]

Parameter	Units	Value
Average Open Circuit $V_{oc}$	[V]	2.654
Average Short Circuit $I_{sc}$	[mA]	514
Voltage at max. Power $V_{mp}$	[V]	2.290
Current at max. Power $I_{mp}$	[mA]	500.6
Efficiency	[%]	28

Table 5.2 : Case Study

Parameter	Units	Value
Average Open Circuit $V_{oc}$	[V]	7.962
Average Short Circuit $I_{sc}$	[A]	1.028
Voltage at max. Power $V_{mp}$	[V]	6.870
Current at max. Power $I_{mp}$	[A]	1.0012
Efficiency	[%]	28

The input solar cell array is emulated with a programmable DC power supply reference E4351B of Agilent according to the described case study. Output load is emulated with a DC Electronic Load model 8500 of BK Precision.

### 5.1.1 Simulation results

As discussed in [Section 2.1.2](#), there exists a relationship between the fractal and exponential PVM model, and one of them can be expressed in terms of the other. Based on the [Equations \(2.4\) and \(2.5\)](#) and the electrical parameters for the desired scenario described in [Table 5.2](#) :

$$n + q = 24.7225$$

$$b = 0.036$$

The simulation of the solar cell was developed using Simulink<sup>®</sup> [40] as shown in [Figure 5.1](#) ; where the PVM has been modeled using the mathematical model described in [Equation \(2.1b\)](#).

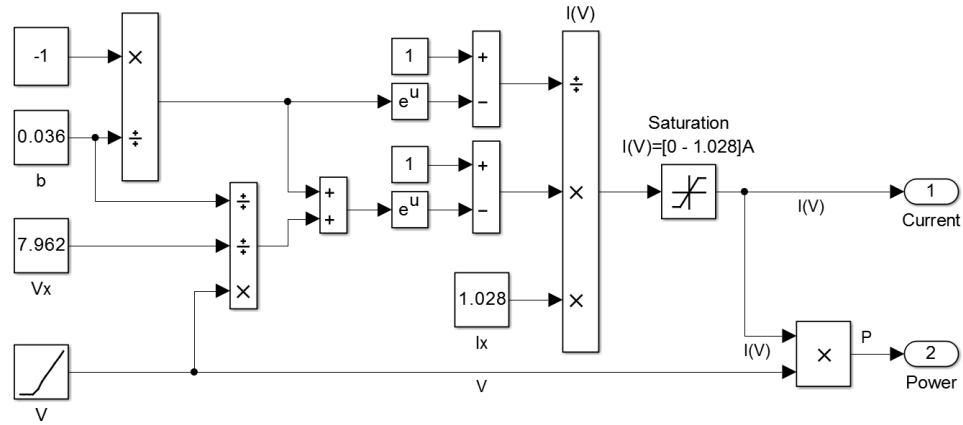


Figure 5.1 : EPVM Model implementation - Simulink<sup>®</sup>

In [Figure 5.2 \(a\)](#) is shown the response of the PV array current for different load values. The PV array response in terms of power in [Figure 5.2 \(b\)](#) can be observed.

Table 5.3 : Case Study - Matlab Simulation

	$V_{oc}(V)$	$I_{sc}(A)$	$V_{op}(V)$	$I_{op}(A)$	$P_{max}(W)$	$b$	$n + q$
Theory	7.962	1.028	6.8782	1.0012	6.870	0.036	24.7225
Simulated	7.962	1.028	7.062	1.003	6.946	0.0343	27.2242

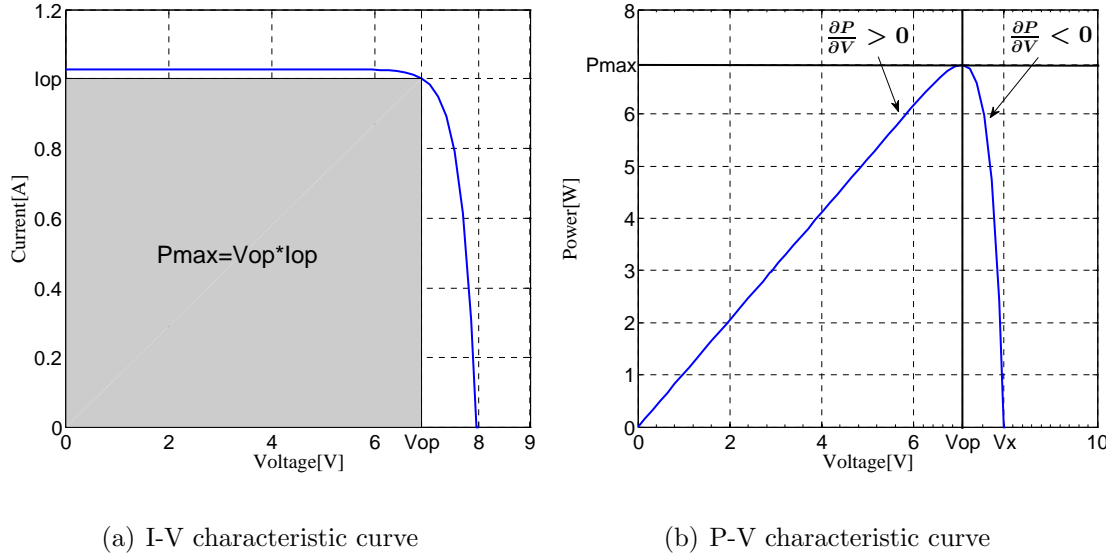


Figure 5.2 : Simulation characteristic curves

As shown in Figure 5.2 the simulation fulfills the parameters set out to recreate the desired scenario that will be used.

### 5.1.2 Experimental results

The experiment consists of a voltage sweep that considers maximum power point given by the solar cell array in Table 5.2 . Figures 5.3 (a) and 5.3 (b) show the comparison between the data obtained from the solar array simulator and the simulation. Exists some differences between real and simulated data, but the fill factor of the solar array simulator and the simulation response is similar.

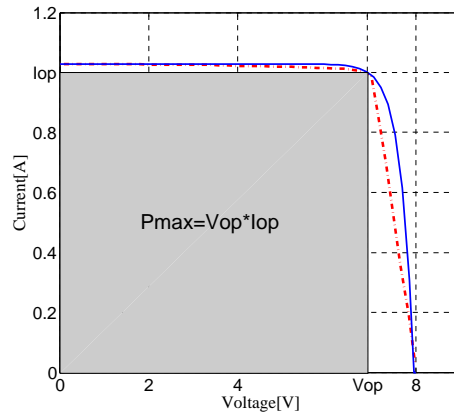
The voltage sweep was conducted with steps of  $0.2V$  in order to have the minimum and enough points to obtain a curve that may describe the behavior of the solar

array simulator. As can be seen in Figure 5.3 the parameters established for the work setting are also met by the solar array simulator.

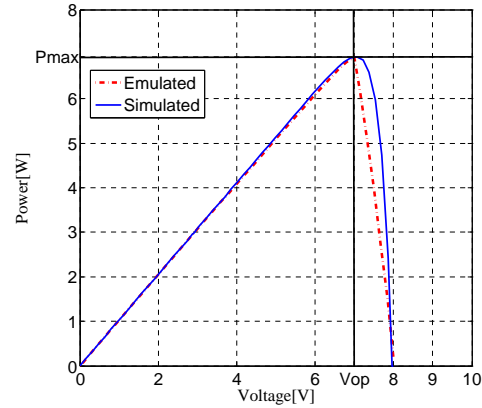
According to the maximum power point as one of the main parameters to compare the performance of the solar array simulator, it can be said that the simulator performance is acceptable to do the tests.

Table 5.4 : Case Study - Solar Array Emulator

	$V_{oc}(V)$	$I_{sc}(A)$	$V_{op}(V)$	$I_{op}(A)$	$P_{max}(W)$	$b$	$n + q$
Theory	7.962	1.028	6.8782	1.0012	6.870	0.036	24.7225
Simulated	7.962	1.028	7.062	1.003	6.946	0.0343	27.2242
Emulated	7.99	1.029	7	0.992	6.944	0.0394	23.7001



(a) IV characteristic curve



(b) PV characteristic curve

Figure 5.3 : Simulation and Experimental characteristic curves

Figure 5.4 show the real solar cell. This cell type is a GaInP/GaAs/Ge on Ge substrate triple junction solar cell (efficiency class 30% advanced).



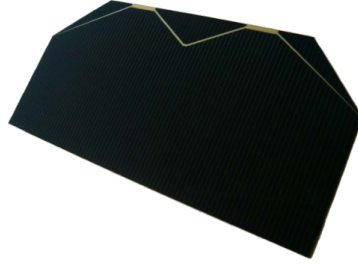


Figure 5.4 : Triple Junction Solar Cell 5E14 - Azur Space [1]

## 5.2 Developed system based on Microcontroller and SEPIC converter

As mentioned above, some controllers depend on the state variables of the system and input and output signals. Thus, these signals must be conditioned in order to be read and operate by the microcontroller. A block diagram of the fully developed system is shown in Figure 5.5 . In addition to the solar array simulator and the load, the system consists of four PCB boards.

Initially, Figures 5.6 (a) and 5.6 (b) show a high-side current sensor and low-side current sensor, respectively. The high-side current sensor board is based on INA168 of Texas Instruments incorporated. This sensor is used to measure currents that are not connected directly to the ground. On the other hand, the low-side current sensor is only used to measure current through the inductor  $L_2$ . The low-side current sensor board is based on INA200 of Texas Instruments incorporated. Ideally, these current sensor boards must be on the same board, but in order to obtain flexibility and versatility are separated for the tests. The third board is the SEPIC converter designed in Chapter 2. This PCB includes different test points in order to measure each state variable of the system, Figure 5.6 (c). As a fourth PCB board, the microcontroller board is a commercial board used to develop each of the algorithms of the controllers. The Arduino DUE is a microcontroller board based on the Atmel SAM3X8E ARM Cortex-M3 CPU. In order to avoid restriction on both the PWM

resolution and analog to digital converter resolution, this Arduino DUE has been chosen.

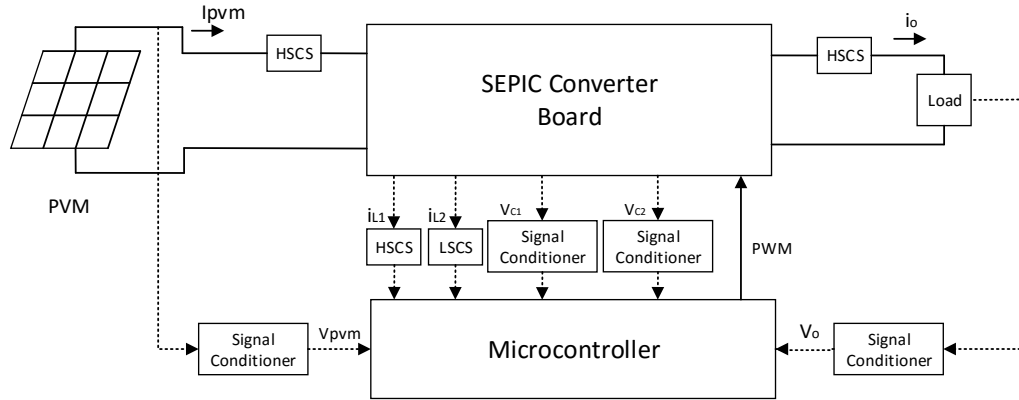
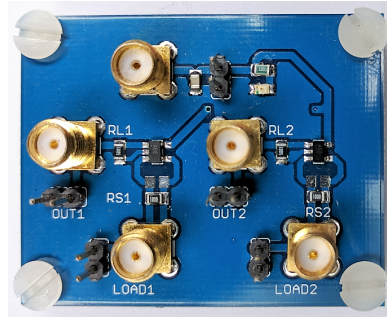
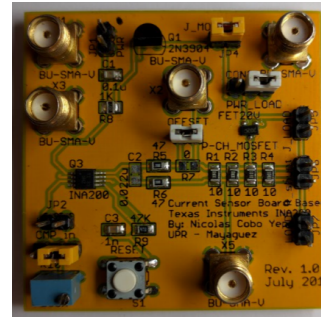


Figure 5.5 : Block Diagram of the developed system



(a) Dual High-Side Current Sensor Board



(b) Low-Side Current Sensor Board



(c) SEPIC Converter Board

Figure 5.6 : PCB Boards

The experimental setup is shown in Figure 5.7 . This setup is used to implement the studied control methods: Fuzzy Logic Controller, and Passivity-Based Control as an output voltage control.

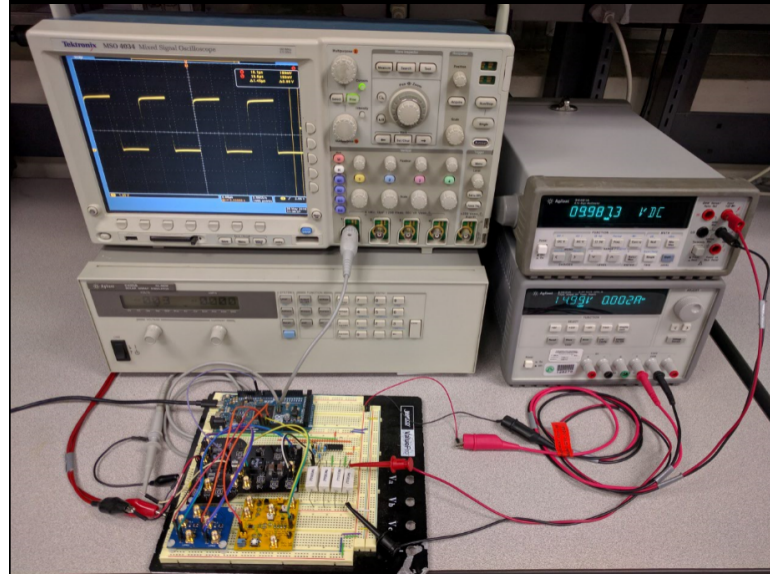


Figure 5.7 : Experimental Setup

### 5.3 DC/DC Converter

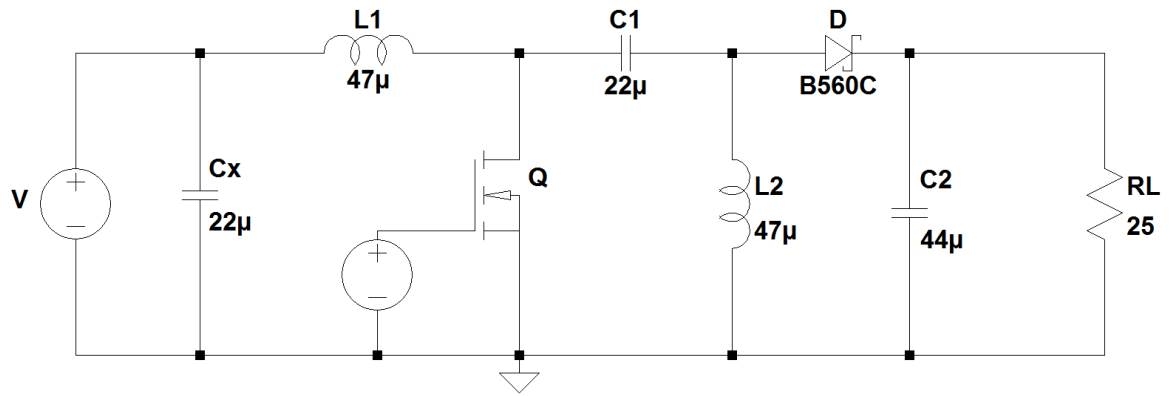
#### 5.3.1 Open-Loop Performance

Below the circuit diagram for Matlab and LT-Spice simulation of SEPIC converter is presented. The aim is to measure the output voltage, current waveform in both directions, input and output.

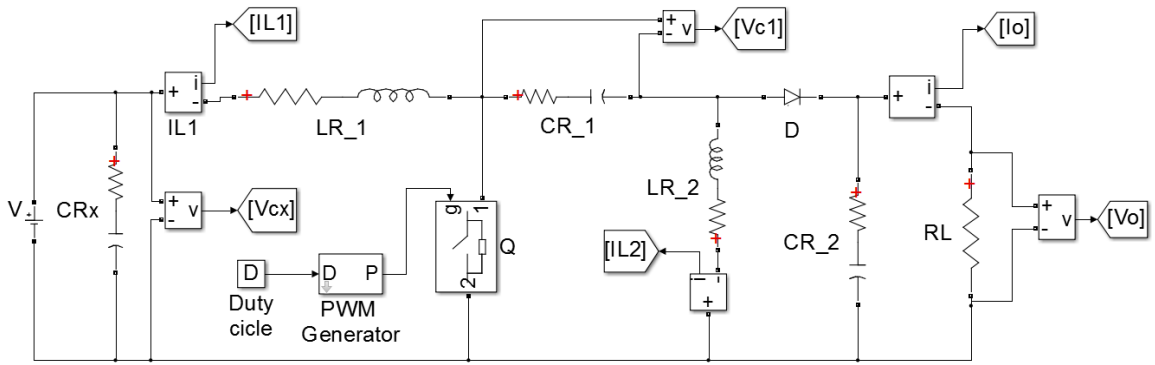
In order to analyze each of the stages of the system and the open loop performance, three cases were considered: step-down, step-up, and hold-mode. These tests were realized for each mode of the SEPIC converter. The component values did not change for the tests. The open loop test was carried out in two forms. An open loop and a fixed DC source are performed as a first way of testing circuit simulation. To evaluate this open-loop test Simulink and LT-Spice are used. LT-Spice has complete

models than some other simulators, including the model for the transistor and diode, for that reason the data to be extracted is more consistent.

Simulink was also used as a second way of testing, in order to evaluate the response of SEPIC converter to the input of the solar panel. The scenario and its specific conditions are explained in the Table 5.4 . Each of the tests that were performed to open-loop was based on schemes that are seen in Figure 5.8 , LT-spice and Simulink<sup>®</sup> respectively. The converter was designed considering output requirements and entry restrictions due to the power system to be used in the entire system.



(a) Battery-Sepic LT-Spice implementation



(b) PVM-Sepic Simulink<sup>®</sup> implementation

Figure 5.8 : Open Loop simulation systems - a) LT-Spice b) Matlab Simulink<sup>®</sup>

## Simulations & Experimental Results

According to the design that was realized in [Section 2.2.2](#), the operating frequency for the simulation and testing of the inverter must be above or equal to  $100kHz$  because the inductors and the other components were chosen to design the PCB and were calculated at a minimum frequency of this range. For this reason, it is necessary that the operating frequency must be equal or greater than  $100kHz$  to meet this parameter. The tests presented below were determined for a load of  $25\Omega$  and  $100kHz$  of frequency. With these values, the power output will not be the maximum power delivered by the solar panel, but the efficiency of the DC/DC converter is not ideal. According to this, the power delivered and received by the load for each of the output voltages is evaluated.

### DC/DC Converter & Fixed Power Supply

Below the Simulink®, LT-Spice simulation and experimental results of the converter in open-loop with a fixed power supply are presented, as well as the graphs that demonstrate the comparison between the simulations and experimental results. In order to evaluate each state of the SEPIC converter, Buck mode, Boost mode, and hold mode, it was decided to use 40%, 50% and 60% in each case respectively for the duty cycle signal. These parameters may determine the accuracy of the implemented system. The parameters to be evaluated are the following:

$T_s$  = Settling time

$T_r$  = Rise time

$I_p$  = Peak Current

$V_p$  = Peak Voltage

$\Delta I$  = Ripple Current

$\Delta V$  = Ripple Voltage

### SEPIC as a Buck converter

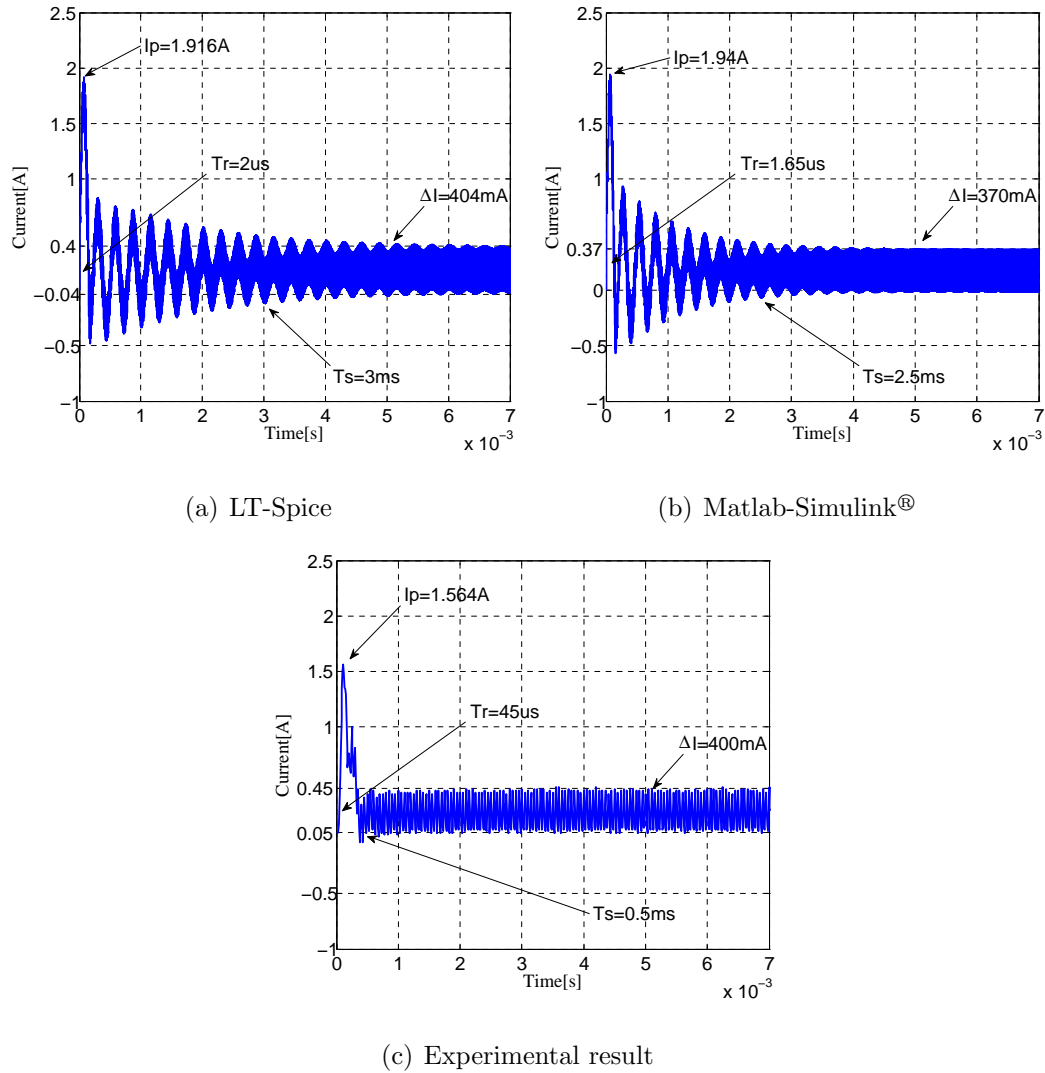
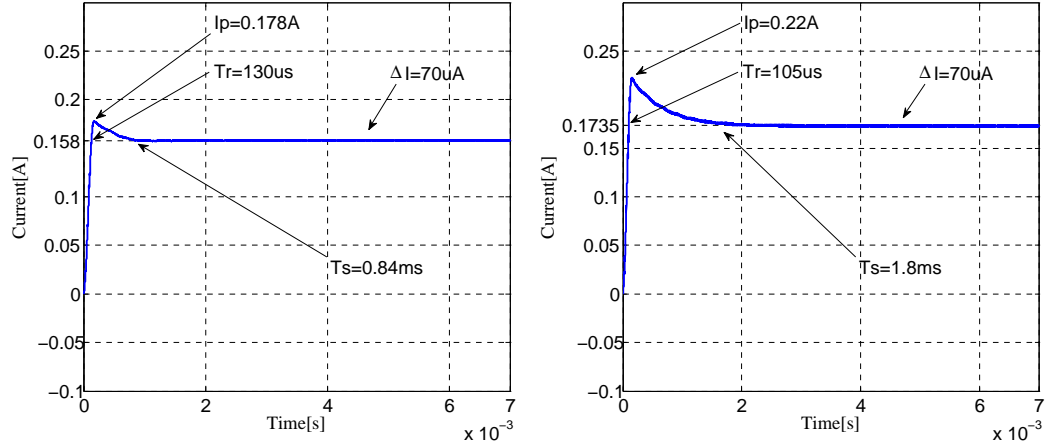


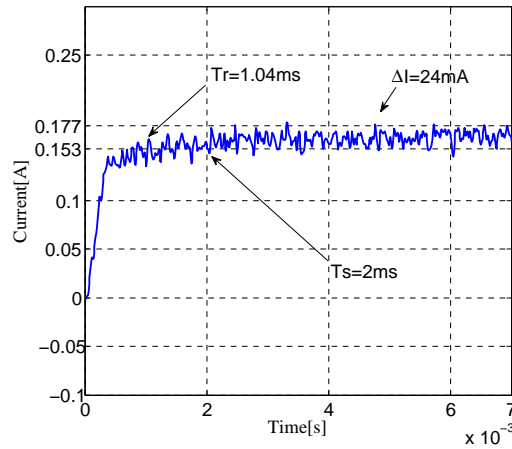
Figure 5.9 : Input Current response - SEPIC as a Buck converter

In Figure 5.9 is shown the comparison about the input current between simulations and real response. Figure 5.9 (c) shows the real response for the input current of SEPIC converter. As can be seen, the simulation responses that can be observed in the Figures 5.9 (a) and 5.9 (b) have a similar response to the real response. As can be observed, the  $T_s$  in the real response is less than the simulations response.  $I_p$  is highest in simulation responses. The final value ( $\Delta I$ ) of each of the answers is similar.



(a) LT-Spice

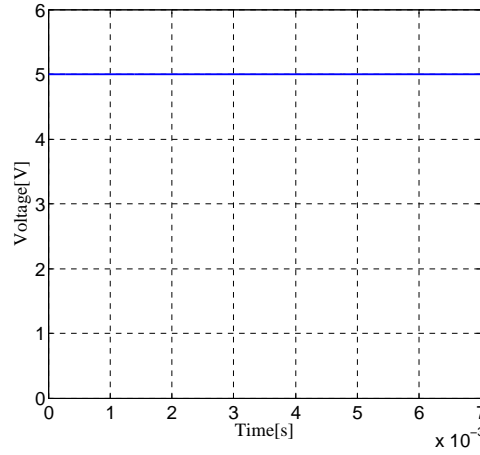
(b) Matlab-Simulink®



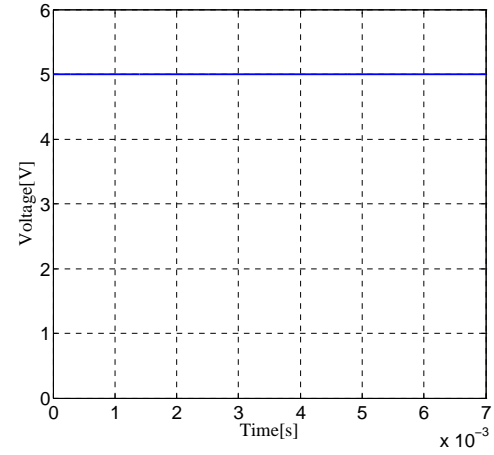
(c) Experimental result

Figure 5.10 : Output Current response - SEPIC as a Buck converter

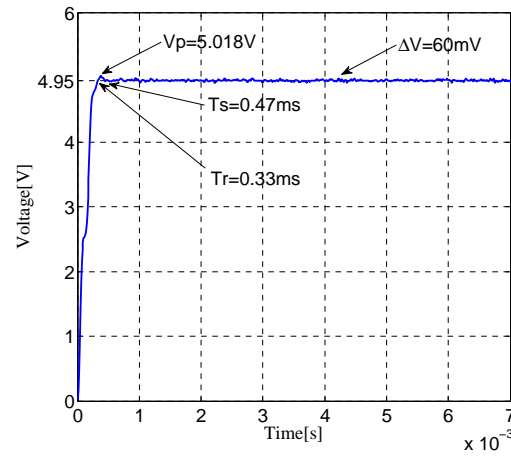
In addition, the output current is observed in Figure 5.10 . Figure 5.10 (c) shows the real response for the output current of SEPIC converter. Figures 5.10 (a) and 5.10 (b) shown the simulation responses for the output current. These responses of the output current are very similar. For this case,  $\Delta I$  over the real response is greater than the simulation responses. In addition, the  $I_p$  does not show up at the real response. On the other hand, the  $T_s$  in simulation responses is less than the real response. The real response presents a little oscillation due to the data acquisition of the sensor. This oscillation is a noise in the current sensor.



(a) LT-Spice



(b) Matlab-Simulink®

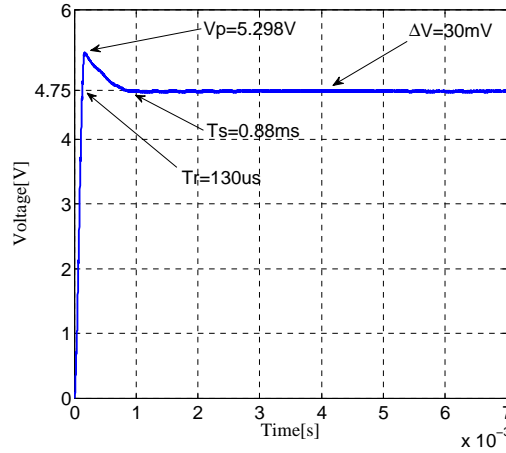


(c) Experimental result

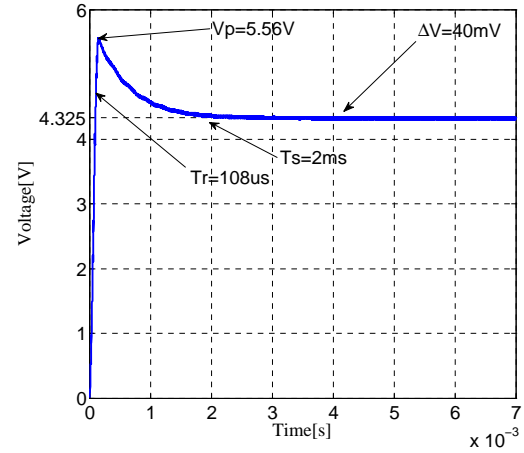
Figure 5.11 : Input Voltage response - SEPIC as a Buck converter

In Figure 5.11 it can be seen the simulation and real responses of the input voltage of the SEPIC converter. In this case, the simulation responses are ideal signals. On the other hand, the real response has a  $T_r$  and  $T_s$  greater than the simulation responses. This is because the real power supply needs time to achieved the final value.

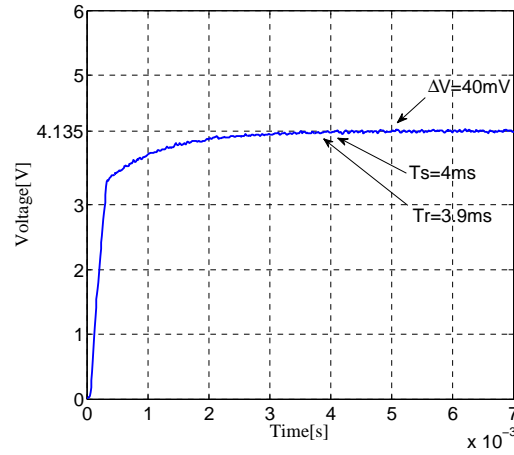




(a) LT-Spice



(b) Matlab-Simulink®



(c) Experimental result

Figure 5.12 : Output Voltage response - SEPIC as a Buck converter

On the other hand, Figure 5.12 shows the output voltage of the SEPIC converter responses. The simulation responses, Figures 5.12 (a) and 5.12 (b), shown a peak voltage that does not present in the real response. This is due to the  $T_s$  present in the real response for the input voltage. Furthermore, the final voltage value is below the final value of the simulations. This output voltage does not present very high ripple.

### SEPIC at 50% duty cycle

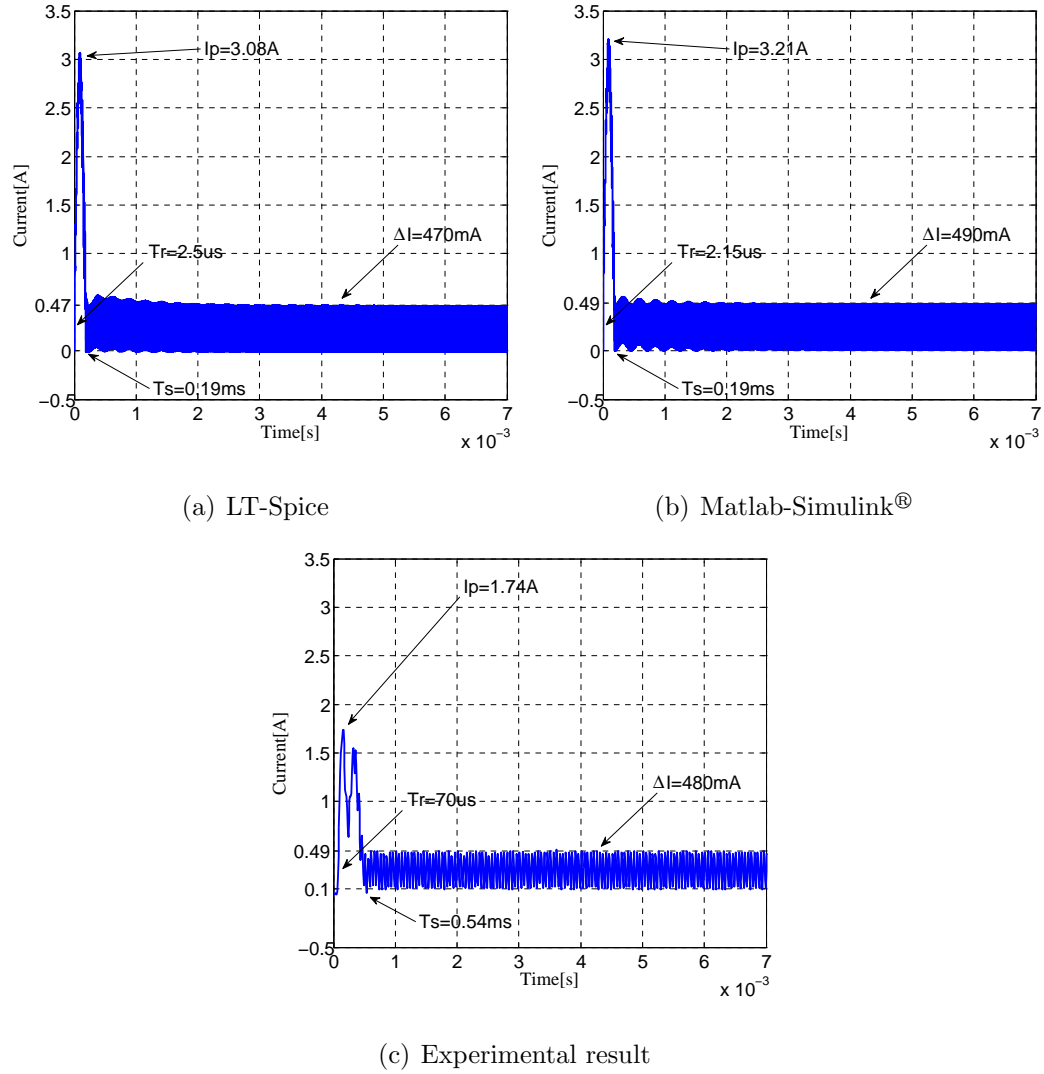
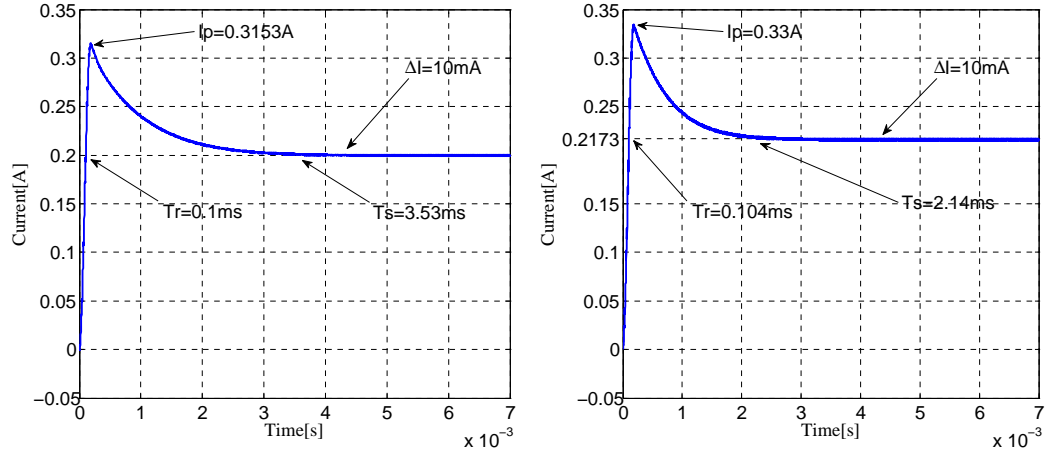


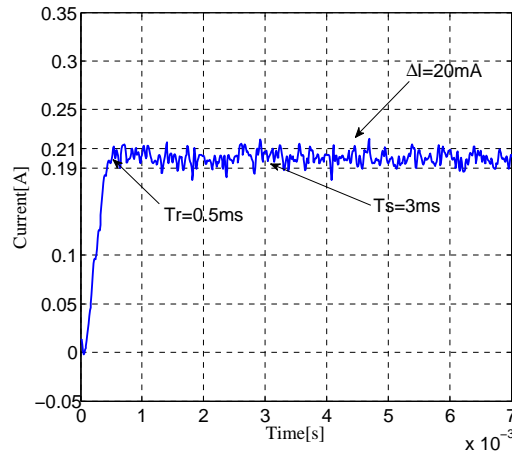
Figure 5.13 : Input Current response - SEPIC at 50% duty cycle

In this case, the real response of the input current (Figure 5.13 (c)) has little difference with respect to the simulation responses. In the responses of the simulators (Figures 5.13 (a) and 5.13 (b)),  $I_p$  has a greater value than the real response. But the value  $\Delta I$  around which the oscillation occurs is the same. The  $T_s$  in the real response is greater than the simulations.



(a) LT-Spice

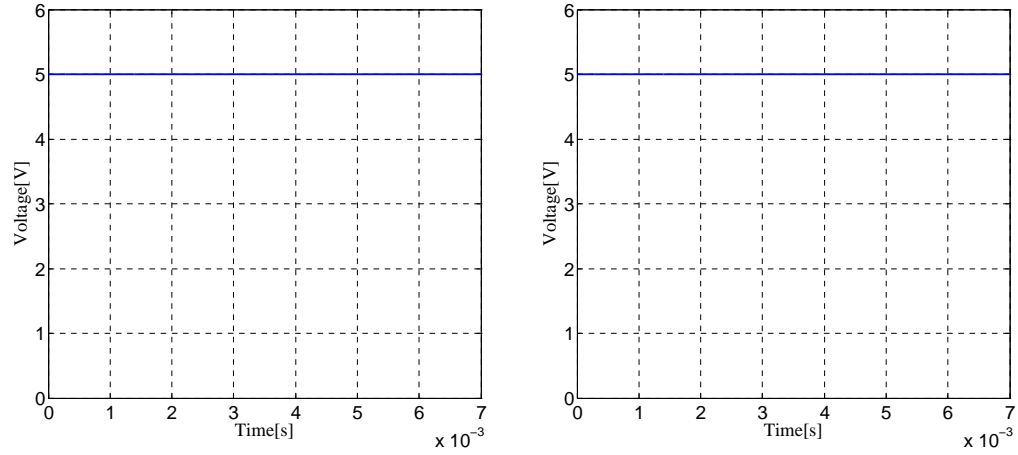
(b) Matlab-Simulink®



(c) Experimental result

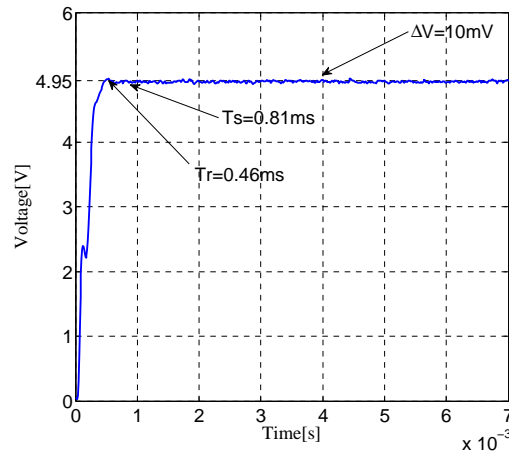
Figure 5.14 : Output Current response - SEPIC at 50% duty cycle

As the responses of the output current in the case for 40% of duty cycle, the output current in case of 50% does not present an overshoot in the real response and also presents an oscillation around the final value,  $\Delta I$ . The average value of the experimental response is very close to the final value that occurs in the simulations. Figures 5.14 (a) and 5.14 (b) shown the simulation responses for the output current. In addition, the  $I_p$  does not show up at the real response. On the other hand, the  $T_s$  is simulation responses is less than the real response.



(a) LT-Spice

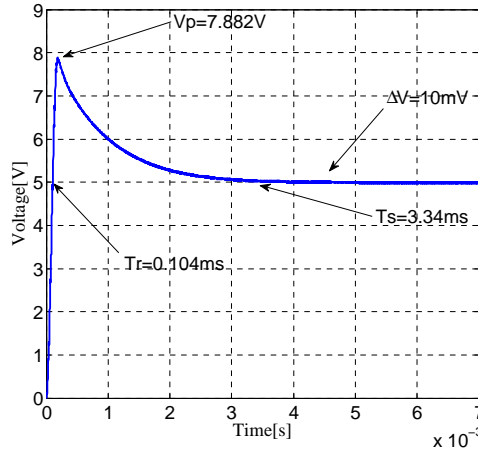
(b) Matlab-Simulink®



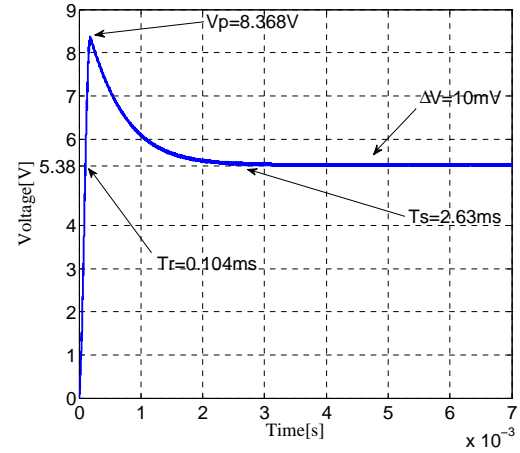
(c) Experimental result

Figure 5.15 : Input Voltage response - SEPIC at 50% duty cycle

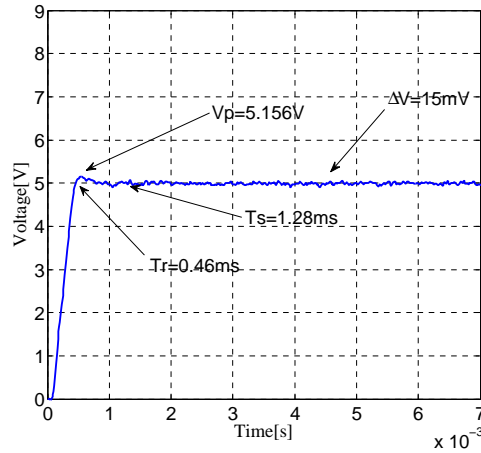
In [Figure 5.15](#) it can be seen the simulation and real responses of the input voltage. In this case, the simulation responses are ideal signals. As can be seen, the real response has a  $T_r$  and  $T_s$  greater than the simulation responses, even greater than the input voltage for a duty cycle at 40%. This is because the real power supply needs time to achieved the final value.



(a) LT-Spice



(b) Matlab-Simulink®



(c) Experimental result

Figure 5.16 : Output Voltage response - SEPIC at 50% duty cycle

In addition, Figure 5.16 shows the output voltage responses. The simulation responses, Figures 5.16 (a) and 5.16 (b), shown a peak voltage that does not present in the real response. This is due to the  $T_s$  present in the real response for the input voltage. Furthermore, the final voltage value is the same value of the LT-Spice simulation. This output voltage does not present very high ripple. This real response has a little overshoot,  $V_p$ . Additionally, there is a difference between the two simulations at the final value. Even so the LT-Spice simulation and experimental signal are very close. Moreover, the Matlab simulation provides a larger output and

could be attributed to the models which are not so successful and the losses in each case are not the same.

### SEPIC as a Boost converter

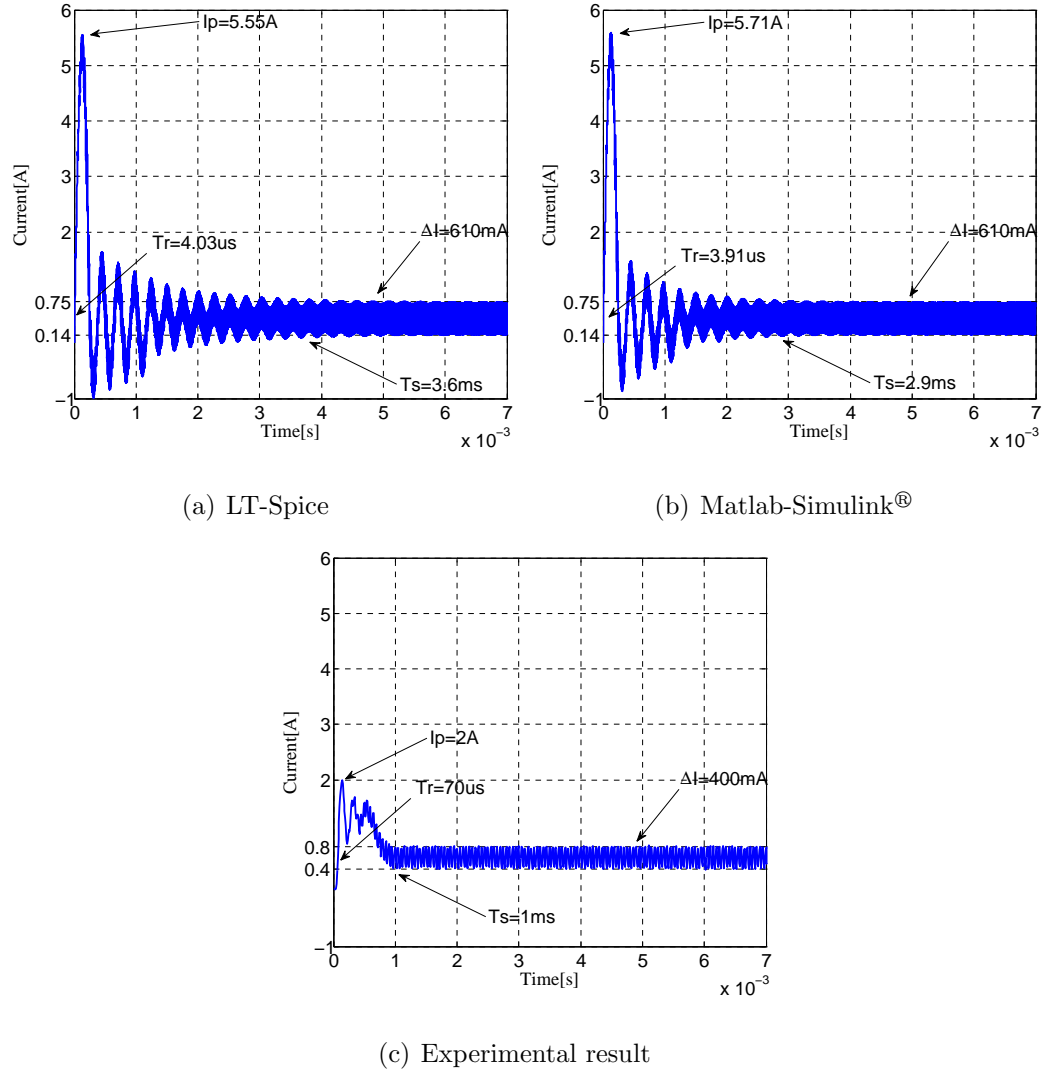


Figure 5.17 : Input Current response - SEPIC as a Boost converter

In the case when the SEPIC converter works like a Boost converter, the input current and output current are shown in Figures 5.17 and 5.18 respectively. Similar to the previous cases, the input current at Figure 5.17, the experimental response

presents a peak lowest in comparison to the simulation responses. In addition, the  $T_s$  and  $\Delta I$  in the real response are less than the simulation responses.

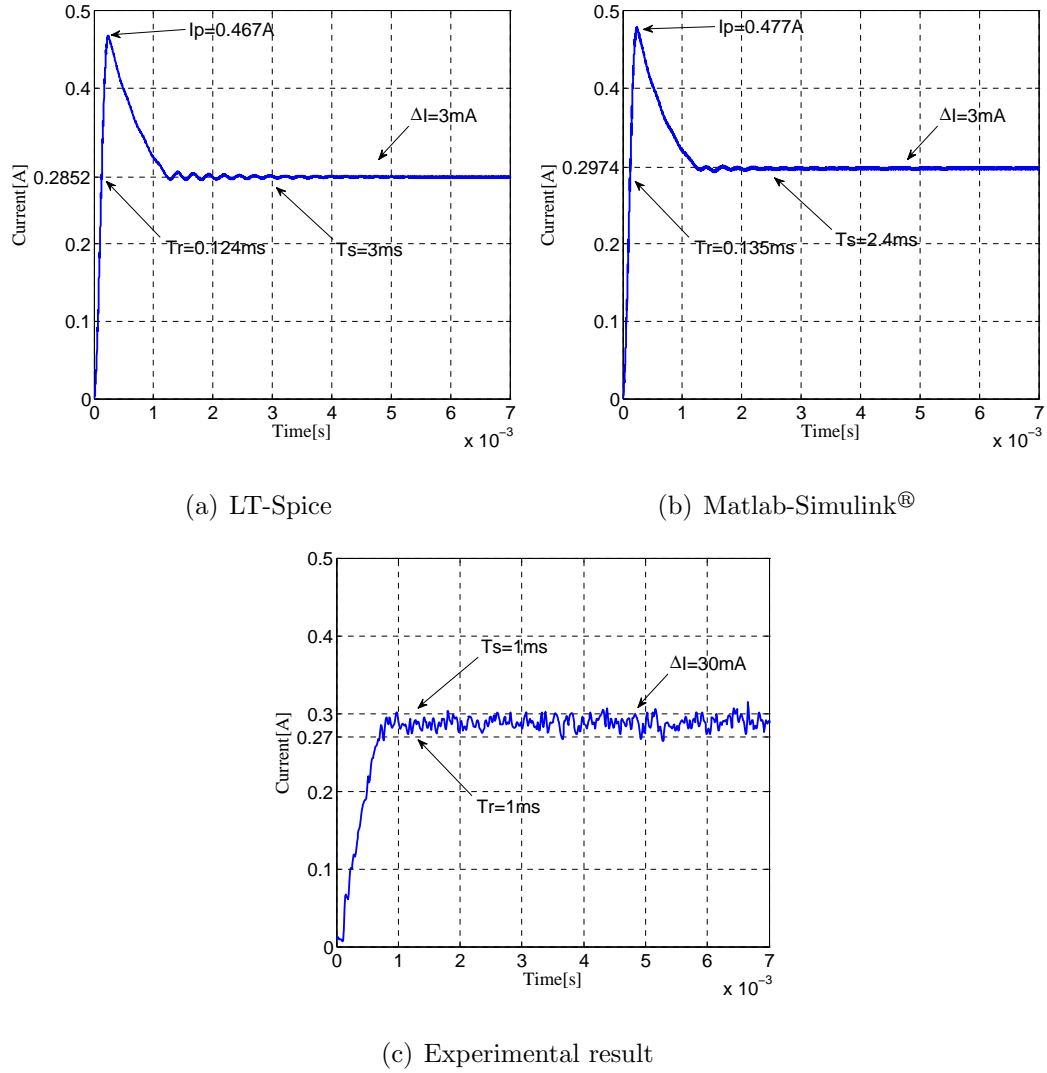
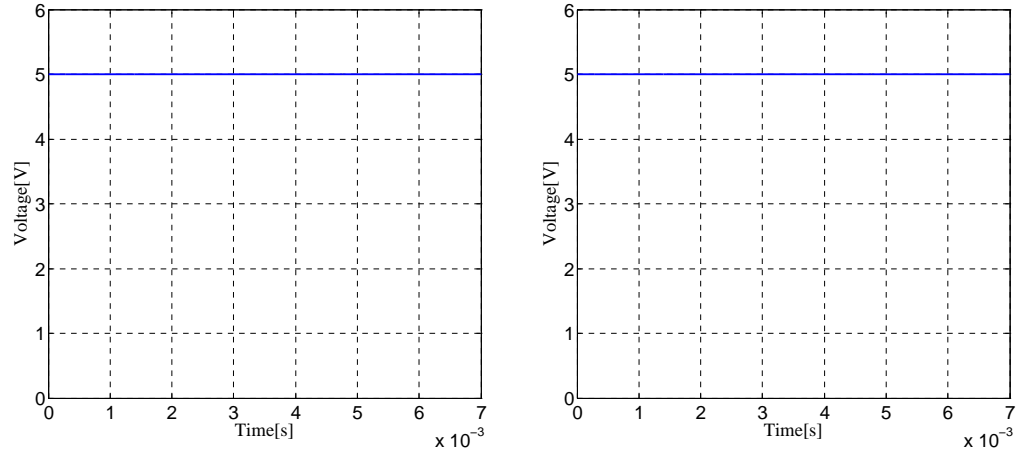


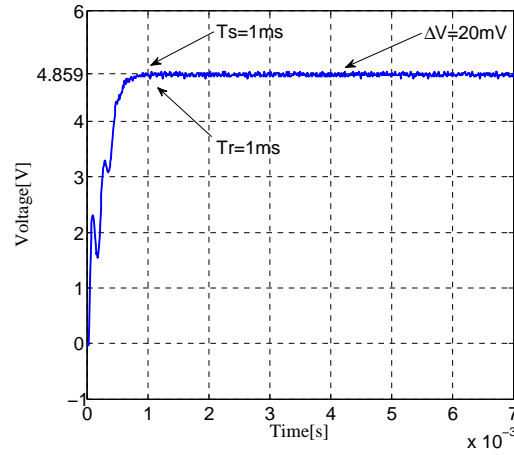
Figure 5.18 : Output Current response - SEPIC as a Boost converter

Figure 5.18 (c) shows the real response for the output current of SEPIC converter. Figures 5.18 (a) and 5.18 (b) show the simulation responses for the output current. Additionally, the output current that is shown in Figure 5.18 (c) does not present overshoot at the beginning of the operation but presents a current ripple ( $\Delta I$ ) higher than the simulation responses.



(a) LT-Spice

(b) Matlab-Simulink®

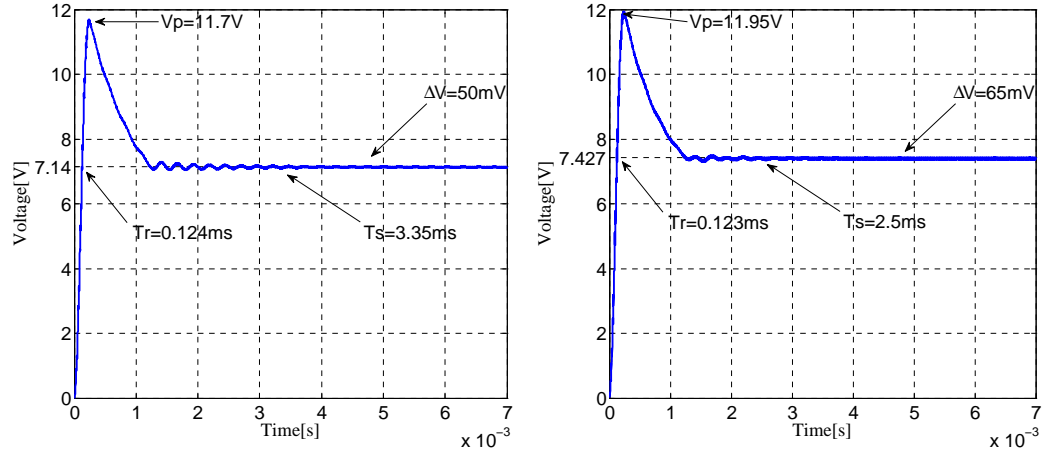


(c) Experimental result

Figure 5.19 : Input Voltage response - SEPIC as a Boost converter

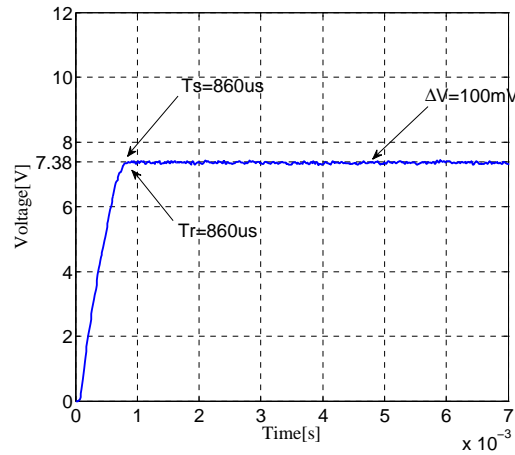
Figure 5.19 shows the responses about the input voltage at 60% of duty cycle. In this case the input voltage of the SEPIC converter, Figure 5.19 (a), has a  $T_s$  and  $T_r$  greater than the other responses. This is because the current need it for this duty cycle is higher.





(a) LT-Spice

(b) Matlab-Simulink®



(c) Experimental result

Figure 5.20 : Output Voltage response - SEPIC as a Boost converter

In Figure 5.20 is shown the comparison of the output voltage between simulations and real response. As can be seen in this case, the output voltage is a good response. This can be said because this response does not present overshoot and the settling time is low. Furthermore, the ripple voltage is minimum. The simulation responses, Figures 5.20 (a) and 5.20 (b), shown a peak voltage that does not present in the real response. This is due to the  $T_s$  present in the real response for the input voltage.

In general terms, it can be said that the open-loop tests achieved the expected values for responses of the fixed power supply. The response of the circuit designed in each of the simulators have the same parameters, component values and characteristics for the power supply, but it should be noted that the components that are used in the LT-Spice simulator are more approximate to real models that are described by Simulink®. Moreover, the response of each of simulators for the same parameters is similar. It is important to note there exists an overshoot in some cases of the signals. This overshoot is not present in the experimental results due to the real elements having parasitic values such as  $ESR$ ,  $ESL$  and others. Furthermore, the switching elements present in the system can cause losses and abnormal behaviors.

### DC/DC Converter & Solar Array Simulator

After verification of operation in open-loop of the SEPIC converter connected to a fixed power supply, performing the tests in the same converter with the photovoltaic cell as input signal proceeds. For the development of the tests with the solar panel the scheme described in Equation (2.1a) was used. This system has a controlled current source and PV array block to represent the photovoltaic cell. This current source is controlled by the solar panel model implemented above. The generated current is driven by the output signal of the PV array block. Below the input and output

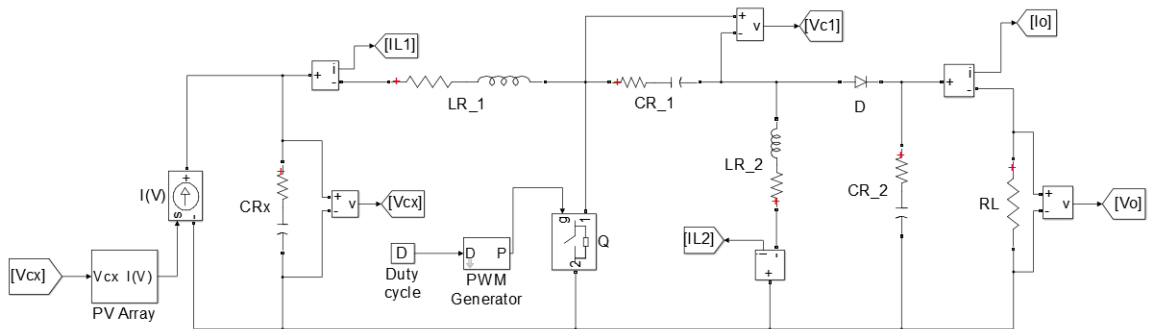


Figure 5.21 : PVM-SEPIC simulation system - Simulink®

signals of the photovoltaic cell and the SEPIC converter respectively are observed at 50% duty cycle. The aim is to know about transient and steady state behavior. As mentioned above, the photovoltaic cell is emulated with a solar array simulator. The simulation parameters were set forth above in [Table 5.3](#).

### Simulations results

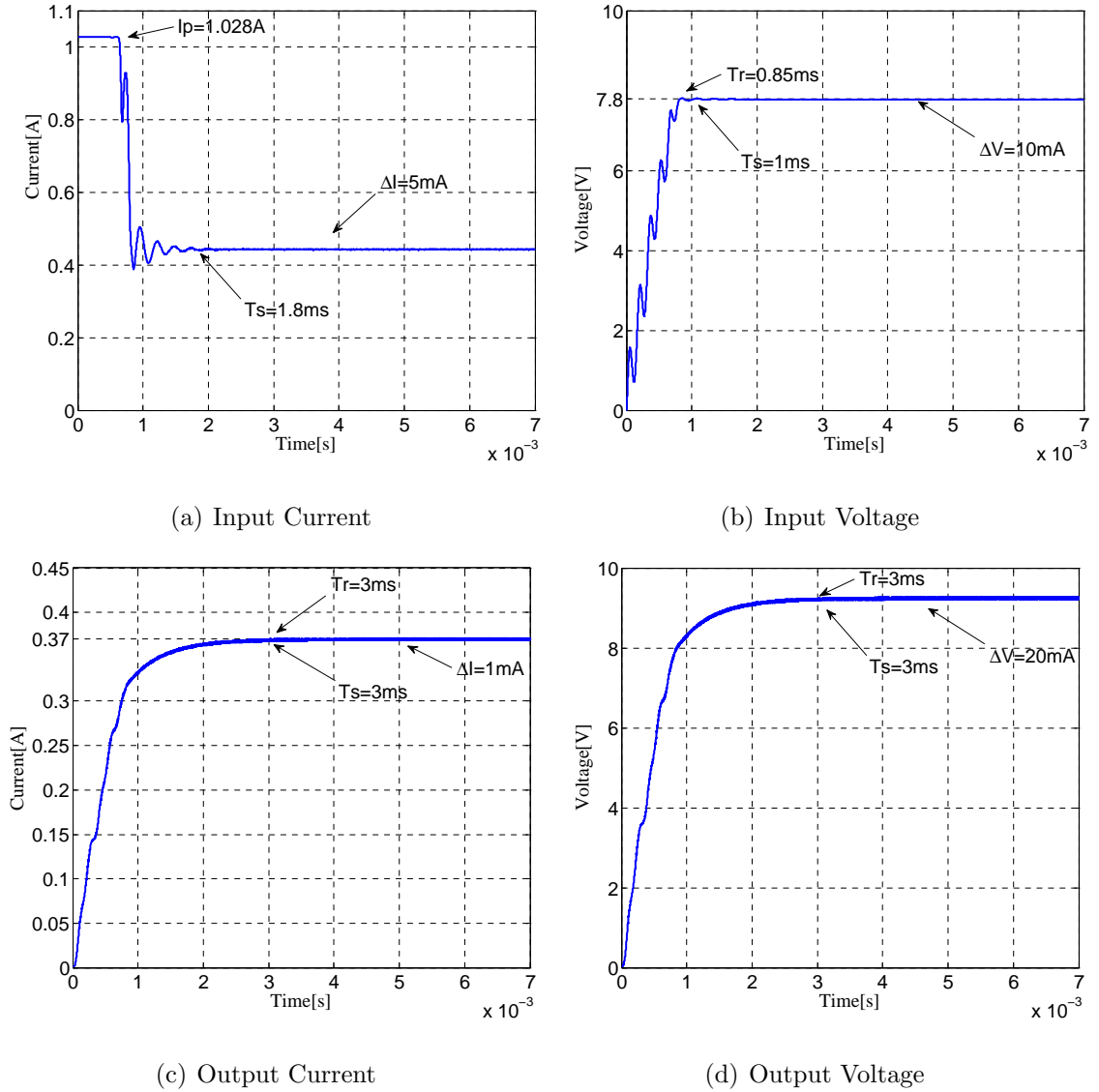


Figure 5.22 : PVM Model Open-Loop simulation response

Figure 5.22 shows the simulation responses for input current, output current, input voltage, and output voltage for photovoltaic cell and SEPIC converter at open-loop performance. As shown in Figure 5.22 (a) the current that is required from the PV cell is saturated by the ability to deliver power from this source. This is because the input voltage, Figure 5.22 (b), has a  $T_r$  necessary to achieve the final value. The  $I - V$  curve, Figure 5.3 (a), says that when the output voltage from the solar panel is low the output current is the maximum available. After that, the input current decreases as the output voltage of the photovoltaic cell increases. Figure 5.22 (b) shows that the input voltage increases over time until achieving the final value. It can also be observed that the limit for the current and voltage respectively is near the limit established above. On the other hand, the output signals present a normal behavior and without overshoot.

## Experimental results

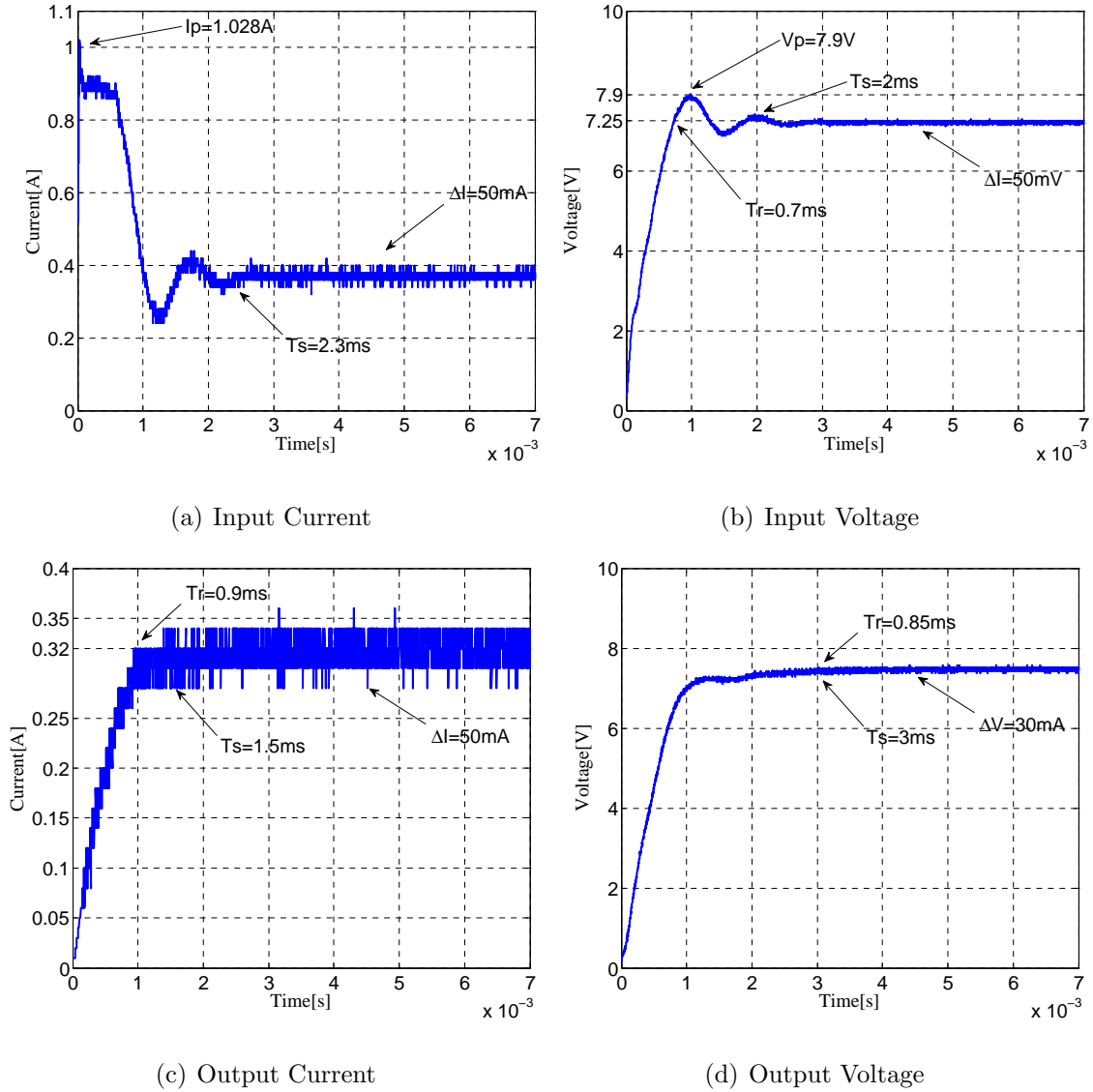


Figure 5.23 : PVM Model Experimental response

Figure 5.23 shows the real responses for input current, output current, input voltage, and output voltage for photovoltaic cell and SEPIC converter at open-loop performance. As can be seen, all signals in the simulation responses, Figure 5.22, are very similar to the real responses shown in Figure 5.23.

The comparison of each of the images presented in the Figures 5.22 and 5.23 shown the similarity between each of the measured parameters. In the case of

the experimental results it can be seen that there exists an overshoot in the voltage signals. This overshoot does not overcome the 10% of the final value. Thus, this overshoot is negligible and not able to damage some component. Also as can be seen the final value for the output voltage signal is lowest than the input voltage signal. This indicates that there are losses in the converter. It should be noted that the time response is a bit slower because the time response of the photovoltaic cell is slower than the DC power supply.

In [Figure 5.23 \(a\)](#) it can be observed that there exists a big consumption about current while the solar panel achieves the final value for the current needed to the system. The average final value is  $420mA$  approximately. Also, it can be seen that the current peak observed in [Figure 5.22 \(a\)](#) is not achieved by the real current delivered by the solar array simulator. This thing can be because there exists a discrepancy between the transient response of the real solar cell and the solar array simulator. The output current that is observed in [Figure 5.23 \(c\)](#) achieves the lowest value than the expected value due to the losses.

[Figure 5.22 \(b\)](#) shows an abnormal behavior between the  $0ms$  and  $1ms$ . But this behavior can not be seen at the real response observed in [Figure 5.23 \(b\)](#). This behavior can be attributed to the mathematical process developed by Matlab. This process

### 5.3.2 Maximum Power Point Tracking

The proposed scheme with Perturb and Observe algorithm was simulated using Simulink<sup>®</sup>. Figure 5.24 shows the details of the Perturbation and Observation flow chart, which is based on [41]. The PVM model and the power converter were simulated using Simulink<sup>®</sup>. The parameters used are cited in Chapter 2.

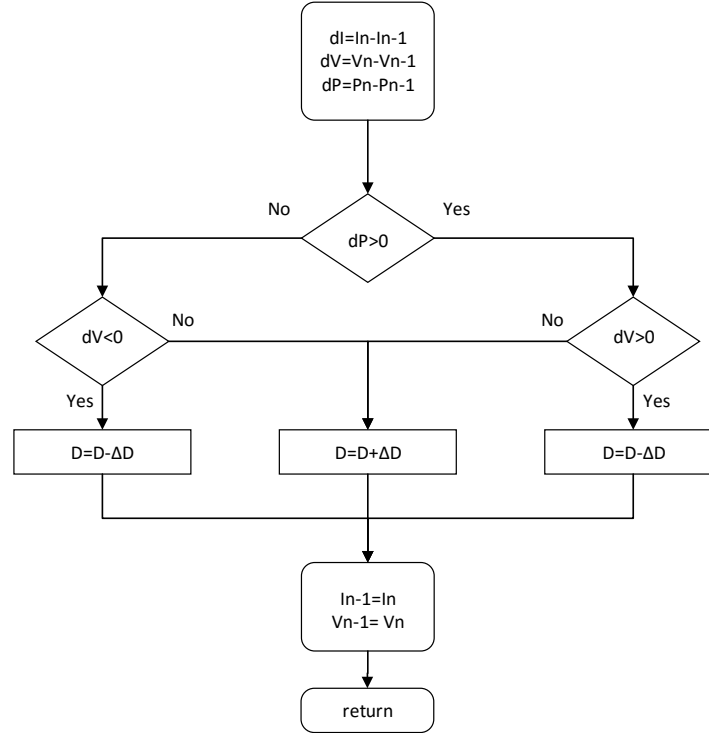


Figure 5.24 : Flow chart of P&O algorithm

In order to determine the P&O algorithm performance, a search of maximum power point in different initial conditions is evaluated. Figure 5.25 shows the simulation results considering different initial points for the search.

The most commonly used initial points for the P&O algorithm are 0 and  $V_x$ , but between these values, exist many values that can be used as an initial point for the search algorithm. Two of these values were calculated in Chapter 4. As mentioned above, these values ( $V_{ap}$ ,  $V_{am}$ ) are a good approximation of the optimal value  $V_{op}$ . In

addition, between  $V_{ap}$  and  $V_{am}$  exist also many values even more close to the optimal value. According to this, one of them is the middle point between  $V_{ap}$  and  $V_{am}$ . Thus, in Equation (5.1) the initial points are can be observed.

$$\left[ 0, V_{ap}, \frac{V_{ap} + V_{am}}{2}, V_{am}, V_x \right] \quad (5.1)$$

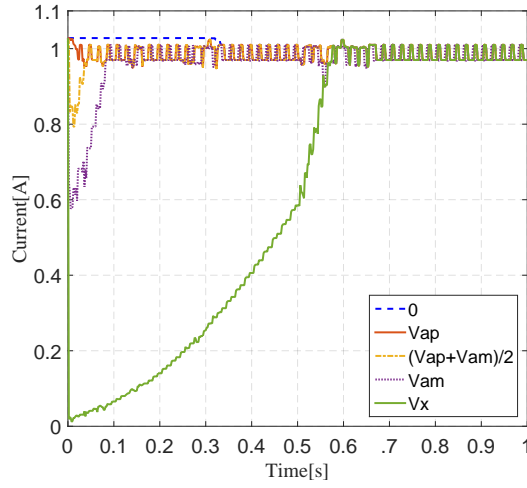
The P&O method tracked the maximum power successfully for all these initial points; however, the PV power had a small oscillation. Table 5.5 summarizes the results of P&O method, showing the minimum and maximum value of the fluctuation of PVM power.

Table 5.5 : Simulation results of P&O method

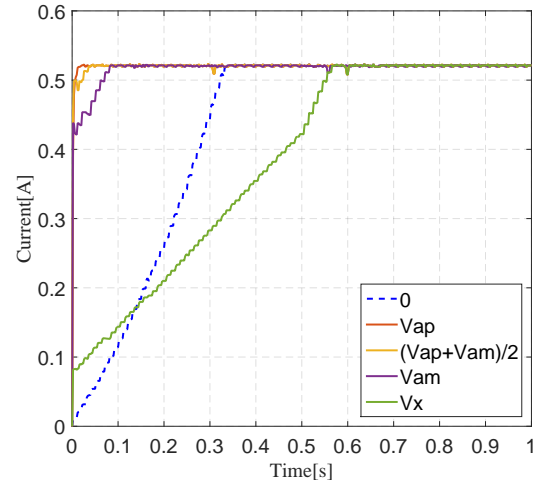
Min. PV Power	Max. PV Power	Power in MPPT
6.9 W	6.94 W	6.94 W

As can be observed, each of the initial points (voltage values) taken as a starting point is a good choice to find the maximum power point. Even when all starting points have a good performance and achieved the MPP, the 0 and  $V_x$  values have a greater settling time than the others initial points for power response. Figure 5.25 shows the variations of the input current, output current, input voltage, output voltage, input power, and output power for the whole system. As can be seen in Figure 5.25 (e), each simulation response in terms of the initial conditions have different behavior. In addition, as can be seen, the others three values have a great response in terms of the final value of power and settling time. These three values have a settling time less than  $100ms$  while the 0 and  $V_x$  value even have a settling time ten times higher than the others. Thus, it can be noted the importance of the starting point of search. As mentioned above, a new search region can be established between  $V_{ap}$  and  $V_{am}$ , which can accelerate the convergence of the P&O algorithm. Figure 5.26 shows a zoom-in of the simulation responses of the P&O.

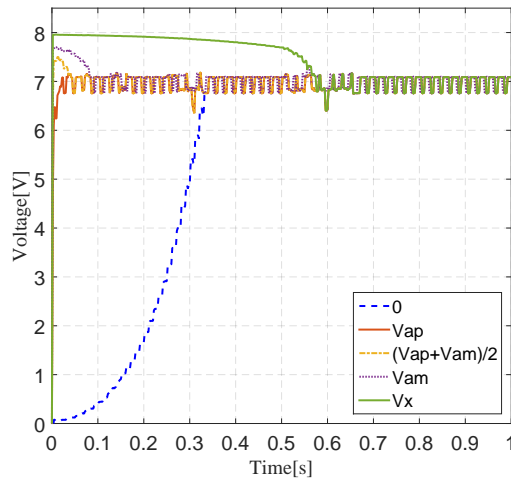




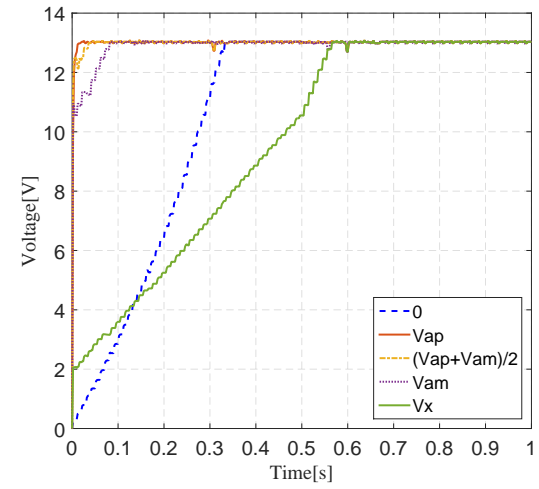
(a) Input Current



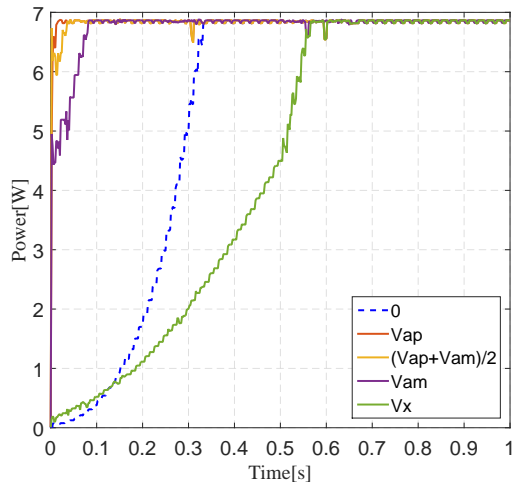
(b) Output Current



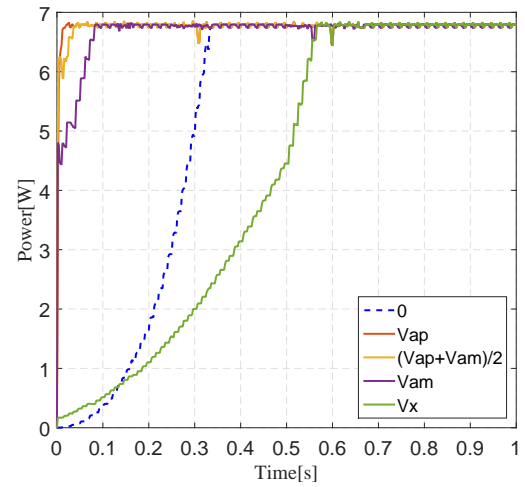
(c) Input Voltage



(d) Output Voltage

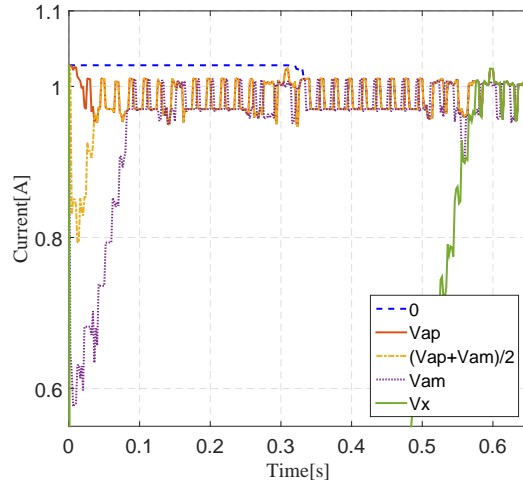


(e) Input Power

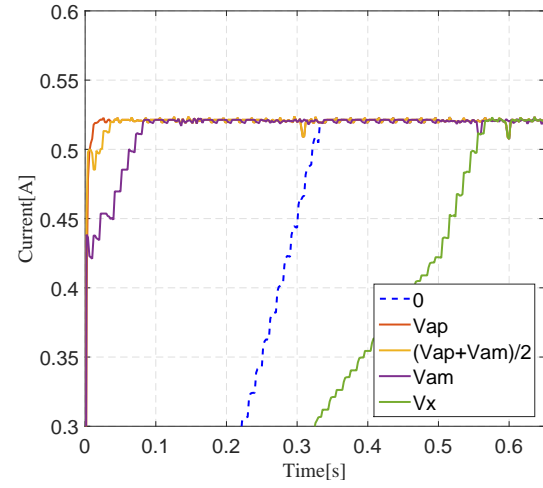


(f) Output Power

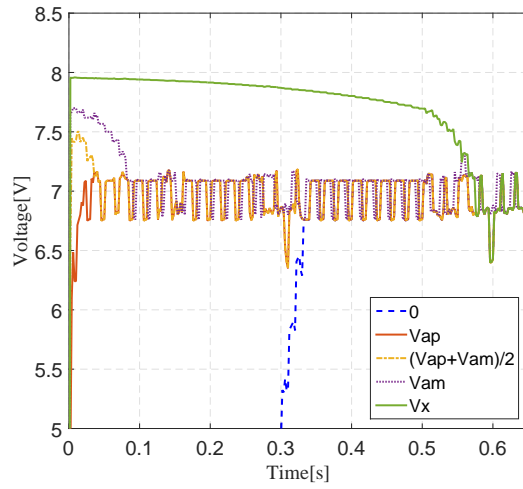
Figure 5.25 : P&amp;O simulation responses



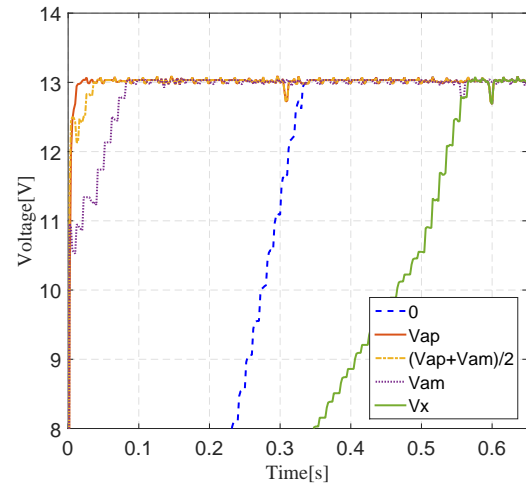
(a) Input Current



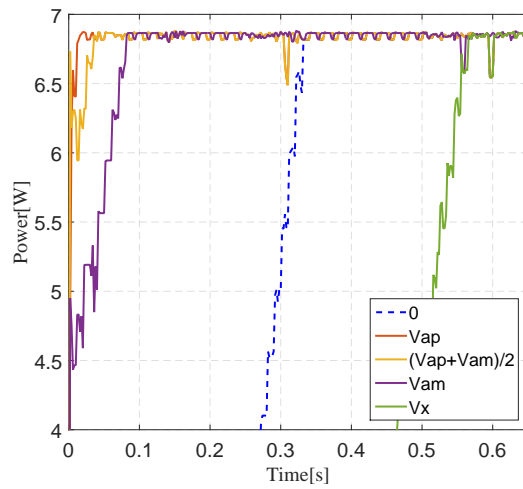
(b) Output Current



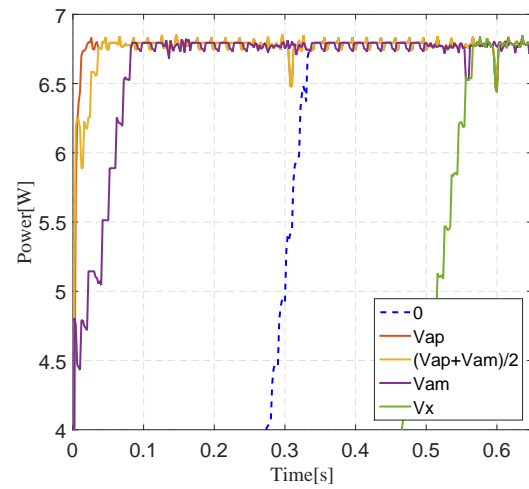
(c) Input Voltage



(d) Output Voltage



(e) Input Power



(f) Output Power

Figure 5.26 : Zoom-in of Figure 5.25

### 5.3.3 Output Voltage Control

In order to determine the influence of some of the control techniques applied to low power converters, the evaluated control schemes are presented. The simulation and experimental results over each control technique are presented as well. Each of the above control techniques is tested under the same test conditions.

The test conditions are as follows:

$$V_{ref} = [6 \ 10 \ 8 \ 4]V, R = 25\Omega$$

#### Fuzzy Logic Control

As mentioned above, the control law must be a little change of the duty cycle in order to avoid big changes in the output voltage. In [Figure 5.27](#) the Simulink® implementation is can be observed. According to this, the system signals are as follow:

$$u(k) = u(k - 1) + \Delta u(k) \quad (5.2)$$

The error  $e$  and difference of error  $\Delta e$  are defined as:

$$e(k) = V_{ref}(k) - V_o(k) \quad (5.3)$$

$$\Delta e(k) = e(k) - e(k - 1) \quad (5.4)$$

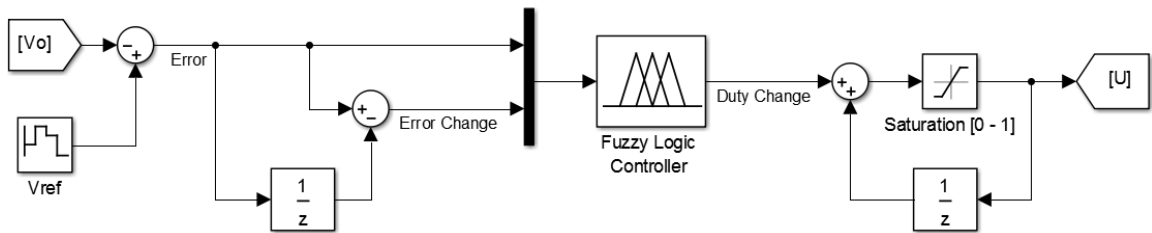


Figure 5.27 : Fuzzy-Logic Control implementation - Simulink®

Figure 5.28 shows a rules analyzer used in Simulink<sup>®</sup> and each rule mentioned above in Table 4.1 . Figure 5.29 presents the convex at zero because of the focused membership functions. Thus, the membership functions in Figure 4.13 are guaranteed to produce the stable output signal. The design of the focused membership function values depends on the nature of the signal. In addition, in the fuzzy logic controllers the ranges and form of memberships to define the inputs and outputs it is something that is done by knowledge of the system.

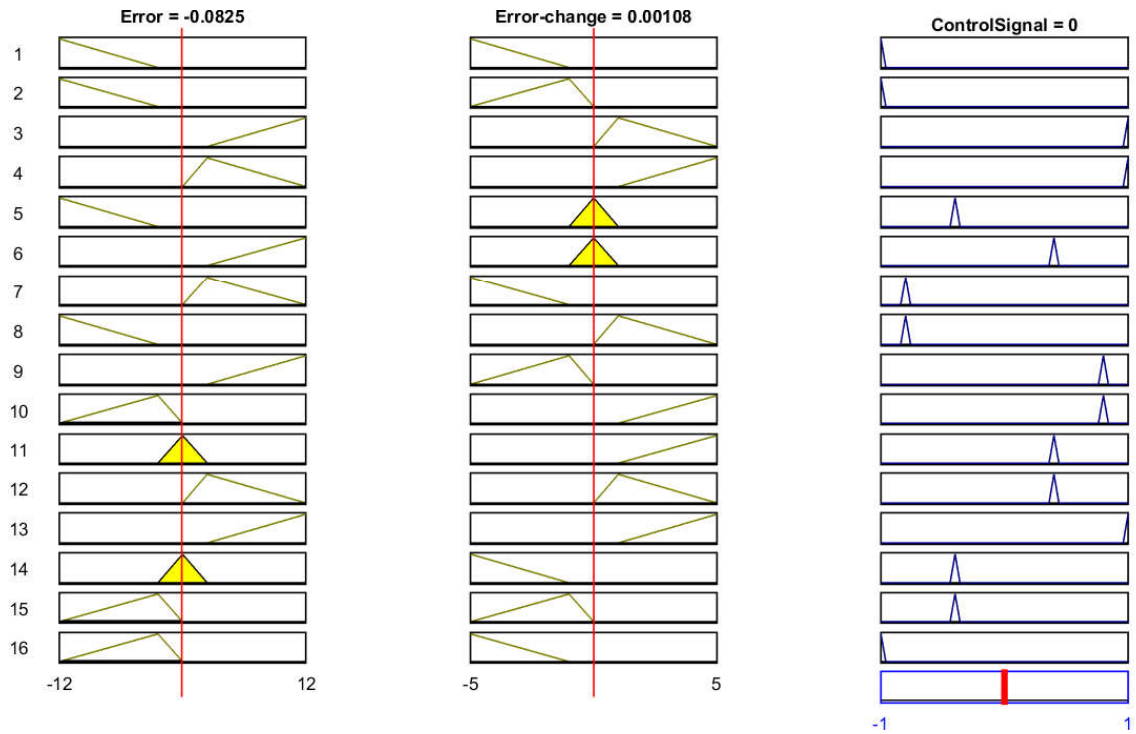


Figure 5.28 : Fuzzy-Logic Control rules validation - Simulink<sup>®</sup>

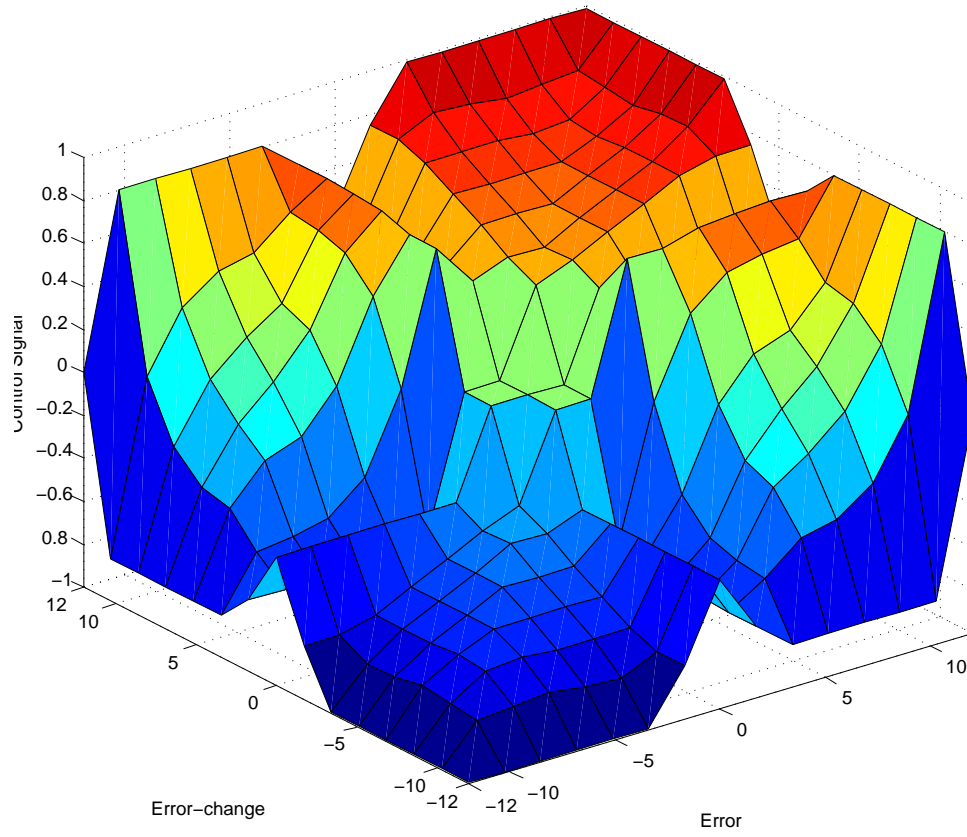


Figure 5.29 : 3-D surface of Memberships in [Figure 4.13](#)

## Simulations results

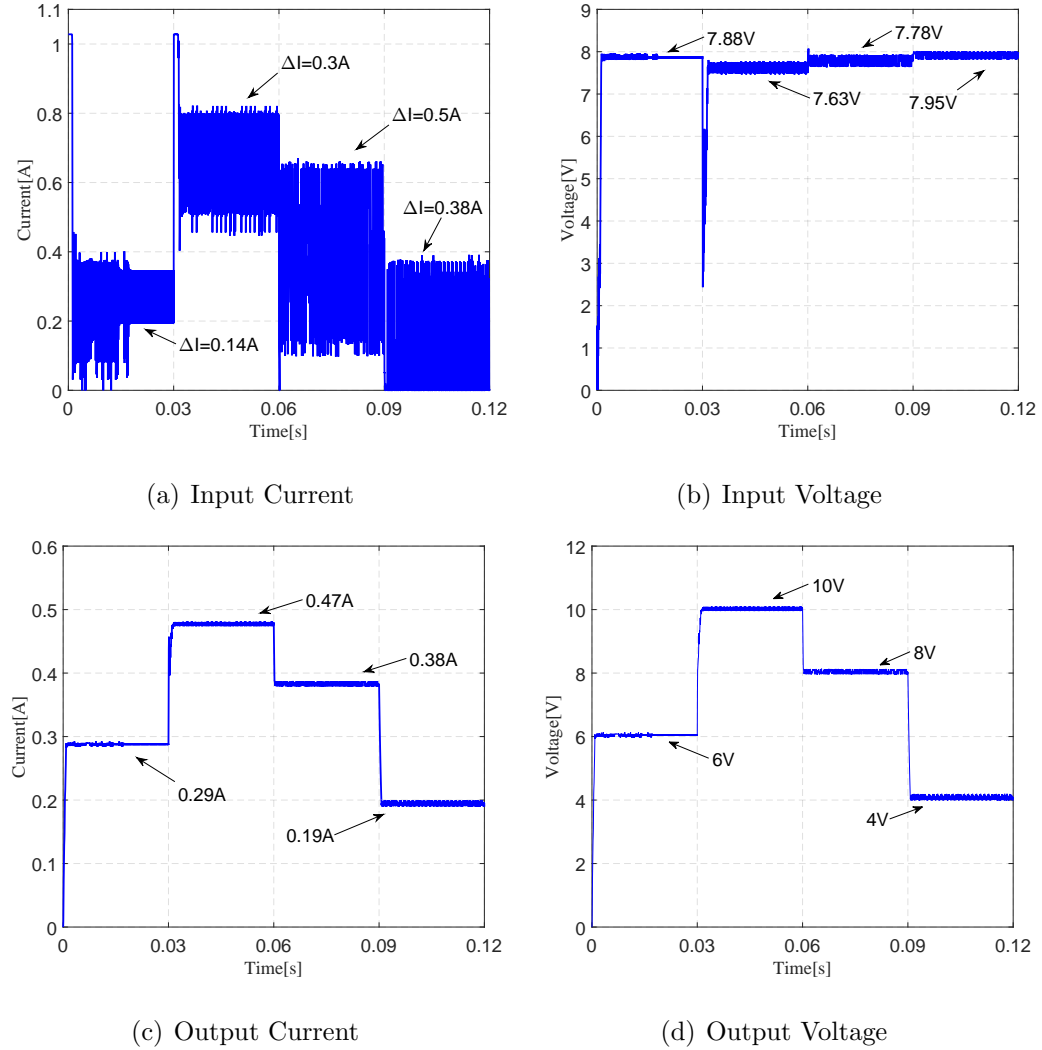


Figure 5.30 : Fuzzy Logic Control simulation response

In this case, the controller achieves the final value at the output (Figure 5.30 (d)). In addition, this signal has a little ripple and little settling time. This result can be considered as a good response. Additionally, the output current also has a little ripple. On the other hand, the input voltage, Figure 5.30 (b), has a little output ripple and their values always are almost the maximum voltage of the photovoltaic panel. This cause that the output current from the solar panel can change abruptly. This property can be observed in  $I-V$  curve. As can be seen, Figure 5.30 (a) shows

that this control technique requires significant current delivered by the solar cell. This can also cause problems because the input current has a significant oscillation.

### Experimental results

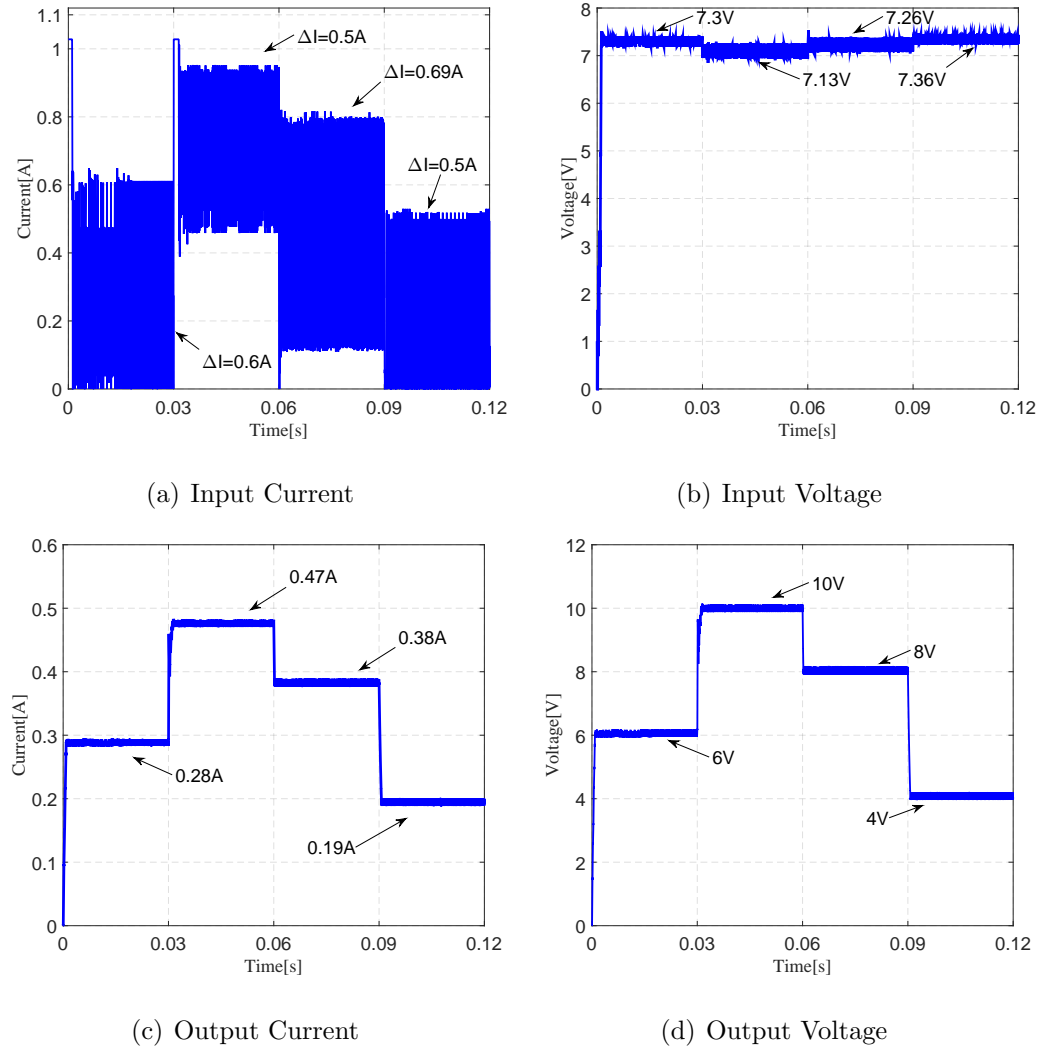


Figure 5.31 : Fuzzy Logic Control Experimental response

Figure 5.31 shows the experimental results for Fuzzy Logic Controller. Similar to the simulation response, the output current from the solar panel has a big ripple. Even greater than the simulation ripple. Additionally, the input voltage of the DC/DC converter also has an oscillation that is not present at the simulation. Thus, this can cause the input current oscillation. Furthermore, the output signals,

Figures 5.31 (c) and 5.31 (d), have a similar behavior with respect to the simulation response. These signals present little oscillations, but the average value is the same and the time response is very similar too.

### Passivity-Based Control

As mentioned above in Section 4.3.2, this type of controller is responsible for bringing the system to a passive state by canceling the components that bring it to this state. Below the control system implemented in simulation and then the experimental results of the control technique are presented. Based on Equation (4.59) the control law to be applied to the system to ensure passivity must be as follows:

$$u = u_k + D_{eq} \quad (5.5)$$

where,

$$D_{eq} = \frac{-I_x R + I_x R \left( \frac{V_{cx}}{V_x} \right)^{n+q} + \sqrt{V_{cx} I_x R - V_{cx} I_x R \left( \frac{V_{cx}}{V_x} \right)^{n+q}}}{-I_x R + I_x R \left( \frac{V_{cx}}{C_x} \right)^{n+q} + V_{cx}} \quad (5.6)$$

$$u_k = -k \left( \frac{1}{R} (J_1(e_1 + e_2) + J_2(e_3 + e_4)) \right) \quad (5.7)$$

and,

$$J_1 = R \left( V_{cx} + \sqrt{-I_x R V_{cx} \left( -1 + \left( \frac{V_{cx}}{V_x} \right)^{n+q} \right)} \right) \quad (5.8)$$

$$J_2 = - \left( I_x R + \sqrt{-I_x R V_{cx} \left( -1 + \left( \frac{V_{cx}}{V_x} \right)^{n+q} \right)} - I_x R \left( \frac{V_{cx}}{V_x} \right)^{n+q} \right)$$

The controller takes each of the state variables to bring the system to a state of passivity.



## Simulations results

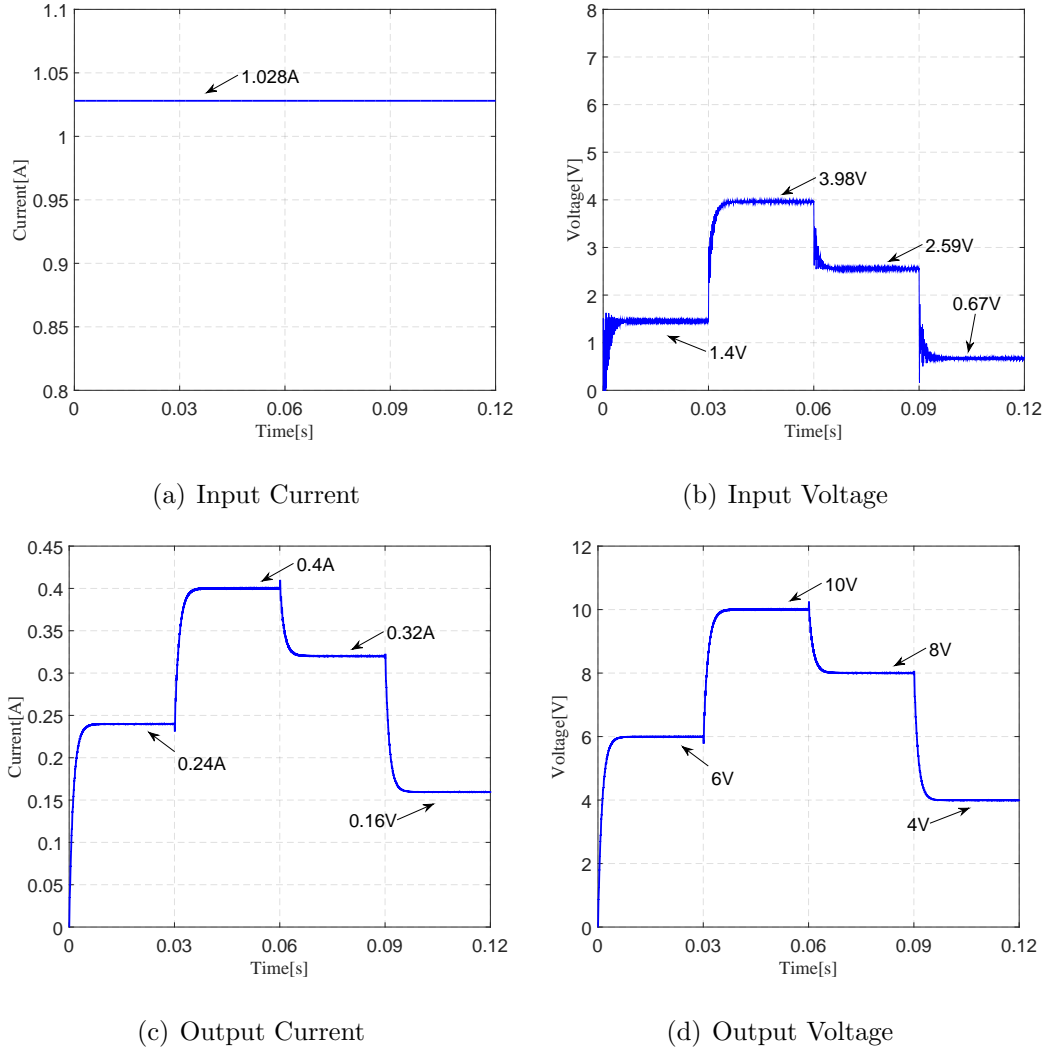


Figure 5.32 : Passivity-Based Control simulation response

Figure 5.32 (a) shows that while the power consumption at the output is low the voltage delivered by the solar panel will be low. Therefore, the output current of the solar panel will be the maximum current that can be delivered while that this power consumption demands the maximum power. The output voltage for each case of the vector of references is achieved and presents low ripple voltage. In a few cases, some spikes are present but these are not big enough that can cause damage. The

steady state that is achieved at the same time of the open loop simulation with solar array simulator can also be observed.

### Experimental results

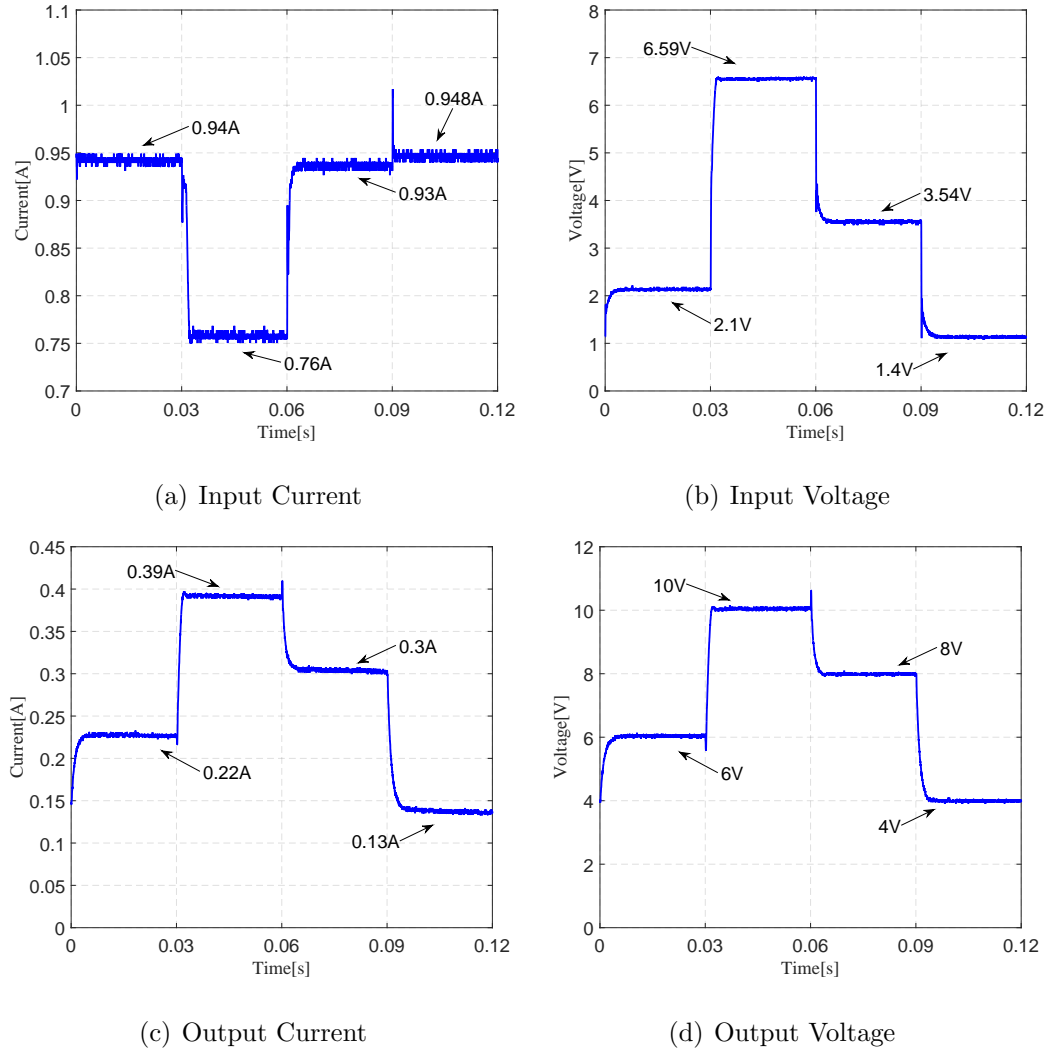


Figure 5.33 : Passivity-Based Control Experimental response

Equal to the previous case, as the Figure 5.33 present, the output signals observed for this technique reached the desired values for the current and voltage over the established load. As can be seen, the settling time is very close to the settling time simulation. Additionally, also is can be observed that the input signals (current and voltage) have other final values. As mentioned earlier, these signals are

different due to the power losses in the DC/DC converter and therefore the efficiency is not 100%. In the output signals can be observed some spikes, but these spikes do not have a long time duration.

## 5.4 Summary of results

Below a summary of results is presented. In order to determine the appropriateness of the use of control techniques, an analysis for each of the cases previously evaluated is presented.

### 5.4.1 Open-Loop Performance

Initially, the results obtained for open loop tests are presented. These tests as mentioned above were made for two different inputs. As a first input, a fixed power supply is used and secondly the simulator solar array. [Table 5.6](#) shows the results of comparison between the simulation in Matlab against the real results of the PCB designed. As can be seen, the efficiency of simulation is almost ideal efficiency for any circuit. Moreover, the results for the efficiency of the real converter are also shown. As for the real efficiency, it can be seen that there are losses in the converter that cause that the efficiency decreases. As mentioned above, there are many reasons that cause losses in normal operation of the DC/DC converter.

Table 5.6 : Open-Loop efficiency - fixed power supply

	Buck		Hold-Mode		Boost	
	Sim.	Exp.	Sim.	Exp.	Sim.	Exp.
$P_{in}(W)$	0.7	0.99	1.225	1.188	2.45	2.915
$P_{out}(W)$	0.69	0.682	1.169	1	2.209	2.103
$n$ (%)	99.6	68.9	95.4	84.2	90.2	72.1

[Table 5.7](#) shows the results of simulation and real results for the converter operating in open-loop and a solar array simulator as input. As can be observed,

the power supply is not a fixed signal and depends on of the current required by the system. This current can change due to the output power or the PWM signal.

Table 5.7 : Open-Loop efficiency - Solar array simulator

	Sim	Exp
$P_{in}(W)$	3.432	2.828
$P_{out}(W)$	3.367	2.16
$\eta$ (%)	98.1	76.4

#### 5.4.2 MPPT

Many systems based on solar systems have the need to have a second power supply such as a battery. A charge controller with MPPT is an electronic device that regulates the charging of these batteries controlling the point at which the solar panels work to deliver the maximum power. Below a summary of results obtained for the Perturb and Observe algorithm is presented.

Table 5.8 : Convergence time of the MPPT algorithm

Initial point	Time (ms)
0	340
$V_{ap}$	15
$\frac{V_{ap}+V_{am}}{2}$	35
$V_{am}$	85
$V_x$	570

As Table 5.8 shows, if the search starts at any point inside the new region, between  $V_{ap}$  and  $V_{am}$ , the time response to achieve the maximum power point is reduced. In one case, the time response is at least 50 times more than the other one. This shows that the search starting point in this class of algorithms is a very important factor for the resource consumption and efficiency. In addition, it can set that even though the final value of the power is the same, the consumption of energy in that time is wasted energy to reach that point and that energy can be delivered to the system being loaded at the exit.

### 5.4.3 Close-Loop Performance

Below the simulation and real results for each controller are presented. These results present the close-loop performance. In this case, the efficiency is evaluated for each voltage reference. In this Section, the results for input voltage control and output voltage control are presented.

#### Output Voltage Control

In the case of output control, the efficiency results are compared for each controller implemented. In addition, an analysis of convenience according to the efficiency and the time response is presented. As mentioned above, the implemented controllers need access to system signals to know its actual status and so know the control action to be taken to bring about the desired state. For this reason, there is a power consumption attached to the power converter which is also assumed by the system and is included in efficiency. It should be noted that the results presented below are results with average values of voltage and current to facilitate them.

Table 5.9 : Average Output Voltage Control efficiency - Fuzzy Logic Controller

	1		2		3		4	
	Sim.	Exp.	Sim.	Exp.	Sim.	Exp.	Sim.	Exp.
$P_{in}(W)$	1.812	2.555	4.883	6.4	3.112	4.356	0.676	1.104
$P_{out}(W)$	1.740	1.680	4.7	4.7	3.04	3.040	0.63	0.76
$\eta$ (%)	96	65.8	96.2	73.4	97.7	69.8	93.2	68.8

Table 5.10 : Output Voltage Control efficiency - Passivity-Based Controller

	1		2		3		4	
	Sim.	Exp.	Sim.	Exp.	Sim.	Exp.	Sim.	Exp.
$P_{in}(W)$	1.439	1.974	4.091	5.008	2.663	3.292	0.689	1.04
$P_{out}(W)$	1.4	1.320	4	3.9	2.560	2.4	0.630	0.520
$\eta$ (%)	97.3	66.9	97.8	77.9	96.1	72.9	91.5	50

Table 5.11 : Output Voltage Control efficiency - Summary

	1		2		3		4	
	Sim.	Exp.	Sim.	Exp.	Sim.	Exp.	Sim.	Exp.
FLC	96	65.8	96.2	73.4	97.7	69.8	93.2	68.8
PBC	97.3	66.9	97.8	77.9	96.1	72.9	91.5	50

As can be observed, the efficiency obtained from the real system for each controller has a difference with respect to the efficiency of the simulation. One of the big factors that can cause this efficiency decrease is the transmission line in the PCB (Print Circuit Board). The simulation in Matlab take into account parasitic elements in  $L$  or  $C$  but does not take into account losses due to the transmission line. In terms of experimental results it can be seen that there is a similarity in the convergence point of converter efficiency.

A very important factor, in this case, is the current that requires each driver to meet the power that is required to output. As shown in the graphs for controlling output by FLC, there is a big oscillation in the input current, and the current values are not small. These changes of the current through the connecting lines may have large amount of losses that may cause, in this case, the lower efficiency presented to the converter.

Another very important factor is shown in [Table 5.12](#) , as can be seen, the time response is different for each controller.

Table 5.12 : Settling Time

	Time ( <i>ms</i> )	
	Sim	Exp
FLC	320	330
PBC	355	340

As can be seen, the times of simulation compared to actual response times are quite similar. This may also be a deciding factor in determining which driver is the one.

The two control techniques, Passivity-Based control, and Fuzzy Logic control have different parameters for the output signals. While the FLC controller requires a low input current for almost each output voltage, the Passivity-Based controller requires almost the highest value delivered for the solar array simulator. This current value just decreases when the output power requires a high power of input. As for the FLC, the input current required by the controller has a big oscillation that causes losses.

If the settling times are compared, it can be observed that both the Passivity-Based controller and FLC have almost the same settling time. This settling time is small because the change of the duty cycle is quickly. In case of the Passivity-Based Control the duty cycle is calculated for the equilibrium points established for each desired case. As can be seen in the [Equation \(5.5\)](#) there are two terms. One of them is the  $u_{eq}$ , that is the ideal duty cycle. The other term is an adjust term used to correct the error of the state variables.

## Chapter 6

### CONCLUSIONS

Application of Two control techniques for the output voltage control methods based on design procedure and dynamic responses for DC/DC converters are presented. The relationship between the duty cycle of PWM and output of each controller is presented based on recent studies. Simulation results showed that the PWM based on Fuzzy Logic Controller, and Passivity-Based control has the acceptable performance for the output voltage control. With consideration of design procedure and hardware implementation, the Fuzzy Logic controller is better than the other controller. This is because the hardware need it to implement the controller is more simple. But with respect to the dynamic response, the Passivity-Based control and Fuzzy Logic control have a similar performance. Despite robustness and dynamic performances of the Passivity-Based controller, the hardware implementation of this controller needs more devices and more mathematical procedures than the Fuzzy Logic controller.

Additionally, an improvement to the convergence of search of one of the most used algorithms to find the maximum power point of photovoltaic systems is presented. This demonstrates that the starting point influences the elapsed time to achieve the maximum power point in order to reduce power losses.



# Bibliography

- [1] Azure Space Power Solar GmbH. 28% Triple Junction GaAs Solar Cell Type: TJ Solar Cell 3G28C. [Online]. Available: <http://www.azurspace.com/index.php/en/products/products-space/space-solar-cells>, 2010.
- [2] Ta-Tau Chen, Ming-Ying Hsiao, Shun-Hung Tsai, and Che-Nan Lin. Design of digital battery charger system based on pv-module. In *Fuzzy Systems (FUZZ), 2011 IEEE International Conference on*, pages 1860–1865. IEEE, 2011.
- [3] Hung-Chih Lin and Tsin-Yuan Chang. Analysis and design of a sliding mode controller for buck converters operating in dcm with adaptive hysteresis band control scheme. In *Power Electronics and Drive Systems, 2007. PEDS '07. 7th International Conference on*, pages 372–377, Nov 2007.
- [4] M. Kovacevic, A. Knott, and M.A.E. Andersen. A vhf interleaved self-oscillating resonant sepic converter with phase-shift burst-mode control. In *Applied Power Electronics Conference and Exposition (APEC), 2014 Twenty-Ninth Annual IEEE*, pages 1402–1408, March 2014.
- [5] A. Kavitha, G. Indira, and G. Uma. Analysis and control of chaos in sepic dc-dc converter using sliding mode control. In *Industry Applications Society Annual Meeting, 2008. IAS '08. IEEE*, pages 1–6, Oct 2008.
- [6] A. Jaafar, P. Lefranc, E. Godoy, Xuefang Lin-Shi, A. Fayaz, and Nan Li. Experimental validation with a control point of view analysis of the sepic converter. In *Industrial Electronics, 2009. IECON '09. 35th Annual Conference of IEEE*, pages 462–497, Nov 2009.
- [7] S. Venkatanarayanan and M. Saravanan. Control of sepic converter using neural network tuned pi controller. In *Power, Energy and Control (ICPEC), 2013 International Conference on*, pages 458–462, Feb 2013.
- [8] Shi bing Wang, Yufei Zhou, H.H.-C. Iu, and Jun ning Chen. Complex phenomena in sepic converter based on sliding mode control. In *Circuits and Systems, 2007. ISCAS 2007. IEEE International Symposium on*, pages 2407–2410, May 2007.

- [9] SJ Chiang, Hsin-Jang Shieh, and Ming-Chieh Chen. Modeling and control of pv charger system with sepic converter. *Industrial Electronics, IEEE Transactions on*, 56(11):4344–4353, 2009.
- [10] A.R. Kashyap, R. Ahmadi, and J.W. Kimball. Input voltage control of sepic for maximum power point tracking. In *Power and Energy Conference at Illinois (PECI), 2013 IEEE*, pages 30–35, Feb 2013.
- [11] Chok-You Chan. A nonlinear control for dc–dc power converters. *Power Electronics, IEEE Transactions on*, 22(1):216–222, 2007.
- [12] SJ Chiang, Hsin-Jang Shieh, and Ming-Chieh Chen. Modeling and control of pv charger system with sepic converter. *Industrial Electronics, IEEE Transactions on*, 56(11):4344–4353, 2009.
- [13] W. Lim, Byungcho Choi, and Jiemyung Ko. Current-mode control to enhance closed-loop performance of asymmetrical half-bridge dc-to-dc converters. In *Circuits and Systems, 2004. ISCAS '04. Proceedings of the 2004 International Symposium on*, volume 5, pages V–896–V–899 Vol.5, May 2004.
- [14] G.K. Jerin. Direct control method applied for improved incremental conductance mppt using sepic converter. In *Green Computing Communication and Electrical Engineering (ICGCCEE), 2014 International Conference on*, pages 1–6, March 2014.
- [15] J.E. Salazar-Duque, E.I. Ortiz-Rivera, and J. Gonzalez-Llorente. Analysis and non-linear control of sepic dc-dc converter in photovoltaic systems. In *Power Electronics and Power Quality Applications (PEPQA), 2015 IEEE Workshop on*, pages 1–6, June 2015.
- [16] Eduardo Ivan Ortiz Rivera. *Modeling and analysis of solar distributed generation*. 2006.
- [17] E.I. Ortiz-Rivera. A mppt method based on the approximation of a pvm model using fractional polynomials. In *Power Electronics Specialists Conference, 2007. PESC 2007. IEEE*, pages 951–954, June 2007.
- [18] Eduardo Ortiz-Rivera et al. Maximum power point tracking using the optimal duty ratio for dc-dc converters and load matching in photovoltaic applications. In *Applied Power Electronics Conference and Exposition, 2008. APEC 2008. Twenty-Third Annual IEEE*, pages 987–991. IEEE, 2008.

- [19] Martin A Green, Keith Emery, Yoshihiro Hishikawa, and Wilhelm Warta. Solar cell efficiency tables (version 33). *Progress in Photovoltaics: Research and Applications*, 17(1):85–94, 2009.
- [20] G. Petrone, G. Spagnuolo, R. Teodorescu, M. Veerachary, and M. Vitelli. Reliability issues in photovoltaic power processing systems. *Industrial Electronics, IEEE Transactions on*, 55(7):2569–2580, July 2008.
- [21] Daniel W Hart. *Power electronics*. Tata McGraw-Hill Education, 2011.
- [22] Rino Micheloni and Luca Crippa. *Charge pumps, voltage regulators and HV switches*. Springer, 2010.
- [23] Sudhakar Rao .P Rajeshwari Y Baraddi. 2d converter combining ky and buck converter. In *International Journal for Scientific Research & Development—Vol. 3, Issue 02, 2015 — ISSN (online): 2321-0613*, 2015.
- [24] Jianbo Yang, Weiping Zhang, Faris Al-Naemi, and Xiaoping Chen. Analysis and modeling of buck converter in discontinuous-output-inductor-current mode operation. *Energy and Power Engineering*, 5(04):850, 2013.
- [25] Ned Mohan and Tore M Undeland. *Power electronics: converters, applications, and design*. John Wiley & Sons, 2007.
- [26] Hebertt Sira-Ramírez and Ramón Silva-Ortigoza. *Control design techniques in power electronics devices*. Springer Science & Business Media, 2006.
- [27] Dongbing Zhang. An-1484 designing a sepic converter. *Texas Instrumants*, 2006.
- [28] Hung T Nguyen, Nadipuram R Prasad, Carol L Walker, and Elbert A Walker. *A first course in fuzzy and neural control*. CRC press, 2002.
- [29] Bingyuan Wang and Yuling Ma. Research on the passivity-based control strategy of buck-boost converters with a wide input power supply range. In *Power Electronics for Distributed Generation Systems (PEDG), 2010 2nd IEEE International Symposium on*, pages 304–308. IEEE, 2010.
- [30] Hassan K Khalil and JW Grizzle. *Nonlinear systems*, volume 3. Prentice hall Upper Saddle River, 2002.
- [31] E. I. rtiz Rivera and Fang Peng. A novel method to estimate the maximum power for a photovoltaic inverter system. In *Power Electronics Specialists Conference, 2004. PESC 04. 2004 IEEE 35th Annual*, volume 3, pages 2065–2069 Vol.3, June 2004.

- [32] E. I. Ortiz Rivera and F. Z. Peng. Linear reoriented coordinates method. In *2006 IEEE International Conference on Electro/Information Technology*, pages 459–464, May 2006.
- [33] National Instruments. Ni-tutorial-7230. 2012.
- [34] David Roger Smart. *Fixed point theorems*, volume 66. CUP Archive, 1980.
- [35] Ahmad El Khateb, Nasrudin Abdul Rahim, and Jeyraj Selvaraj. Fuzzy logic controller for mppt sepic converter and pv single-phase inverter. In *Industrial Electronics and Applications (ISIEA), 2011 IEEE Symposium on*, pages 182–187. IEEE, 2011.
- [36] SA Elankurisil, VP Deepika, and J Baskaran. Comparison of controllers in sepic dc-dc converter with high gain. In *Computation of Power, Energy Information and Commuincation (ICCPEIC), 2015 International Conference on*, pages 0110–0116. IEEE, 2015.
- [37] Bingyuan Wang and Yuling Ma. Research on the passivity-based control strategy of buck-boost converters with a wide input power supply range. In *Power Electronics for Distributed Generation Systems (PEDG), 2010 2nd IEEE International Symposium on*, pages 304–308. IEEE, 2010.
- [38] Brad Lehman and Richard M Bass. Extensions of averaging theory for power electronic systems. *IEEE Transactions on Power Electronics*, 11(4):542–553, 1996.
- [39] Jesus Gonzalez-Llorente, David Rodriguez-Duarte, Sergio Sanchez-Sanjuan, and Andres Rambal-Vecino. Improving the efficiency of 3u cubesat eps by selecting operating conditions for power converters. In *Aerospace Conference, 2015 IEEE*, pages 1–7. IEEE, 2015.
- [40] Mathworks Simulink. Simulation and model-based design, 2005.
- [41] Muralidhar Killi and Susovon Samanta. Modified perturb and observe mppt algorithm for drift avoidance in photovoltaic systems. *IEEE Transactions On Industrial Electronics*, 62(9):5549–5559, 2015.